OUKA
The University of Osaka
Institutional Knowledge Archive

Title	Development of Hybrid DFT Method for Strongly Correlated Electron Systems and Its Application to Polynuclear Transition Metal Complexes
Author(s)	北河, 康隆
Citation	大阪大学, 2003, 博士論文
Version Type	VoR
URL	https://hdl.handle.net/11094/746
rights	
Note	

The University of Osaka Institutional Knowledge Archive : OUKA

https://ir.library.osaka-u.ac.jp/

The University of Osaka

Development of Hybrid DFT Method for Strongly Correlated Electron Systems and Its Application to Polynuclear Transition Metal Complexes

Yasutaka Kitagawa

Department of Chemistry
Graduate School of Science
Osaka University

2003

Acknowledgements

The present work in this thesis has been completed under the supervision of Professor Kizashi Yamaguchi at the Department of Chemistry, Graduate School of Science, Osaka University. The author would like to express sincere gratitude to him for his many fruitful discussions, valuable suggestions and encouragement. He is deeply grateful for Professor Yasunori Yoshioka, Associate Professor Masayosi Nakano, Associate Professor Hidemi Nagao and Dr. Mitsutaka Okumura for helpful discussions, suggestions and encouragement.

The author is deeply indebted to Dr. Shusuke Yamanaka and Dr. Yasuteru Shigeta for helpful discussions and guidance about theoretical background (Chapter two). He gratefully acknowledges Professor Wasuke Mori, Professor Kazushi Mashima, Professor Sadamu Takeda, Dr. Satoshi Takamizawa and Dr. Goro Maruta for their helpful suggestions and discussions about the magnetic interactions in d-d and d-π conjugated systems and the experimental magnetic measurements (Chapter three).

The author would like to express his sincere gratitude to Dr. Takashi Kawakami and Dr. Shinji Kiribayashi for their continuous efforts about the administration of the computer system, which he has used in the Yamaguchi laboratory.

The author acknowledges Dr. Masaki Mitani, Dr. Takao Kobayashi, Dr. Daisuke Yamaki, Dr. Satoru Yamada, Dr. Kenji Ueda, Dr. Tadafumi Osaku, Dr. Masamichi Nishino, Dr. Akifumi Oda, Mr. Shigehiro Kubo, Mr. Tsunaki Tsunesada and Dr. Yu Takano for their helpful discussion, advice and encouragement.

The author wishes to thank Mr. Tomohisa Soda, Mr. Yusuke Odaka, Mr. Taku Onishi and Mr. Hiroshi Isobe for their friendship as the same grade students in the same laboratory. He also thanks Mr. Shuhei Nakano for collaboration, cooperation and discussion.

Many thanks are given to all the members and secretaries in the Yamaguchi laboratory, especially Mr. Fumitake Matsuoka, Mr. Yoshifumi Yamashita, Mr. Shun Tanaka, Mr. Masahiro Takahata, Mr. Harunori Fujita, Mr. Tadashi Maruta, Mr. Ryo Takeda, Mr. Takeshi Taniguchi, Mr. Ken-ichi Koizumi, Mr. Mitsuo Shoji, Mr. Yusuke Nishiyama, Mr. Yusuke Maruno and Mr. Tomohiro Hamamoto for the author's full, fruitful and enjoyable life in the laboratory.

Numerical calculations were carried out on the super computers at the Institute for Molecular Science and workstations at Yamaguchi Laboratory. The author's work was supported by Research Fellowships of the Japan Society for the Promotion of Science for Young Scientist from April 2000 to March 2003.

Finally, the author would like to express his sincere thanks to his family, especially his parents Mr. Takashi Kitagawa and Mrs. Michiko Kitagawa, his sister Miss Yuko Kitagawa and his fiancée Keiko for their constant support and hearty encouragement.

CONTENTS

CHAPTER ONE

GENERAL INTRODUCTION OF THIS THESIS

Chapter One

General Introduction of This Thesis

Strongly correlated systems i.e. the systems that have strong electron correlation effects were found in various place, such as unstable metal-metal bond in polynuclear complexes, mixed valence systems, organic ferro (or antiferro) magnet, hydrogen bonding systems and electron transfer systems in vivo, copper oxide superconductor, and so on. Those systems are interesting in terms of a scientific viewpoint, of course. Besides, they were focused on in terms of the development of new materials. If we consider from a viewpoint of electron correlation, various phenomena (that seem to be completely different such as superconductivity and biochemical reactions) might be able to understand systematically. The detail about a relation between the electronic structure and physical properties, chemical reaction does not have been elucidated well in those strong correlating systems. Therefore the investigation of it is a subject as pressing need.

In the field of quantum chemistry, it is becoming possible to calculate electronic states of large-sized electron systems that are almost similar to real systems because of the recent development of computers and *ab initio* methods. Thereby, the more concrete theoretical approach to various

directions, such as physical properties and a chemical reaction, is expected. In the strong correlation systems, however, there is still a restriction that stems from a computing size and the effective *ab initio* calculation technique for those systems has not been established. On the other hand, there is a density functional theory (DFT) method as another method of quantum chemical calculations. The DFT method has a merit that electron correlation effects are taken into account at a low computing cost. In the strong correlation systems that localized spins appear, however, the DFT method can not express the electronic state well, especially spin-spin interaction. So, DFT method must be improved to apply it to those strong correlating systems.

Polynuclear complexes that involve the linearly aligned metal chain are known as one of the strongly correlated systems. In those complexes, electron spins are localized on metal ions because of strong electron correlation. In recent years, many reports about these metal string complexes have been presented in a field of the coordination chemistry. Those aligned metal systems usually have unique bonding nature such as d orbital - d orbital direct bonds between metal ions (metal-metal bond), d orbital - p orbital interactions between metal and ligands (metal-ligand bond) and so on. Some interesting phenomena related to them also have been investigated. So, they are interesting in terms of fundamental studies of their peculiar bonding characters and applications to functional materials. From the above facts, the author proposed the original hybrid DFT schemes, which have variable ratio of HF exchange term and DFT exchange-correlation term for the magnetic measurement between radical species in those strong correlating systems. And the author verified it using several models and applied it to the linearly aligned metal complexes to investigate their electronic states in terms of magnetic interactions between metal ions.

In chapter two, the author developed the hybrid DFT method for magnetic measurement between spins in strongly correlated systems, namely MEDF and verified it using several radical dimer models. Instabilities of radical orbitals were estimated by several methods and the author found close relation between the instabilities and hybrid parameter.

In chapter three, the author investigated linearly aligned metal systems that were also strongly correlated electron systems. By MEDF, quantitative analyses of J_{ab} values become possible. The electronic states and magnetic interactions of Cotton type di-nuclear complexes were investigated in detail. From these results, experimental J_{ab} values were explained by theoretical calculations. Linearly aligned tetra-nuclear complexes also examined in terms of magnetic interactions. This J_{ab}

analyses for linearly aligned tetra-nuclear complexes by theoretical calculations were the first time in the world.

The approach to magnetic interaction between radical species by the improved hybrid DFT for magnetic measurement has not been reported yet. So, this study is newly and unique.

CHAPTER TWO

DEVELOPMENT OF HYBRID DFT METHOD FOR STRONGLY CORRELATED ELECTRON SYSTEMS

Chapter Two

Development of Hybrid DFT Method for Strongly Correlated Electron Systems

2.1 Introduction

In recent years, a density functional theory (DFT) is becoming increasingly popular in quantum chemistry[1][2][3]. Especially, it is applied to large-sized molecules such as transition metal complexes[4][5][6][7][8], polymers[9][10], bio-molecules with proteins[11] and so on, because it has an advantage that exchange-correlation effects are taken at a lower computing cost. The exact exchange-correlation functional of the DFT method should cover 'all' electron correlation effects. Up to now, many researchers have been developed the E_{xc} terms to express the electron-correlation effects to reproduce appropriate electronic structure[3]. Three different approaches of exchange-correlation functions have been used in standard DFT methods (for instance, [1][2][3][12][13][14][15][16][17]). Typical representatives of the first generation were the local density approximation (LDA) such as SVWN, which combined the Slater exchange functional[12] with the Vosko-Wilk-Nusair correlation

functional[16]. The second generation of DFT was based on the generalized gradient approximation (GGA) such as BLYP which combined Becke's exchange[13] and Lee-Yang-Parr correlation[17]. The third generation of functionals is based on a mixing of HF an DFT exchange to obtain a more realistic account of the exchange-correlation effects, as first suggested by Becke, such as B3LYP[18]. Despite the effort of these pioneers, DFT methods have not been able to 'all' electronic properties[3], especially magnetic properties.[19][20][21]

Intermolecular magnetic interactions between radical species have been studied by using unrestricted HF (UHF), unrestricted post HF and unrestricted DFT (UDFT)[21]. The intermolecular effective exchange interactions play important roles for long-range magnetic ordering in molecule-based magnetic materials. However the effective exchange integrals (J_{ab}), which revealed by magnetic measurements are usually weak[27][28][29][30]. Calculated results showed that conventional methods such as UB3LYP and UBLYP were powerful and reliable for computations of through-bond J_{ab} values in these species[9][10]. In the case of through-space interactions, however, the magnitude of the calculated J_{ab} values for the radical dimers were too large as compared with the UCCSD(T) values[18][19][20]. It suggested that further improvements are necessary for computations of intermolecular (through-space) J_{ab} for radical clusters.

Here, the author examined hybrid UDFT methods, which have variational ratio of HF exchange for effective computations of intermolecular J_{ab} values for radical clusters[20][21]. First, the author examined whether hybrid UDFT methods could reproduce J_{ab} values which were calculated by UCCSD(T) or Full CI methods by calibrating mixing parameter using several models. Next, the author investigated the relations between hybrid parameters and instabilities of the systems. Takatsuka et al. [22] and Yamaguchi et al. [23] discussed about distributions of odd electrons in ground state molecules and determined the diradical character. On the other hand, the information entropy is applied to the matters of quantum chemistry such as the stability of small molecules[24][26]. The author examined that the instabilities of several diradical models by using these chemical indices and relation between the instability of a system and the hybrid parameter. The present computational results indicated a possibility of effective magnetic density functional (EMDF) theory for radical clusters.

2.2 Hybrid density functional methods

2.2.1. *Hybrid procedure for magnetic measurements*

In the Kohn-Sham formulation of DFT[31], the electronic energy is separated in parts[1][32],

$$E_{total} = T_S + V_{n-e} + J + E_{XC} \tag{2.1}$$

where

$$\rho = \sum_i^N |\psi_i|^2 \tag{2.2}$$

$$T_S = \sum_i^N \langle \psi_i | -\frac{1}{2}\nabla^2 | \psi_i \rangle \tag{2.3}$$

$$V_{n-e} = -\sum_A^{nucl} Z_A \int \rho(r) |r - r_A|^{-1} dr \tag{2.4}$$

$$J = \frac{1}{2}\iint \rho(r_1) |r_1 - r_2|^{-1} \rho(r_2) dr_1 dr_2 \tag{2.5}$$

and E_{xc} is expressed as follows,

$$E_{XC} = T - T_S + V_{e-e} - J. \tag{2.6}$$

Here, T and V_{n-e} are kinetic and electron-nuclear interaction energies and J is the coulomb interaction, respectively. T_S is a kinetic energy of a single Slater determinant. T - T_S and V_{e-e} - J are expressing the difference between a multi-reference and a single-reference of kinetic and electron-electron interactions, respectively. In this way, E_{XC} involves the remainder between multi- and single-Slater determinant *i.e.* electron-correlation effect.

As mentioned before, the present exchange-correlation functionals could not reproduce 'all' electron-correlation effects in spite of the effort of these pioneers. To answer the question why these E_{XC} methods could not reproduce appropriate electron-correlation energies, one has to consider two types of electron-correlation effect[3]. One is dynamical correlation and another is non-dynamical correlation. The dynamical correlation is a short range interaction that is usually explained as the collision of alpha and beta electron pair. While non-dynamical (static) correlation effect is known to result from near-degeneracy of orbitals, i.e. strong interactions of ground and exited states, which are

result from near-degeneracy of orbitals, i.e. strong interactions of ground and exited states, which are close in energy[3]. (Hence, non-dynamical electron correlation in system-specific contrary to dynamical correlation.) This non-dynamical correlation causes the localized spins such as in the biradical singlet state. So, it is important how to treat this non-dynamical correlation in case of magnetic measurements. DFT is a correlation collected method, however, it is still unclear which electron correlation effects are covered by the various exchange-correlation functionals presently in use. The approximate exchange-correlation functional available today are considered to describe only dynamical correlation effects, because conventional functions was developed starting from an approximation of a homogeneous electron gas[2].

In this decade, several developments about the hybrid DFT which couples DFT to HF, namely adiabatic connection method (ACM) [33][34][35], and improvement of them for practical use (for instance, [36][37][38][39]) were reported. Recently, it is considered that the hybrid DFT is a promising method for the combining the long-range (non-dynamical) interaction and short-range (dynamical) interaction[40][41]. Because missing long-range correlations of DFT might be compensated by HF exchange[42]. Iikura et al. improved the DFT exchange functional with HF exchange[41]. However non-dynamical correlation effect was not fully involved.

In case of the magnetic measurement between radical clusters, the treatment of two effective factors becomes important. One is the non-dynamical correlation effects and another is self-interaction correlation (SIC) effect. The author improve the hybrid DFT method to overcome those problems based on unrestricted broken-symmetry (BS) scheme[20][21].

In the case of restricted Hartree-Fock (RHF) calculation of wave function theory (WFT), the effects of multi-reference must be considered to involve both correlations. While unrestricted Hartree-Fock (UHF) calculations are approximately including the non-dynamical correlation by splitting alpha and beta electrons into two different orbitals, namely different orbitals for different spins (DODS) approach. In the DODS approach, orbital mixing is used[43],

$$\begin{cases} \psi^{\alpha}_{HOMO} = \cos\theta\psi_{HOMO} + \sin\theta\psi_{LUMO} & (2.7a) \\ \psi^{\beta}_{HOMO} = \cos\theta\psi_{HOMO} - \sin\theta\psi_{LUMO}, & (2.7b) \end{cases}$$

and Fock for each orbital are written as

$$\begin{cases} f^{\alpha}(r) = h(r) + \sum_{i}^{n^{\alpha}} \left[J_i^{\alpha}(r) - K_i^{\alpha}(r) \right] + \sum_{j}^{n^{\beta}} J_i^{\beta}(r) & (2.8a) \\ f^{\beta}(r) = h(r) + \sum_{i}^{n^{\beta}} \left[J_i^{\beta}(r) - K_i^{\beta}(r) \right] + \sum_{j}^{n^{\alpha}} J_i^{\alpha}(r). & (2.8b) \end{cases}$$

And total energy is written as follows,

$$E_0 = \sum_{i}^{n^{\alpha}} h_{ii}^{\alpha} + \sum_{i}^{n^{\beta}} h_{ii}^{\alpha} + \frac{1}{2} \sum_{i}^{n^{\alpha}} \sum_{j}^{n^{\alpha}} \left[J_{ij}^{\alpha\alpha}(r) - K_{ij}^{\alpha\alpha}(r) \right] + \frac{1}{2} \sum_{i}^{n^{\beta}} \sum_{j}^{n^{\beta}} \left[J_{ij}^{\beta\beta}(r) - K_{ij}^{\beta\beta}(r) \right] + \sum_{i}^{n^{\alpha}} \sum_{j}^{n^{\beta}} J_{ij}^{\alpha\beta}. \quad (2.9)$$

In comparison with RHF, Coulomb repulsive energy between alpha and beta electrons was taken into account in the UHF scheme. Similarly, BS-UDFT was also developed. Gunnarsson et al successfully indicated that BS-UDFT reproduced H_2 dissociation[44], which could not reproduced using restricted DFT (RDFT). The spin restricted DFT (Eqs(2.2)-(2.5)) were usually extended to spin unrestricted DFT as follows;

$$T_S = \sum_{i}^{n^{\alpha}} \left\langle \psi_i^{\alpha} \left| -\frac{1}{2} \nabla^2 \right| \psi_i^{\alpha} \right\rangle + \sum_{i}^{n^{\beta}} \left\langle \psi_i^{\beta} \left| -\frac{1}{2} \nabla^2 \right| \psi_i^{\beta} \right\rangle \quad (2.10)$$

$$V_{n-e} = -\sum_{A}^{nucl} Z_A \int \rho(r) |r - r_A|^{-1} dr \quad (2.11)$$

$$J = \frac{1}{2} \iint \rho(r_1) |r_1 - r_2|^{-1} \rho(r_2) dr_1 dr_2 \quad (2.12)$$

$$E_{XC} = \int f(\rho^{\alpha}, \rho^{\beta}) dr \quad (2.13)$$

where

$$\rho^{\alpha} = \sum_{i}^{n^{\alpha}} \left| \psi_i^{\alpha} \right|^2, \quad (2.14a)$$

$$\rho^{\beta} = \sum_{i}^{n^{\beta}} \left| \psi_i^{\beta} \right|^2 \quad (2.14b)$$

$$\rho = \rho^{\alpha} + \rho^{\beta}. \quad (2.15)$$

Using the E_{XC} of UDFT, appropriate collections for the dynamical correlation for UHF seems to be effective. The hybrid UDFT method has the merit of UHF-based treatment of exchange and it helps for understanding of dynamical correlation correction.

Here, two schemes are assumed that have one parameter hybridizing the HF exchange and DFT exchange-correlation terms. In the first scheme, the author generalize the exchange-correlation potential, which involve both HF and DFT terms as follows[20][21],

$$E_{XC} = E_X + E_C \tag{2.16a}$$

$$= c_1 E_X^{HF} + (1 - c_1) E_X^{DFT} + E_C^{DFT} \tag{2.16b}$$

And in the second scheme[21],

$$E_{XC} = c_1 E_X^{HF} + (1 - c_1) E_{XC}^{DFT} \tag{2.17a}$$

$$= c_1 E_X^{HF} + (1 - c_1)\left(E_X^{DFT} + E_C^{DFT}\right) \tag{2.17b}$$

Those two schemes are based on Becke's procedures. The first scheme is based on B3LYP procedure[18]. Becke presumed E_{XC} energy as

$$E_{XC} = E_{XC}^{LSDA} + c_1\left(E_X^{exact} - E_X^{LSDA}\right) + c_X \Delta E_X^{GGA} + c_C \Delta E_C^{GGA}. \tag{2.18a}$$

Here if $E_X^{exact} = E_X^{HF}$, $c_X = 1 - c_1$ and $c_C = 1$ were presumed then

$$E_{XC} = c_1 E_X^{HF} + (1 - c_1)\left(E_X^{LSDA} + \Delta E_X^{GGA}\right) + E_C^{LSDA} + \Delta E_C^{GGA}. \tag{2.18b}$$

The second scheme is based on Becke's ACM (this scheme is so-called Beche's Half and Half)[33],

$$E_{XC} \cong c_1 E_X + c_2 E_{XC}^{LSDA} \tag{2.19}$$

here assuming that $c_2 = 1 - c_1$ and GGA correction then

$$E_{XC} = c_1 E_X^{HF} + (1 - c_1)\left(E_X^{LSDA} + \Delta E_X^{GGA} + E_C^{LSDA} + \Delta E_C^{GGA}\right) \tag{2.20}$$

In this way, eqs.(2.18b) and (2.20) are derived. Eqs(2.18b) and (2.20) consist of only one parameter, which is adjustable for the appropriate dynamical correlation. Here, Slater's exchange functional[12], Becke's exchange functional[13] and VWN correlation functional[16] LYP correlation functional[17] are used as E_x^{LSDA}, ΔE_X^{GGA}, E_C^{LSDA} and ΔE_C^{GGA}, respectively. The hybrid parameter c_1 means a correction for the HF exchange potential by two types of schemes. The mixing coefficients in conventional DFT: BLYP and B3LYP and HF are summarizing in Table 2.1 in comparison with these two schemes.

2.1.2 Self-interaction correlation (SIC) problem

Another problem that occurs in DFT is self-interaction correlation (SIC) error. In HF theorem, it is easily understood that SIC is removed in eq 2.9 (J_{ii} - K_{ii} = 0). However, V_{ee} does not

vanish in DFT[1]. Usually, this SIC error is canceled out by subtraction in calculations such as ionization potential, binding energy and so on[1]. In the case of magnetic calculations, however, another problem occurs.

Let us consider the linear chain of hydrogen atoms as illustrated in Figure2.1. It is often classified into three regions[20][21]. The region I is characterized by strong orbital interactions and formations of strong covalent bonds. On the other hand, the region III is regarded as a dissociation region. There are scarcely intermolecular interactions between two hydrogen atoms in this region. The region II is around a bifurcation point and a transition region from the region I to the region III[45]. Near the dissociation region in III, the total wavefunction of H_2 can be described by a Slater determinant constructed of DODS orbitals which are localized on each hydrogen atoms.

$$\lim_{r\to\infty}\left|\Psi_0\right\rangle = \lim_{r\to\infty}\left|\psi^{\alpha}_{HOMO}\overline{\psi}^{\beta}_{HOMO}\right\rangle = \left|\phi_a\overline{\phi}_b\right\rangle \tag{2.21}$$

where ϕ_a and ϕ_b are atomic orbitals of H_a and H_b.

Under this approximation, the pair function $P_2^f(r_1,r_2)$ of parallel spin pairs are given by density P_1 and spin density Q_1 obtained by the DODS orbitals. [46][47][48]

$$P_2^f(r_1,r_2) = \frac{\left\{\left[P_1(r_1)P_1(r_2) - P_1(r_1,r_2)^2\right] + \left[Q_1(r_1)Q_1(r_2) - Q_1(r_1,r_2)^2\right]\right\}}{2} \tag{2.22}$$

Similarly the pair function $P_2^c(r_1,r_2)$ of antiparallel spin pairs is expressed by

$$P_2^c(r_1,r_2) = \frac{\left[P_1(r_1)P_1(r_2) - Q_1(r_1)Q_1(r_2)\right]}{2} \tag{2.23}$$

The correlation effects of the same and opposite spins are described by these functions, respectively. The pair function of the same spin clearly vanishes for r_2 - r_1, since two terms in density and spin density become equal, respectively and cancel exactly. This type of correlation prevents two electrons of the same spin being found at the same point in space. Thus there exists Fermi hole in the same spin pairs. The pair function of opposite spin, however, does not vanish for r_2 - r_1 as

$$P_2^c(r) = \frac{\left[P_1(r)^2 - Q_1(r)^2\right]}{2} \tag{2.24}$$

The true pair function of different spins should vanish for r_2 - r_1 due to the Coulomb repulsion between different spins. Thus, spin density is closely related to Coulomb correlation between different spins, and its magnitude directly expresses the size of the Coulomb hole [46][47][48]. And its product

$Q_1(r)Q_1(r')$ is nothing but the classical part of spin correlation function related to spin exchange in eq. 1[46][47]. The spin density and spin correlation function can be observed in the antiferromagnetically ordered state, though they remain useful indices to express exchange-correlation phenomena in small radical clusters.

The electron-electron repulsion at site r, which is a part of the self interaction correction (SIC), is given by

$$\lambda V_{ee}(r) = P_2^c(r)U \qquad (U = \text{on-site repulsion integral}). \tag{2.25}$$

From eq. (9), the electron-electron repulsion diminishes in special case, $(P_1)^2 = (Q_1)^2$, for example the pure biradical or dissociation limit. This indicates that the UHF exchange potential is correct at the dissociation limit of hydrogen radical clusters. On the other hand, the electronic structure of the hydrogen chain in the regions I and II cannot be described exactly by one Slater determinant because of the nonzero electron-electron interaction ($V_{ee}(r)$). The Kohn-Sham approximation can be used to evaluate the kinetic energy part in the regions I and II, though the exact form of the remaining exchange-correlation potential is not discovered yet. However, it is well known that UBLYP, B3LYP[18] or EDF[49] works well in the strong bond region I, though the self interaction correction (SIC) term remains because of $(P_1)^2 \neq (Q_1)^2$. These circumstantials evidence indicate that the exchange potential should vary from the UBLYP-type to the UHF-type in the course of the dissociation process from I to III through II. It is convenient that the exchange potential in the intermediate region II-III is given by the mixing of UDFT and UHF, in conformity with the hybrid DFT approach. Hybrid DFT method is one of the approach to overcome the problem.

2.2 Size-consistent spin projection

The magnetic properties of transition metal complexes have been investigated by the use of the Heisenberg-Dirac-van Vleck spin Hamiltonian. For example, the effective exchange interaction between localized spins is described by the spin-coupling Hamiltonian[28][29][30][50][51];

$$H = -2\sum J_{ab} S_a \bullet S_b , \tag{2.26}$$

where J_{ab} is the orbital-averaged effective exchange integral between the metal a and b with total spin operators $\mathbf{S}_a$ and $\mathbf{S}_b$. J_{ab} can be experimentally determined by magnetic susceptibility. Recent development in computational quantum chemistry enabled us to perform *ab initio* calculations of J_{ab} values using broken-symmetry (BS) approach such as UHF or UDFT[8][52]. The BS approach can be performed at a low computing cost but for singlet biradicals and low-spin species suffer from the spin contamination arising from high-spin states. For example, HF wavefunction of singlet H_2 molecule are described by

$$\left|\Psi_0\right\rangle = \left|\psi_1^{\alpha}\overline{\psi}_1^{\beta}\right\rangle. \tag{2.27}$$

If eq (2.7a) and (2.7b) are substituted in eq (2.27), UHF wavefunction of H_2 is described as follows[43];

$$\left|\Psi_{UHF}\right\rangle = \cos^2\theta\left|\psi_1\overline{\psi}_1\right\rangle - \sin^2\theta\left|\psi_2\overline{\psi}_2\right\rangle - \frac{1}{\sqrt{2}}\cos\theta\sin\theta\left|{}^3\Psi_1^2\right\rangle. \tag{2.28a}$$

And $\langle S^2\rangle$ becomes as follows,

$$\left\langle S^2\right\rangle_{UHF} = \left\langle S^2\right\rangle_{exact} + N^{\beta} - \left|S^{\alpha\beta}_{SOMO-SOMO}\right|. \tag{2.28b}$$

where $\langle S^2\rangle_{exact} = S(S+1)$. In this way, BS-UHF contains triplet state. This spin-contamination is leading to spin-projection procedures[8][50][52].

Several computational schemes of J_{ab} have been reported such as eqs. (2.29) - (2.31) with different BS methods[8][50][52].

$$J_{ab}(1) = \frac{E(LS) - E(HS)}{S^2} \quad \text{where } S = \left|S_a\right| + \left|S_b\right| \tag{2.29}$$

$$J_{ab}(2) = \frac{E(LS) - E(HS)}{S(S+1)} \tag{2.30}$$

$$J_{ab}(3) = \frac{E(LS) - E(HS)}{\left\langle S^2\right\rangle(HS) - \left\langle S^2\right\rangle(LS)} \tag{2.31}$$

where $E(X)$ and $\langle S^2 \rangle(X)$ denote the total energy and total spin angular momentum for the spin state X, respectively. S_a and S_b are spin magnitude of site a and b, respectively. $J_{ab}(1)$ is a scheme by Ginsberg[53], Noodleman[54] and Davidson[55], while $J_{ab}(2)$ is a scheme by Bencini[56] and Ruiz[57] and others. $J_{ab}(3)$ is Yamaguchi's spin projection procedure[57]. Through the studies, it is known that $J_{ab}(1)$ is derived when the overlap of magnetic orbitals is sufficiently small, while $J_{ab}(2)$ is applicable when overlap is sufficiently large. $J_{ab}(3)$ can connect $J_{ab}(1)$ and $J_{ab}(2)$ with the strength of the orbital overlap[8][50][52].

Here, the author introduce an approximate but size-consistent spin projection (AP) scheme for UHF and DFT solutions by Yamaguchi et al in eq (2.31)[58][59][60]. Let us consider potential curve of one-dimension clusters with variation of the interatomic distance, as illustrated in Figure 1, again. The spin projection is easy for radical clusters in the region III, since UHF and UDFT orbitals for radical sites are essentially orthogonal. Since the total energies of the HS and LS UHF (or UDFT) solutions correspond to those of the Heisenberg (HB) models, respectively, the energy gap can be used to estimate effective exchange integrals (J_{ab}) as

$$J_{ab}(Z) = \frac{\left[{}^{LS}E(Z) - {}^{HS}E(Z)\right]}{\Delta(Z_I)}, \tag{2.32}$$

where

$$\Delta(Z_I) = 4(N-1)S_aS_b, \tag{2.33}$$

and Z = UHF, post UHF such as UCCSD(T), or DFT, and N is the number of spin sites in clusters under consideration. The S_a and S_b are the sizes of spin at sites a and b. The energy gain by the spin projection can be estimated by eqs. (2.32) and (2.33), since J_{ab}(Z) is determined even for larger systems.

On the other hand, the spin projection of the UHF and UDFT wavefunctions in the region II is a difficult task, since orbital overlaps between radical orbitals are significantly large. Here, the author introduced an approximate but size-consistent spin projection procedure, where the denominator in eq. (2.33) is modified so as to reproduce the values of the total spin angular momentum in regions both I and III as

$$\Delta(Z_{II}) = {}^{HS}\langle S^2 \rangle(Z) - {}^{LS}\langle S^2 \rangle(Z) - S_a g(N)\left[{}^{LS}\langle S^2 \rangle(Z) - S_r(S_r+1)\right], \tag{2.34}$$

where

$$g(N) = \frac{(N-2)^2}{N} \quad (\text{N} \geq 2 \text{ and even numbers}), \tag{2.35}$$

$$= (N-3) \quad (\text{N} \geq 3 \text{ and odd numbers}), \tag{2.36}$$

and S_r denotes the exact spin angular momentum for clusters under discussion.

$$S_r = n(S_a - S_b) \quad (N = 2n), \tag{2.37a}$$

$$S_r = n(S_a - S_b) + S_a \quad (N = 2n+1). \tag{2.37b}$$

The effective exchange integral by the approximate spin projected (AP-) UHF, UCCSD(T) and UDFT methods are, therefore, given by

$$J(AP-Z) = \frac{\left[{}^{LS}E(Z) - {}^{HS}E(Z)\right]}{\Delta(Z_{II})}. \tag{2.38}$$

The J(AP-Z) value almost reduces to that of eq. (2.32) in the magnetic region III, whereas it becomes a theoretical parameter for the spin projection in the intermediate (II) and strong overlap (I) regions, where the spin contamination effects in UHF and UDFT wavefunctions are more or less decreased. The equations (2.32) and (2.38) have the correct size(N)-dependency, though the equation in ref. [58] becomes wrong when N>3. The equations (2.32)-(2.38) are applicable to any hybrid method of UHF and UDFT since only the total spin angular momentum is used for approximate spin projection.

Similar to the procedure for spin projected J_{ab} values, total energy of the pure singlet state is approximately given by[58][59][60]

$${}^{LS}E(AP-Z) = {}^{LS}E(Z) + f \times \left({}^{LS}E(Z) - {}^{HS}E(Z)\right) \tag{2.39}$$

where

$$f = \frac{{}^{LS}\langle S^2 \rangle - S(S+1)}{{}^{HS}\langle S^2 \rangle - {}^{LS}\langle S^2 \rangle}. \tag{2.40}$$

In this way, spin-projected J_{ab} values and low spin state energies are derived. This spin projection scheme is very effective for the region where strong non-dynamical correlation effect exists as discussed in chapter 2.6.2. In this thesis, Yamaguchi's scheme (eq. 2.31 or 2.38) is used to estimate J_{ab} values as long as there is no notice.

2.3 Instability of chemical bonds in open-shell systems

Let us consider potential curve of a hydrogen molecule with variation of the interatomic distance, as illustrated in Figure 2.1, again. In singlet ground state of a hydrogen molecule, σ orbital is considered to be doubly occupied by a pair of electrons having α and β spins in the region I. Unrestricted calculations offer same results to the restricted calculations in this region. However, α and β electrons split spatially and become so-called singlet diradical species in region II and III. There are several methods to assess this diradical character[22][23][24][26]. The relation of them was examined analytically for H_2 by Yamaguchi et al[50].

2.3.1 *Takatsuka's procedure*

Let us consider a singlet ground state. The first-order reduced density matrix is written as [22]

$$\rho(x,x') = \frac{1}{2}\gamma(r,r')\left[\alpha(s)\alpha(s') + \beta(s)\beta(s')\right] \tag{2.41}$$

where r and s respectively denote the space and spin coordinates and where $\gamma(r, r')$ is the spinless first-order density matrix. The necessary and sufficient condition for a wavefunction to be reduced to a single Slater determinant is

$$\rho(x,x') - \int \rho(x,x'')\rho(x'',x)dx''$$
$$= \frac{1}{4}\left[2\gamma(r,r') - \int \gamma(r,r'')\gamma(r'',r')dr''\right]\left[\alpha(s)\alpha(s') + \beta(s)\beta(s')\right] = 0 \tag{2.42}$$

It follows that

$$2\gamma(r,r') - \gamma^2(r,r') = 0 \tag{2.43}$$

where $\gamma^2(r, r')$ has been defined as

$$\gamma^2(r,r') = \int \gamma(r,r'')\gamma(r'',r')dr''. \tag{2.44}$$

Eq.2.43 means that the natural orbitals should be doubly occupied, as long as the wavefunction for which $\langle S^2\rangle=0$ can be represented by a single Slater determinant. On the contrary, when the exact wavefunction can not be expressed by one determinant alone, $2\gamma(r, r') - \gamma^2(r, r')$ should not be nonzero. In such latter cases, the natural orbital pairs must be split to a certain extent. Thus, a spinless density function defined as

$$D(r,r') = 2\gamma(r,r') - \gamma^2(r,r') \tag{2.45}$$

is expected to provide a theoretical clue to the spatial splitting of electron pairs in a given molecular system. Each counterpart electron of an electron pair which is thus split to occupy different portions of space, orthogonally will hereafter be referred to as an 'odd electron'. The extent of generation of such odd electrons and their distribution in molecules are the central problem of our present concern. Let us concern ourselves here primarily with the diagonal element of Eq.2.45. One will express the diagonal element as

$$D(r) = 2\gamma(r) - \gamma^2(r) \tag{2.46}$$

The density function $D(r)$ can be expanded diagonally in terms of the natural orbitals φ_k and their occupation numbers n_k ($0 \le n_k \le 2$). The result is written as

$$D(r) = \sum_k n_k(2 - n_k)\varphi_k^*(r)\varphi_k(r) \tag{2.47}$$

Eq(2.47) indicates that the intensity factor of a natural orbital contributing to the density function D(r) is $n_k(2 - n_k)$. Obviously, the factor $n_k(2 - n_k)$ takes a maximal value of 1 when n_k=1, and diminishes monotonously down to 0 as nk approaches 0 or 2. This could be taken as an implication that $n_k(2 - n_k)$ is the probability that the electrons in φ_k is left unpaired as if it were an odd electron in the singly occupied molecular orbital of a doublet radical. Here, $D(r)$ is called T value in this thesis.

2.3.2 *Yamaguchi's procedure*

In order to elucidate the open-shell characters, the UHF solution is expressed by the corresponding molecular orbitals (CMOs)[23]:

$$\Psi(UHF) = |\chi_1\overline{\eta}_1 \quad \chi_2\overline{\eta}_2 \quad \cdots \quad \chi_N\overline{\eta}_N| \tag{2.48}$$

where χ_i and η_i are CMOs, which are related to the UHF natural orbitals (UHF NO=UNO) φ

$$\chi_{HOMO-i} = (\cos\omega)\varphi_{HOMO-i} + (\sin\omega)\varphi_{LUMO+i} \tag{2.49}$$

$$\eta_{HOMO-i} = (\cos\omega)\varphi_{HOMO-i} - (\sin\omega)\varphi_{LUMO+i} \tag{2.50}$$

where ω is the orbital mixing parameter. The localized natural orbitals (LNO) and magnetic orbitals are defined as the corresponding MOs at the strong correlation limit ω = 45°:

$$\chi_{HOMO-i}(LNO) = \frac{(\varphi_{HOMO-i} + \varphi_{LUMO+i})}{\sqrt{2}} \tag{2.51}$$

$$\eta_{HOMO-i}(LNO) = \frac{(\varphi_{HOMO-i} - \varphi_{LUMO+i})}{\sqrt{2}} \tag{2.52}$$

The LNOs are useful for the valence-bond (VB) -like explanations of the UNO complete active space (CAS) configuration interaction (CI) wavefunctions. The natural orbital pairs (φ_{HOMO-i} , φ_{LUMO+i}) in eq.(2) usually correspond to the bonding and antibonding MOs, and these are spatially symmetry-adapted orbitals in contrast to generalized valence bond (CVB) NOs [24], which are often bonding orbitals. The occupation numbers (n_j) of these NOs are given by the orbital overlap between the corresponding orbital (χ_{HOMO-I} and η_{HOMO-i}) as

$$\eta_{HOMO-i}(UHF) = 1 + T_i \tag{2.53}$$

$$\eta_{LUMO+i}(UHF) = 1 - T_i \tag{2.54}$$

where

$$T_{ij} = \int \chi_i \eta_j dr = \delta_{ij} \tag{2.55}$$

$$T_{ii} = T_i \tag{2.56}$$

The diradical character y is defined by the weight (W_d) of the doubly excited configuration in the MCSCF theory and it is formally expressed by the orbital overlap T_i in the case of the PUHF theory:

$$y_i = 2W_d = 1 - \frac{2T_i}{1 + T_i^2} \tag{2.58}$$

The diradical characters by the PUHF method are 0 and 1 for closed-shell and pure diradical states, respectively. In this sense, the diradical character y_i means the instability of the chemical bonding. Here, the y value is called Y value in this thesis.

2.3.3 *Procedure using the information enthropy*

In recent years, there are some attempts to apply the information theory to the studies of atomic and molecular systems[24]. Ramírez et al indicated that the entropy of the system is calculated as follows;

$$I = -\sum_i n_i \ln n_i . \tag{2.59}$$

Here n_i is occupation number of occupied natural orbital. Perdew et al. examined the diradical character of H_2 using the information entropy[25].

In the case of hydrogen molecule, n_i of σ orbital calculated by UHF is 2 in region I, so I indicates the minimum value. While n_i decreases to 1 in region III and I indicates maximum value,

zero. Thus, this formulation means a stability of the system. To gain a consistent results with other indices by Takatsuka and Yamaguchi, the author improved eq.(2.59) as follows[21];

$$I' = \sum_{i}^{k}\left(1 - \frac{n_i \ln n_i}{2\ln 2}\right) \tag{2.60}$$

where k is a number of magnetic orbitals. The normalized information entropy, I', indicates zero in the region I and the number of magnetic orbitals in fully dissociated region.

2.3.4. Effective bond order

To assess this instability (diradical character), effective bond order[61] for orbital i (b_i) were also used in this thesis as follows,

$$b_i = \frac{n_i - n_i^*}{2} \tag{2.61}$$

where n_i and n_i^* were occupation number of bonding and anti-bonding orbital, respectively. b_i indicates 1.0 where a bond is stable, while b_i indicates zero where a bond is broken down and spins are localized at metal sites.

2.6 Calculations and Results

2.6.1 Computational Details

To elucidate the character of hybrid DFT, the author examined model structures of H_2 (**1**), methylradical dimer (**2**), triplet methylene dimer (**3**) and Cr(II) dimer (**4**) as illustrated in Figure 2.2. The total energies and the spin angular momentums of the lowest-spin and highest-spin states of these radical clusters are calculated by UHF, UDFT, hybrid UDFT and post Hartree-Fock methods using eq.2.38. All calculations except for Cr(II) dimer are carried out by using 6-31G** basis set. MIDI+diffuse [533(21)/53(21)/(41)1] basis set[63] with Hay's diffuse function[64] is used for Cr(II) atom. The present computations were carried out using Gaussian 98[65].

2.6.2. Hydrogen molecule

At first, the author examined a hydrogen molecule. Figure 2.3(a) illustrates the potential curves of RHF and UHF. The curves of RHF and UHF bifurcate at about 1.2-1.3Å and RHF curve becomes unstable at a longer distance than the bifurcation point. On the other hand, UHF curve could express dissociation of H_2 successfully. Because RHF do not take non-dynamical correlation into account and UHF approximate it by DODS. Figure 2.3(b) illustrates the potential curves of RBLYP, UBLYP. Similar to HF, RBLYP could not reproduce the dissociation of H_2 while UBLYP could. From this result, E_{XC} of BLYP i.e. Slater's exchange functional, Becke's exchange functional, VWN correlation functional and LYP correlation functional did not express the non-dynamical correlation well. So, BS approach is necessary to express diradical species by single Slater determinant if DFT is used. Figure 2.4(a) illustrates the correlation energy defined as

$$E_C = E(\text{Full CI}) - E(\text{X})$$

where X is calculation method. High spin state (HS) and low spin state (LS) of UHF and UBLYP were depicted in Figure 2.4(a). One can easily finds that there are two different types of electron correlations exist on H_2 dissociation process because E_C suddenly decreases at a longer distance than bifurcation point. E_c of HS state is small in almost all region and it could be negligible in comparison with LS state. LS curve of UBLYP has a peak at bonding region that is derived from overestimation of binding energy[1]. Both LS and HS curves of UBLYP underestimated the stability in dissociation region. This instability in dissociation region mainly comes from the SIC error, which canceled out

by subtraction such as E(HS)-E(LS) as explained before. Figure2.4(b) illustrates the effects of approximate spin-projection (AP) for LS state. E_c of APUHF suddenly decrease at the bifurcation point and it becomes almost zero. So, AP works well for non-dynamical correlation correction of UHF. To the contrary, unexpected peak around 2.1Å appeared on APUBLYP curve. Cremer reported that DFT involves non-dynamical correlation effect and he warned the double counting of non-dynamical correlation effect if one compensate for it[3]. So, AP-scheme might overestimate the non-dynamical correlation effect in case of APUBLYP.

The calculated J_{ab} between hydrogen atoms are shown in Figure 2.5. J_{ab} curves calculated by scheme 1 hybrid UDFTs are shown in Figure 2.5 (a) and scheme 2 in Figure 2.5 (b). In the figures the author found that J_{ab}(APUHF) has an uneven point around 1.2-1.3Å derived from the bifurcation of unrestricted calculation.

From the Figure 2.5, J_{ab} curves of hybrid UDFTs by scheme 2 reproduce J_{ab}(Full CI) in region III, while hybrid UDFTs by scheme 1 reproduce J_{ab}(Full CI) in region I - II by adjusting the hybrid parameter c_1 in eqs.(6) and (8). Relative energies of high-spin (HS) state and relative energies of spin projected low-spin (AP-LS) state are depicted in Figure 2.6. In the case of HS state, the author could not find significant differences between each method. On the other hand, there are large method and parameter dependencies in relative energies of AP-LS state. Similar to the case of J_{ab} values, hybrid UDFTs by scheme 2 reproduce relative energies by Full CI in region III, while hybrid UDFTs by scheme 1 reproduce in region I - II by adjusting the hybrid parameter c_i. J_{ab} values by conventional DFT methods such as APUB3LYP and APUBLYP methods correspond to J_{ab} by Full CI at region I. From those results, the author found that hybrid UDFTs by scheme 2 reproduce J_{ab} values and relative energies in region III and hybrid UDFTs by scheme 1 reproduce at region I - II by adjusting the hybrid parameter c_1. The AP-UHF potential curve for LS state exhibits a cusp near 1.2Å. While such cusp is not remarkable in the case of hybrid DFT methods, and it almost disappears for pure DFT, BLYP. It was reported that this cusp also disappeared in case of APUMP2 and other electron-correlation collection methods[19].

2.6.3. Methylradical dimer and triplet methylene dimer

The author had another attempt to examine the methylradical dimer (**2**) and triplet methylene dimer (**3**) in order to elucidate the effectiveness of hybrid DFT. These are the simplest models

consist of the pσ-pσ and pσ-pσ, pπ-pπ interactions, respectively. In these models, the author varied the intermolecular distance from 3Å to 5Å in order to elucidate magnetic interactions between radicals. These relatively longer intermolecular distances are considered to be classified in region III in figure 2.1.

The J_{ab} curves of methyl radical dimer are shown in Figure 2.7. J_{ab} curves of hybrid UDFT by scheme 2 reproduces J_{ab}(APUCCSD(T)) by adjusting the hybrid parameter c_1, while the hybrid UDFT by scheme 1 does not reproduce J_{ab}(APUCCSD(T)) well. Within the intermolecular distance from 3Å to 5Å, conventional UDFT methods overestimated J_{ab} values. Relative energies that were determined as 2E(•CH_3)-E($_3$HC:CH_3), of HS state and AP-LS state of methylradical dimer are depicted in Figure 2.8. The author found small energy differences between UCCSD(T) and UDFTs and small parameter dependencies in the calculated HS state. In AP-LS state, parameter dependencies were significantly larger than HS's one. And the author found that relative energies of AP-LS states by UCCSD(T) were reproduced by scheme 2 hybrid UDFT adjusting the hybrid parameter c_1. This result is consistent with hydrogen's one in region III.

The lowest- and highest-spin states of triplet methylene dimer (**3**) are singlet and quinted, respectively. Total energies and total spin angular momentums of both spin states were also calculated by UHF, hybrid UDFT and UDFT methods. The J_{ab} values were calculated using these calculated results according to eq.2.38. J_{ab} curves of **3** are shown in Figure 2.9. The hybrid UDFT by scheme 2 reproduce J_{ab}(APUCCSD(T)) by adjusting the hybrid parameter c_1 similar to a hydrogen molecule and a methyl radical dimer. This results supported that scheme 2 was effective for region III. The calculated results of relative energies were depicted in Figure 2.9. The AP-LS state were also reproduced by scheme 2 hybrid UDFT. The results of **3** were similar to those of methylradical dimer.

2.6.4. Cr(II) dimer

Finally, the author attempted to examine more complicated system; Cr(II) dimer model (**4**). This model has three different types of interactions; dσ-dσ, dπ-dπ and dδ-dδ. In particular, it is known that dδ-electrons are almost localized on the Cr(II) atoms because of strong electron-correlation. In this model, the author varied the intermolecular distance from 3Å to 5Å that were also considered to be classified in region III. The total spin angular momentums of the lowest-spin (LS)

and the highest-spin (HS) states of 4 are S=0 and S=4, respectively. Total energies and total spin angular momentums of both the LS and HS states are calculated by UHF, UDFT, hybrid UDFT and UCCSD(T). The orbital averaged Jab were obtained using them. The Jab values of Cr(II) dimer are shown in Figure 2.11(a) and (b). Similar to other models, Jab values of hybrid UDFT by scheme 2 reproduced J_{ab}(APUCCSD(T)) values by adjusting the parameter c_1.

2.6.5 *Instabilities*

The author have shown that the calculated Jab values by UCCSD(T) and CI methods are reproduced with hybrid UDFT method by adjusting the ratio of HF exchange. However, it is necessary to make a guiding principle to determine the hybrid parameter for the practical use. Therefore, the author next focused on the relation between the instability of the chemical bonding of magnetic orbitals and hybrid parameter.

As mentioned before, this hybrid DFT method aimed to correct dynamical correlation effect presuming that non-dynamical correlation effect was approximated by unrestricted calculation with spin-projection. The non-dynamical correlation effect is system specific[3]. However if one can obtain some universal indices for the degree of non-dynamical, it will be effectual for the estimation of hybrid parameter. Figure 2.13 (a) is depicting the T, Y, I' and b values. From the picture, b value is closely related to I' value. This was described in the reference[50]. Figure 2.13(b) is depicting the T, Y, I' values in comparison with E_c(UHF) and E_c(APUHF) of hydrogen molecule, where

$$E_c(\mathrm{UHF}) = E(\text{Full CI}) - E(\mathrm{UHF})$$

$$E_c(\mathrm{APUHF}) = E(\text{Full CI}) - E(\mathrm{APUHF}).$$

From this figure, it is found that the indices and E_c were mutually correlated, especially E_c(APUHF). Figure 2.13 (b) is depicting the relation between the chemical indices and ΔJ_{ab}. The relation is similar to one of Ec(APUHF) and the chemical indices. From these results, the author concluded that instability of magnetic orbitals reflected the degree of non-dynamical correlation effect well, and instability values were effective to estimate the hybrid parameter.

Table 3.2 is summarizing the instability values (I') of UHF at the crossing points of J_{ab} curves by scheme 2 and a J_{ab} curve by UCCSD(T) or Full CI methods. For the simplification, instability values were expressed by percentage derived as I'/N where N was a number of magnetic orbitals. They showed similar values except for hydrogen model. The relation between the instability values

and hybrid parameters of scheme 2 was depicted in Figure 2.13. From the figure, the author found that hybrid parameters were in proportion to the instability value. It seems that the hybrid parameters could be determined by the information entropy analysis of the UHF solution. Further investigations, however, are needed about this problem.

Discussion and concluding remarks of chapter two

The hybrid UDFT could reproduce the J_{ab} values calculated by post-HF methods by adjusting the ratio of Hartree-Fock exchange. Especially, the hybrid UDFT by scheme 2 reproduced the J_{ab} values well by post-HF methods in region III. The present results clearly indicated that the hybrid DFT methods in scheme 2 were applicable to computations of J_{ab} values for magnetic clusters of both organic radical and transition metal ion with spins, leading to a possibility of the magnetic effective density functional (MEDF) methods. Through-space magnetic interactions between radical species that treated here were mainly classified region III. Actually, experimental J_{ab} values of through-space interactions between organic radicals are very small, therefore they are classified in region III. The hybrid UDFT by scheme 2 is one of the very powerful and reliable approaches to investigations of J_{ab} for those systems. In this sense, the scheme 2 could be referred to as a magnetic effective density functional (MEDF) approach. In addition to J_{ab} values, it is also interesting that the hybrid UDFT of scheme 2 reproduce the energies of spin projected low-spin state in region III. While, there are many interesting phenomena in region II such as magnetism, superconductivity and so on. Up to now, it has been a very difficult task to approach them theoretically. In this study, the author applied the hybrid UDFT by scheme 1 to the calculation of J_{ab} for the radical species in this region. Here, the author only calculated the lowest- and highest-spin states assuming the non-dynamical correlation effect was included in unrestricted calculation. In comparison with the conventional DFTs, the hybrid UDFT by scheme 1 reproduced the J_{ab} and the relative energies of spin projected low-spin state for H_2 in region I - II by adjusting the hybrid parameter c_i. However higher order approximations such as general spin orbitals (GSO) CAS-DFT or DFT natural orbital (DNO) CI methods are surely necessary to discuss the details about LS states around a bifurcation point *i.e.* region II. The CAS-DFT and DNO-CI methods are also useful for investigations of low-lying exited states.

The hybrid parameter was closely related to the instability of the system. An appropriate scheme and parameter c_i could be selected by estimating the instabilities of the systems on the basis of the information entropy defined by the occupation numbers of UHF natural orbital (UNO) or DNO. The procedure was illustrated as shown Figure 2.14. Thus the author could construct the magnetic effective density functional (MEDF) scheme for magnetic clusters in region II-III, where conventional DFT methods had some problems to solve. The MEDF method is applicable to large-sized molecular

magnetic materials for practical use nevertheless a simple approximation, for which the post-HF methods such as UCCSD(T) and CASPT2 are hardly applicable.

The meaning and merit of the hybrid DFT method together with spin-projection is explained as follows. As mentioned before, there are two types of electron-correlations. In case of magnetic measurements, non-dynamical correlation effect by valence electrons is important. The dynamical correlation effect of inner electrons, however, is not negligible as illustrated in Figure 2.15. If one focuses on inner electrons that dominate total energy, one has to use conventional DFT methods that have succeeded closed shell systems. The spin-projection scheme uses the 'energy difference' between low-spin state and high-spin state. The dynamical correlation effect of inner electrons of low-spin state should be similar to one of high-spin state because the difference of shapes of inner MOs between high-spin state and low-spin state are small. The dynamical correlation effect of inner electrons is approximately canceled out by the subtraction (E(LS)-E(HS)). Therefore we can focus on the electron-correlation effect of 'valence electrons'. The MEDF correct dynamical correlation effect by DFT terms under approximation that non-dynamical correlation effect is corrected by BS scheme with spin-projection on valence elections. As a consequence, MEDF means the correction for low-spin state, because E_c of valence electrons on high-spin state is small.

This subtraction is effective to the SIC problems in inner electrons in same strategy. Furthermore, approximated spin-projection scheme, which removes spin-contamination, can make more accurate approximation to non-dynamical correlation of unrestricted methods. Hybrid parameter is expressing the dynamical correlation of valence electrons for low-spin state.

References of chapter two

[1] Parr, R. G.; Yang, W. In Density Functional Theory of Atoms and Molecules (Oxford, New York, 1989),

[2] Nagy,Á. *Physics Reports* **1998**, *298*, 1.

[3] Cremer, D. *Mol. Phys.* **2001**, *99*, 1899.

[4] Cotton, F. A.; Cowley, A. H.; Feng, X. J. *J. Am. Chem. Soc.* **1998**, *120*, 1795.

[5] Ruiz, E.; de Graaf, C.; Alemany, P.; Alvarez, S. *J. Phys. Chem.* **2002**, *106*, 4938.

[6] Kitagawa, Y.; Nakano, S.; Kawakami, T.; Mashima, K.; Tani, K.; Yamaguchi, K. *Mol. Cryst. Liq. Cryst.* **2002**, *379*, 525

[7] Kitagawa, Y.; Kawakami, T.; Yoshioka, Y.; Yamaguchi, K. *Polyhedron* **2001**, *20*, 1189.

[8] Soda, T.; Kitagawa, Y.; Onishi, T.; Takano, Y.; Shigeta, Y.; Nagao, H.; Yoshioka, Y.; Yamaguchi, K., *Chem. Phys. Lett.* **2000**, *319*, 223.

[9] Mitani, M.; Takano, Y.; Yoshioka, Y.; Yamaguchi, K. *J. Chem. Phys.* **1999**, *111*, 1309.

[10] Mitani, M.; Yamaki, D.; Takano, Y.; Kitagawa, Y.; Yoshioka, Y.; Yamaguchi, K. *J. Chem. Phys.* **2000**, *113*, 10486.

[11] Sato, F.; Yoshihiro, T.; Era, M.; Kashiwagi, H. *Chem. Phys. Lett.* **2001**, *341*, 645.

[12] Slater, J. C. In *Quantum Theory of melecular and Solids. Vol.4: The Self-Consistent Field for Molecular and Solids* (McGraw-Hill, New York, 1974)

[13] Becke,A.D.,1988,*Phys.Rev.A.*,**38**,3098

[14] Perdew, J. P.; Wang, Y. Phys. Rev. B, 1992, 45, 13244.

[15] Perdew, J. P. In *Electronic Structure of Solids '91* p.11(Akademie-Verlag, Berlin, 1991).

[16] Vosko, S. H. ; Wilk, L.; Nusair, M. *Can. J. Phys.* **1980**, *58*, 1200

[17] Lee, C.; Yang, W.; Parr, R. G. *Phys. Rev. B*, **1988**, *37*, 785.

[18] Becke, A. D. *J. Chem. Phys.* **1993**, *98*, 5648.

[19] Yamanaka, S.; Kawakami, T.; Nagao, H.; Yamaguchi, K. *Chem. Phys. Lett.* **1994**, *231*, 25.

[20] Kitagawa, Y.; Soda, T.; Shigeta, Y.; Yamanaka, S.; Yoshioka, Y.; Yamaguchi, K. *Int. J. Quant. Chem.* **2001**, *84*, 592.

[21] Kitagawa. Y.; Kawakami, T.; Yamaguchi K. *Mol. Phys.* **2002**, *100*, 1829.

[22] Takatsuka,K.,Fueno,T.,Yamaguchi,K., 1978,*Theoret.Chem.Acta*, **48**,175

[23] Yamaguchi,K.,Okumura,M.,Takada,K.,Yamanaka,S.,1993,*Int.J.Quant.Chem. Quant.Chem.Symp.*, **27**,501

[24] Ramílez,J.C.,Rodolfo,C.S.,Esquivel,O.,Sagar,R.P., 1997,*Phys.Rev.A.*,**56**,4477.

[25] Gersdorf, P.; John, W.; Perdew, J. P.; Ziesche, P. Int. J. Quant. Chem. 1997, 61, 935.

[26] Smith, G. T.; Schmider, H. L.; Smith Jr, V. H. *Phys. Rev. A.* **2002**, *65*, 032508.

[27] Kawakami, T.; Yamanaka, S.; Mori, W.; Yamaguchi. K. In *Molecular Based Magnetic Materials*, p30 (ACS Symposium Series 664, American Chemical Society, Washington, DC, 1995).

[28] Gatteschi, D.; Kahn, O.; Miller, J. S.; Palacio, F. Eds. *Magnetic Molecular Materials*; Kluwer

Academic Publishers: Dordrecht, 1991.

[29] Kahn, O., Ed. *Magnetism: A Supermolecular Function*; NATO ASI Series C, Vol 484,; Kluwer Academic Publishers: Dordrecht, 1996.

[30] Coronado, E., Dekhais, P., Gatteschi, D., Miller, J. S., Eds. *Molecular Magnetism: From Molecular Assemblies to the Devices*; NATO ASI Series E, Vol. 321; Kluwer Academic Publishers: Dordrecht, 1996.

[31] Kohn, W.; Sham, L. D. *Phys. Rev. A*, **1965**, *140*, 1133

[32] Pople, J. A.; Gill, P. M. W.; Johnson, B, G. *Chem. Phys. Lett.* **1992**, *199*, 557

[33] Becke, A. D. *J. Chem. Phys.* **1993**, *98*, 1372

[34] Adamo, C.; Barone, V. Chem. Phys. Lett. 1997, 274, 242.

[35] Burke, K.; Ernzerhof, M.; Perdew, J. P. Chem. Phys. Lett. 1997, 265, 115.

[36] Barone, V. *J. Chem. Phys.* **1994**, *101*, 6834

[37] Barone, V.; Adamo, C. *Chem. Phys. Lett.* **1994**, *224*, 432

[38] Baker, J.; Andzelm, J.; Muir, M.; Taylor, P. R. *Chem. Phys. Lett.* **1995**, *237*, 53

[39] Neumann, R.; Handy, N. C. *Chem. Phys. Lett.* **1996**, *252*, 19

[40] Leininger, T.; Stoll, H.; Werner, H-J.; Savin, A. *Chem. Phys. Lett.* **1997**, *275*, 151.

[41] Iikura, H.; Tsuneda, T.; Yanai, T.; Hirao, K. *J. Chem. Phys.* **2001**, *115*, 3540.

[42] Tao, J.; Paola, G-G.; Perdew, J. P.; McvWeeny, R. *Phys. Rev. A.* **2001**, *63*, 032513.

[43] Szabo, A.; Ostlund, N. S. In *Modern Quantum Chemistry* (Macmillan Publishing Co., Inc.)

[44] Gunnarsson, O.; Lundqvist, B. I. *Phys. Rev. B.* **1976**, *13*, 4274.

[45] Kawakami, T.; Yamanaka, S.; Takano, Y.; Yoshioka, Y.; Yamaguchi, K. *Bull. Chem. Soc. Jpn.*, **1998**, *71*, 2097.

[46] Yamaguchi, K.; Fueno, T. *Chem. Phys.* **1977**, *19* , 35

[47] Yamaguchi, K. *Chem. Phys.* **1978**, 29, 117

[48] Perdew, J. P.; Savin, A.; Burke, K. *Phys. Rev. A.* **1995**, *51*, 4531

[49] Adamson, R. D.; Gill, P. M. W.; Pople, J. A.; *Chem. Phys. Lett.* **1998**, *284*, 6

[50] Yamaguchi,K.; Kawakami, T.; Takano, Y.; Kitagawa, Y.; Yamashita, Y.; Fujita, H. *Int.J.Quant.Chem.* 2002, 90, 370

[51] Yamaguchi, K. In *Self-Consistent Field, Theory and Applications*; Carbeó, R.; Klobukowski, M. Eds.; Studies in physical and theoretical chemistry 70; Elsevier: Amsterdam-Oxford-New Tork-Tokyo, 1990; p727.

[52] Nagao, H.; Nishino, M.; Shigeta, Y.; Soda, T.; Kitagawa, Y.; Onishi, T.; Yoshioka, Y.; Yamaguchi, K. *Coord. Chem. Rev.* **2000**, *198*, 265.

[53] Ginsberg, A. P. *J. Am. Chem. Soc.* **1980**, *102*, 111,

[54] Noodleman, L. *J. Chem. Phys.* **1981**, *74*, 5737,

[55] Noodleman, L.; Davidson, E. R. *Chem. Phys.* **1985**, *109*, 131

[56] Bencini, A.; Totti, F.; Daul, C. A.; Doclo, K.; Fantucci, P.; Barone, V. *Inorg. Chem.* **1997**, *36* 5022,

[57] Ruiz, E.; Cano, J.; Alvarez, S.; Alemany, P. *J. Comp. Chem.* **1999**, *20*, 1391

[58] Yamaguchi, K.; Okumura, M.; Mori, M.; Maki, J.; Takada, K.; Noro, T.; Tanaka, K. *Chem. Phys. Lett.* **1993**, *210*, 201 .

[59] Yamaguchi, K.; Takahara, Y.; Fueno, T. in *Applied Quantum Chemistry*; V.H. Smith et al. Eds., Reidel, Dordrecht, 1986, p155

[60] Yamanaka S. Doctor thesis, 1999

[61] Takano, Y.; Kitagawa, Y.; Onishi, T.; Yoshioka, Y.; Yamaguchi, K.; Koga N.; Iwamura, H. *J. Am. Chem. Soc.* **2002**, *124*, 450.

[62] Staroverov, V. N.; Davidson, E. R. *ChemPhys.Lett.* **2000**, *330*, 161

[63] Tatewaki, H.; Huzinaga, S. 1979,*J.ChemPhys.*,**71**,4339

[64] Hay, P.J. *J. Chem. Phys.* **1977**, *66*, 4377.

[65] Gaussian 98, Frisch,M,J., Trucks,G.W., Schlegel,H.B., Scuseria,G.E., Robb,M.A., Cheeseman,J.R., Zakrzewski,V.G., Montgomery,J.A.,Jr., Stratmann,R.E., Burant,J.C., Dapprich,S., Millam,J.M., Daniels,A.D., Kudin,K.N., Strain,M.C., Farkas,O., Tomasi,J., Barone,V., Cossi,M., Cammi,R., Mennucci,B., Pomelli,C., Adamo,C., Clifford,S., Ochterski,J., Petersson,G.A., Ayala,P.Y., Cui,Q., Morokuma,K., Malick,D.K., Rabuck,A.D., Raghavachari,K., Foresman,J.B., Cioslowski,J., Ortiz,J.V., Stefanov,B.B., Liu,G., Liashenko,A., Piskorz,P., Komaromi,I., Gomperts,R., Martin,R.L., Fox,D.J., Keith,T., Al-Laham,M.A., Peng,C.Y., Nanayakkara,A., Gonzalez,C., Challacombe,M., Gill,P.M.W., Johnson,B., Chen,W., Wong,M.W., Andres,J.L., Gonzalez,C., Head-Gordon,M., Replogle,E.S. and J. A. Pople, Gaussian, Inc., Pittsburgh PA, 1998.

Table 2.1

The mixing coefficients in conventional B3LYP, BLYP and HF in comparison with scheme 1 and scheme 2.

parameter sets[1]					*cf*
a_1	a_2	a_3	a_4	a_5	
0.0	1.0	1.0	1.0	1.0	UBLYP
0.2	0.8	0.72	1.00	0.81	UB3LYP
1.0	0.0	0.0	0.0	0.0	UHF
c_1	1-c_1	1-c_1	1.0	1.0	scheme 1
c_1	1-c_1	1-c_1	1-c_1	1-c_1	scheme 2

1) in eq $E_{XC} = a_1 E_X^{HF} + a_2 E_X^{Slater} + a_3 \Delta E_X^{B88} + a_4 E_C^{VWN} + a_5 \Delta E_C^{LYP}$

Table 2.2

The instability of the system (I')[1] at the crossing points of J_{ab} curves by scheme 2 and a J_{ab} curve by post HF

	c_1[2]			
model	0.5	0.6	0.7	0.8
H_2			55	65
$(CH_3)_2$	85	88	92	95
$(CH_2)_2$		91	93	96
$Cr(II)_2$	87	91	94	97

1) [%], 2) in eq. 2.20

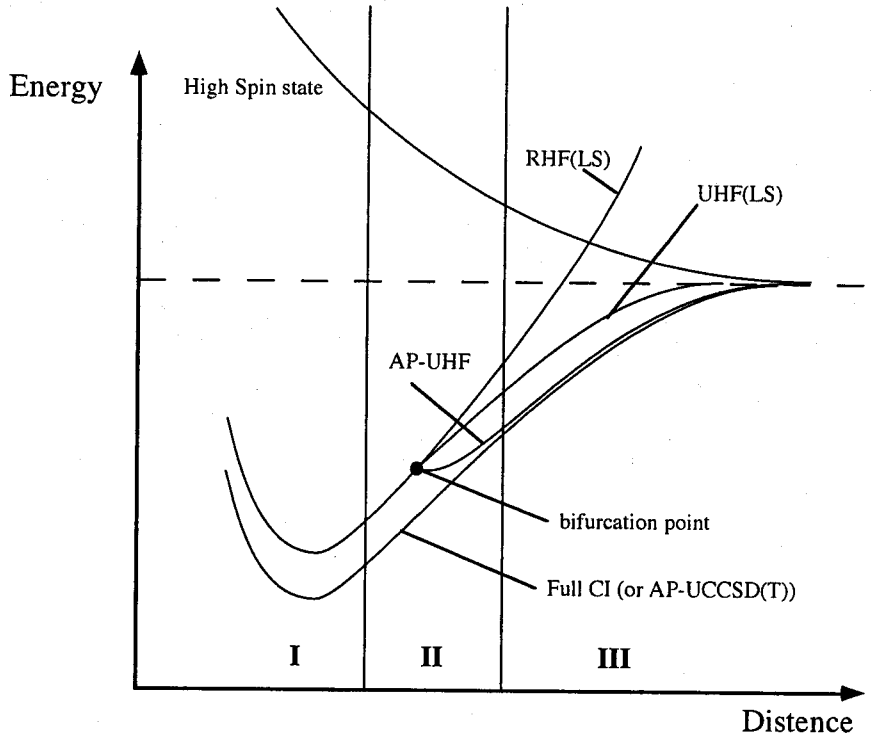

Figure 3.1

Potential curve of hydrogen molecule with variation of the interatomic distance.

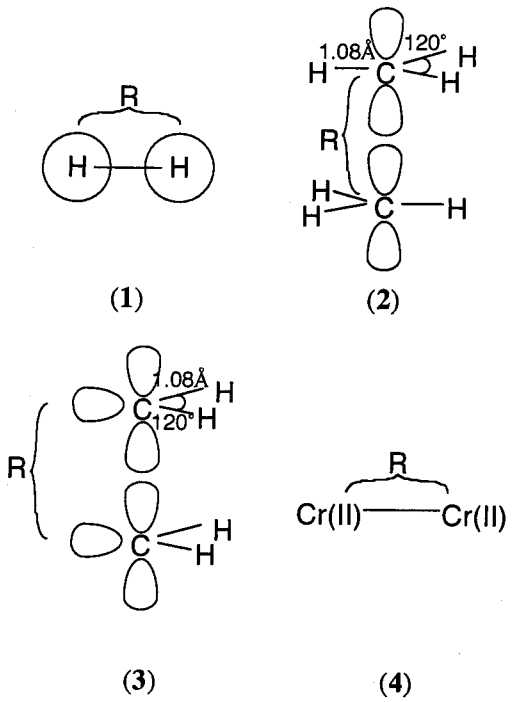

Figure 3.2

Model figures of (**1**) hydrogen molecule, (**2**) methyl radical dimer, (**3**) triplet methylene dimer and (**4**) Cr(II) dimer.

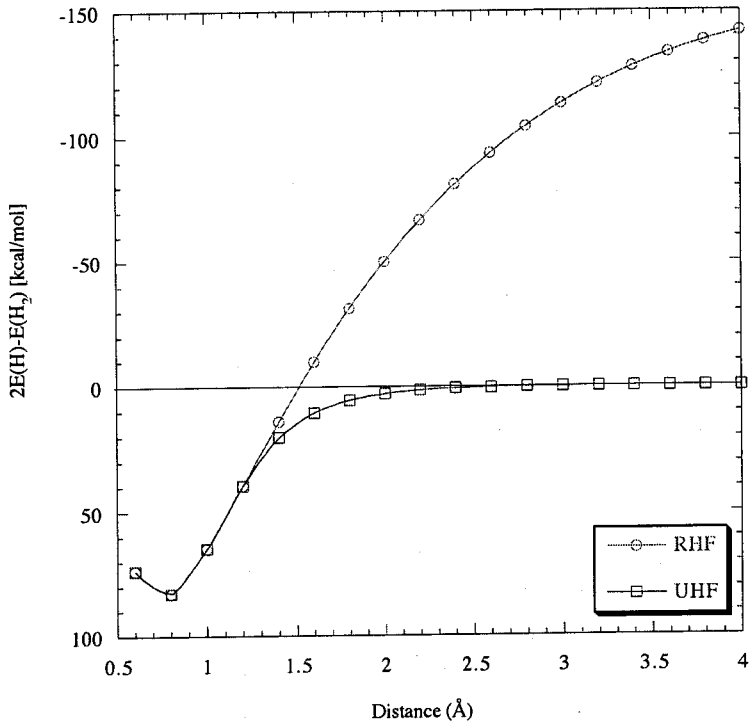

(a)

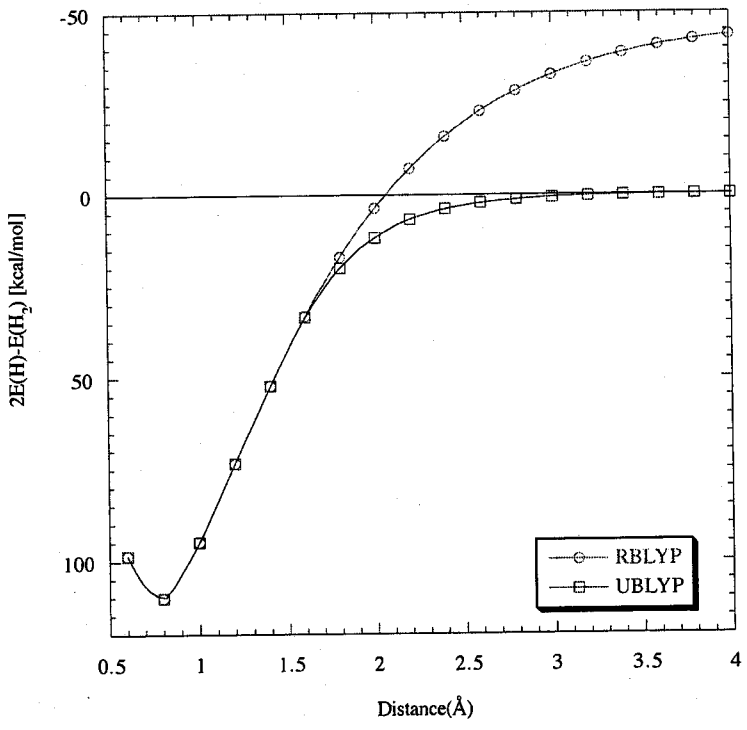

(b)

Figure 2.3 Relative energies of (a) RHF and UHF, (b) RBLYP and UBLYP.

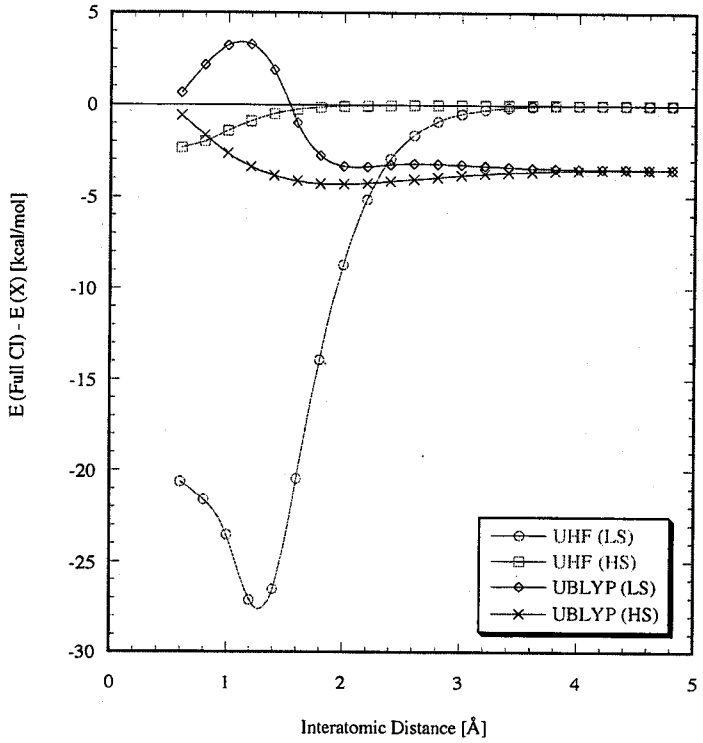

(a)

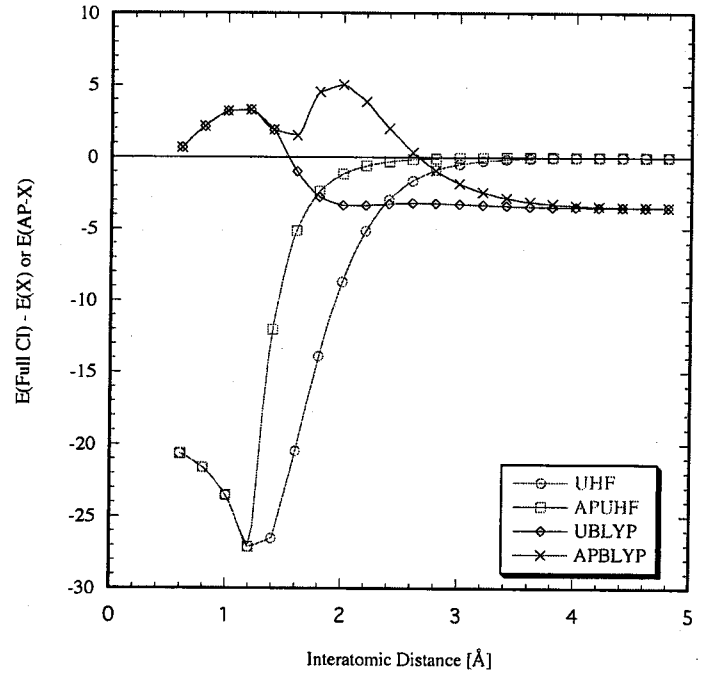

(b)

Figure 2.4

(a) E_c of low spin state and high spin state calculated by UHF and UBLYP respectively. (b) E_c of low spin state calculated by UHF, APUHF, UBLYP and APUBLYP.

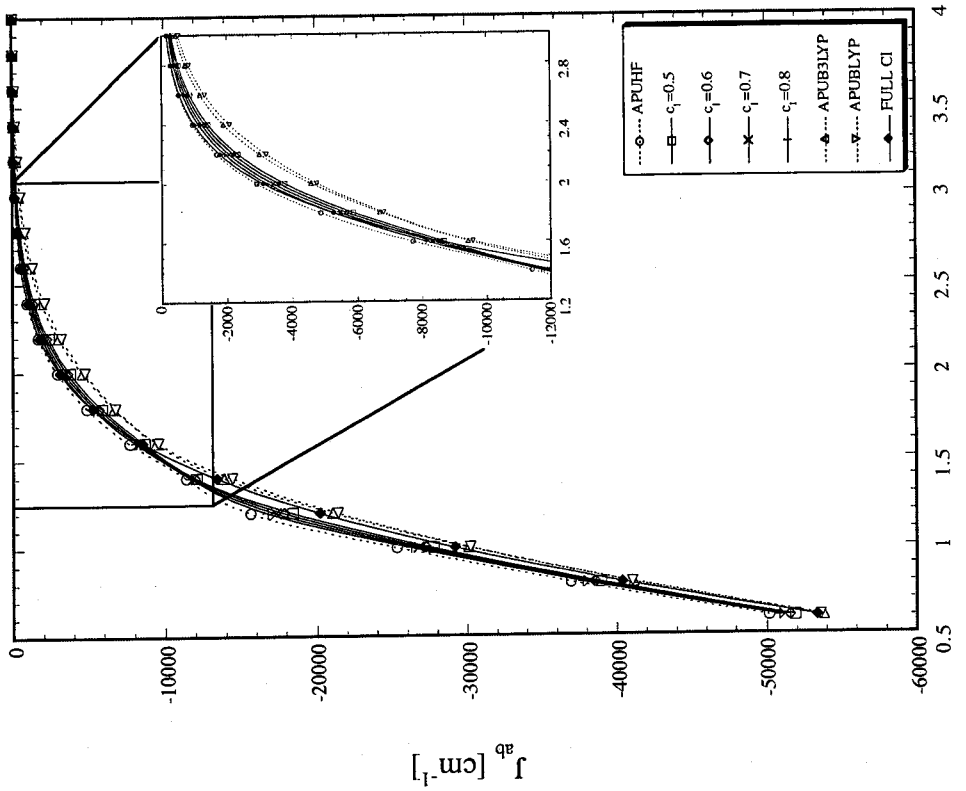

(b)

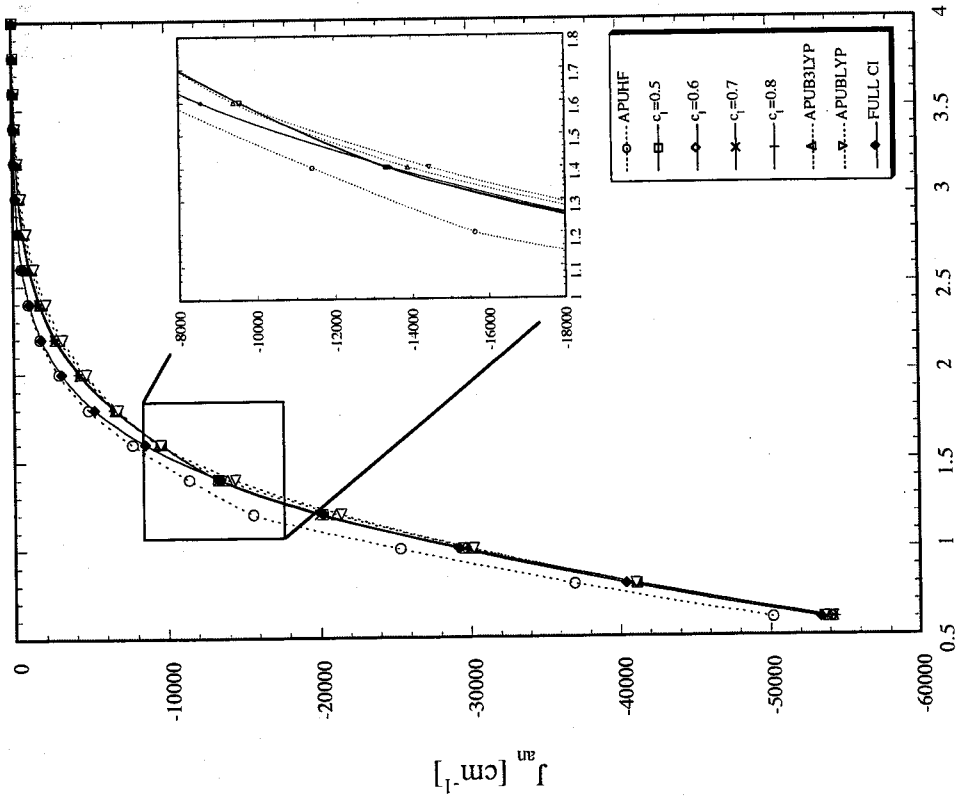

(a)

Figure 2.5 The effective exchange integrals J_{ab} between hydrogen molecule (1) calculated by (a) scheme 1 and (b) scheme 2.

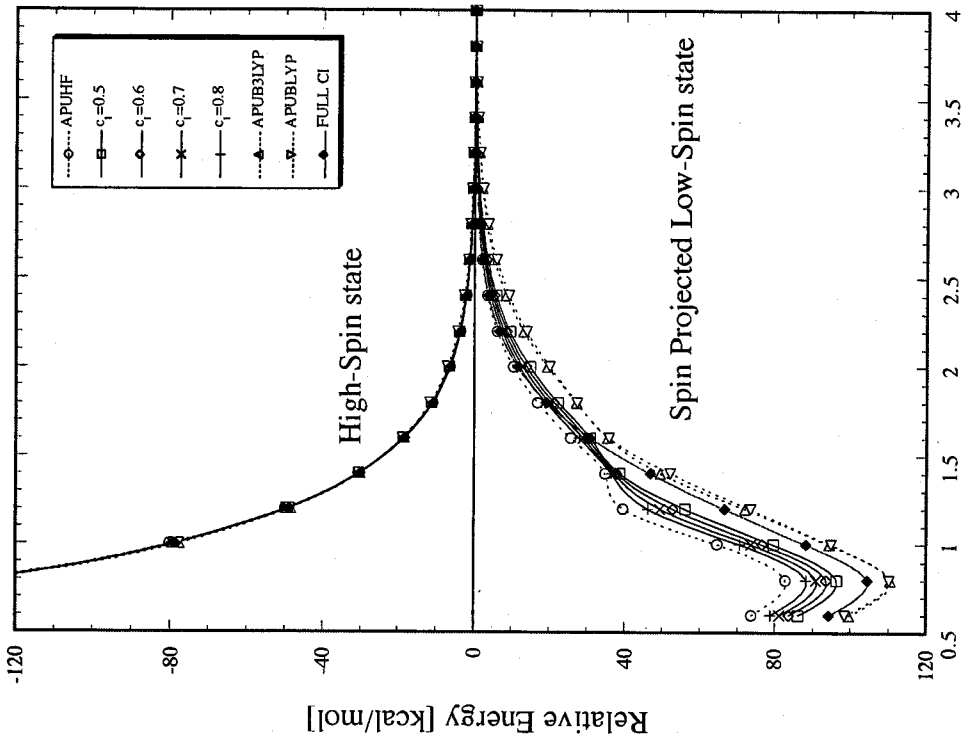

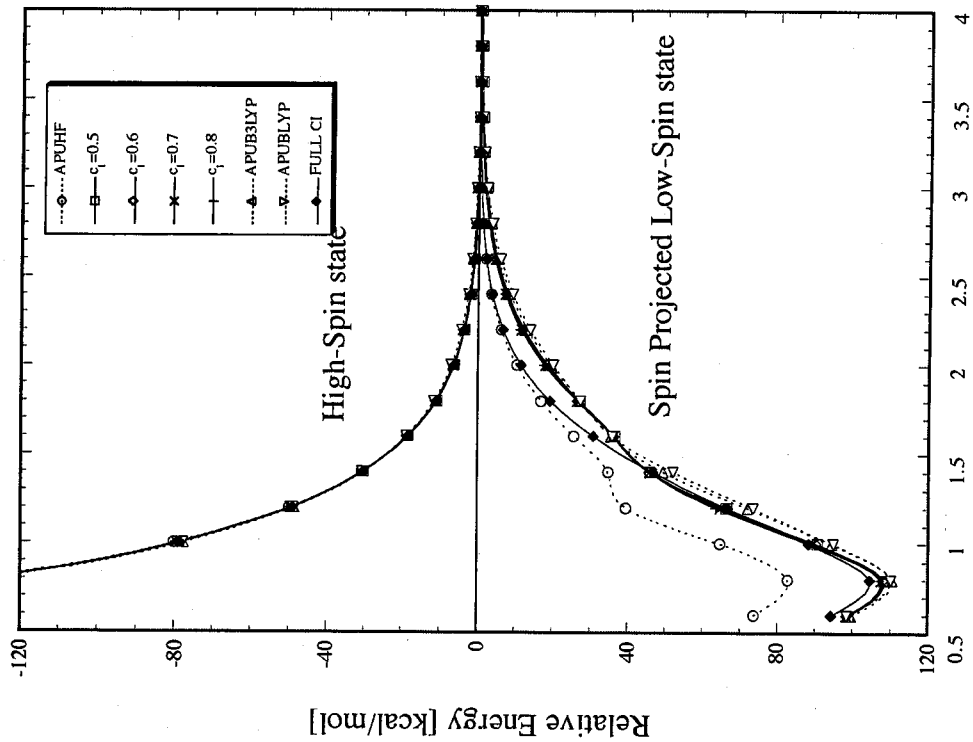

Figure 2.6 The relative energies of HS and AP-LS states of **1** calculated by (a) scheme 1 and (b) scheme 2.

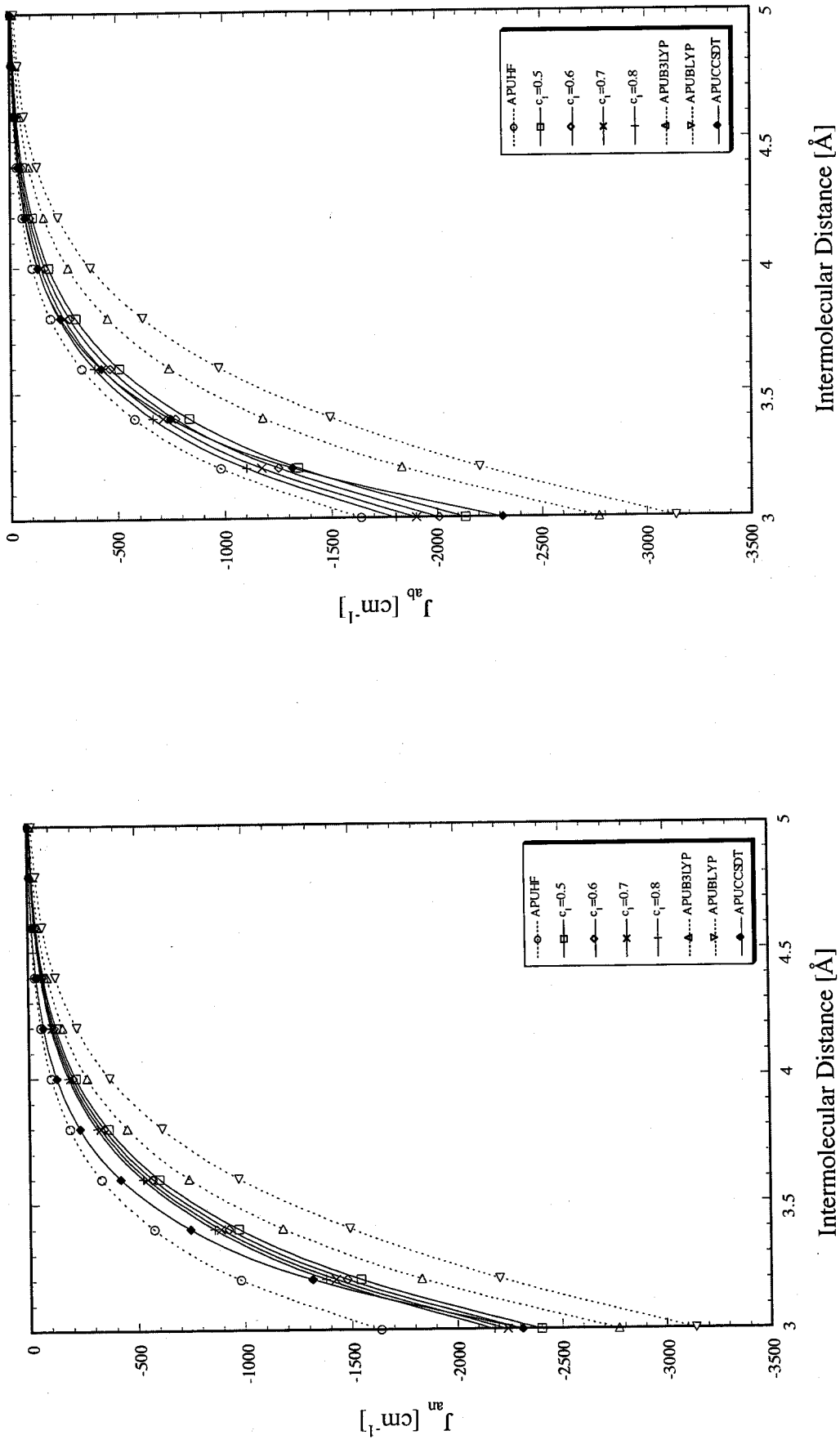

Figure 2.7 The effective exchange integrals J_{ab} between methyl radical dimer (**2**) calculated by (a) scheme 1 and (b) scheme 2.

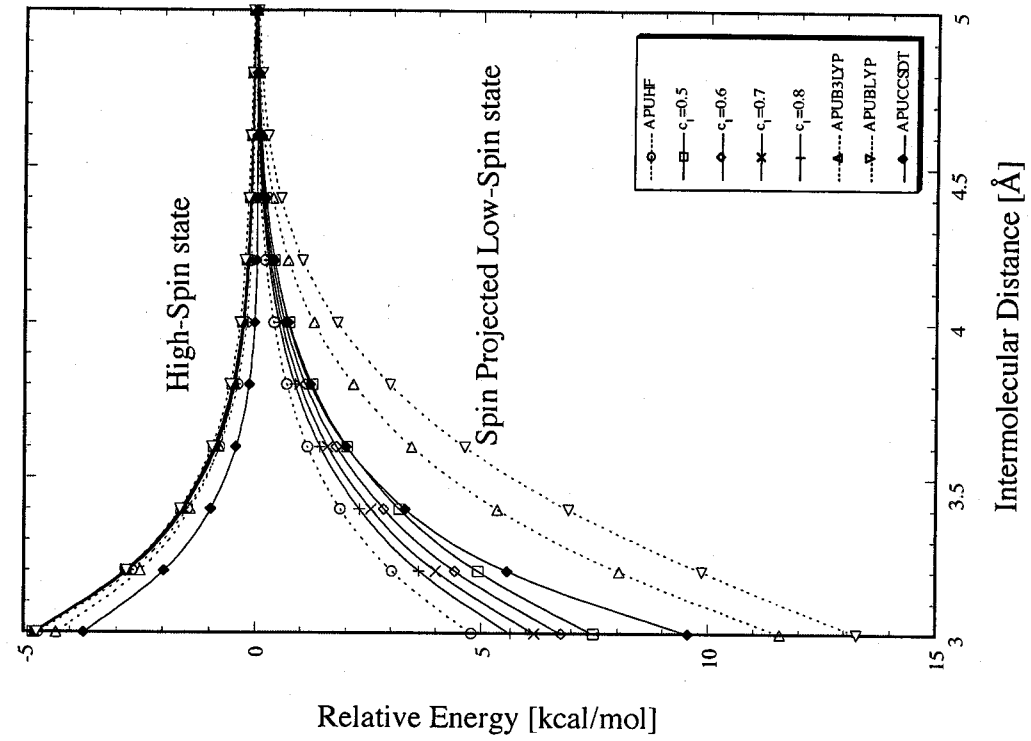

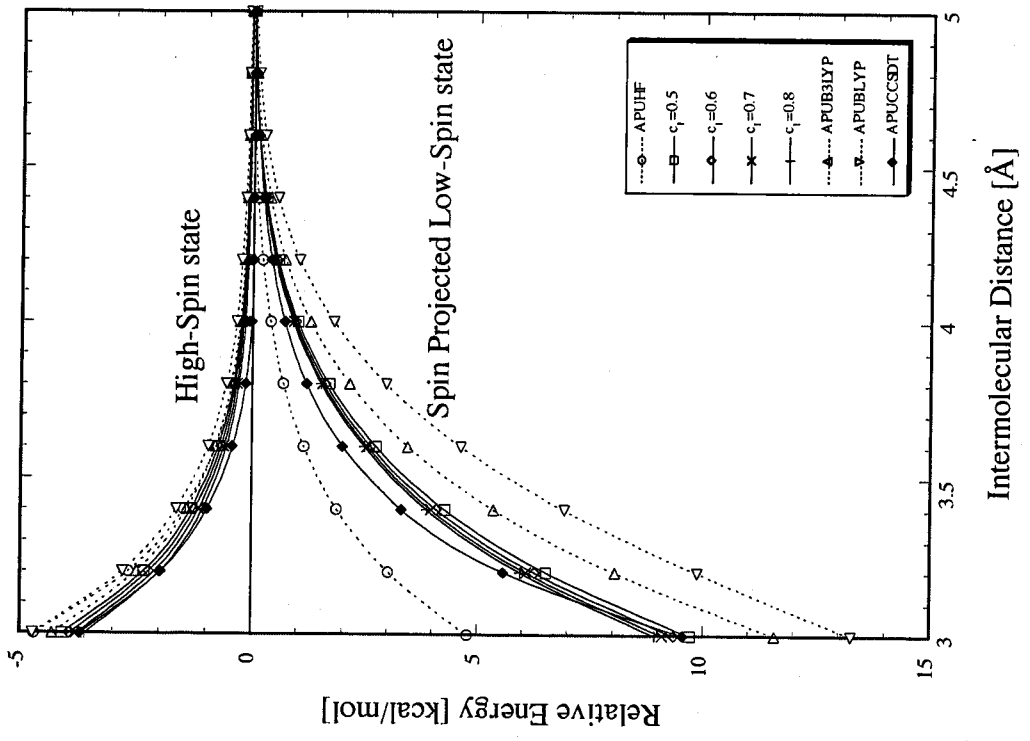

Figure2.8 The relative energies of HS and AP-LS states of **2** calculated by (a) scheme 1 and (b) scheme 2.

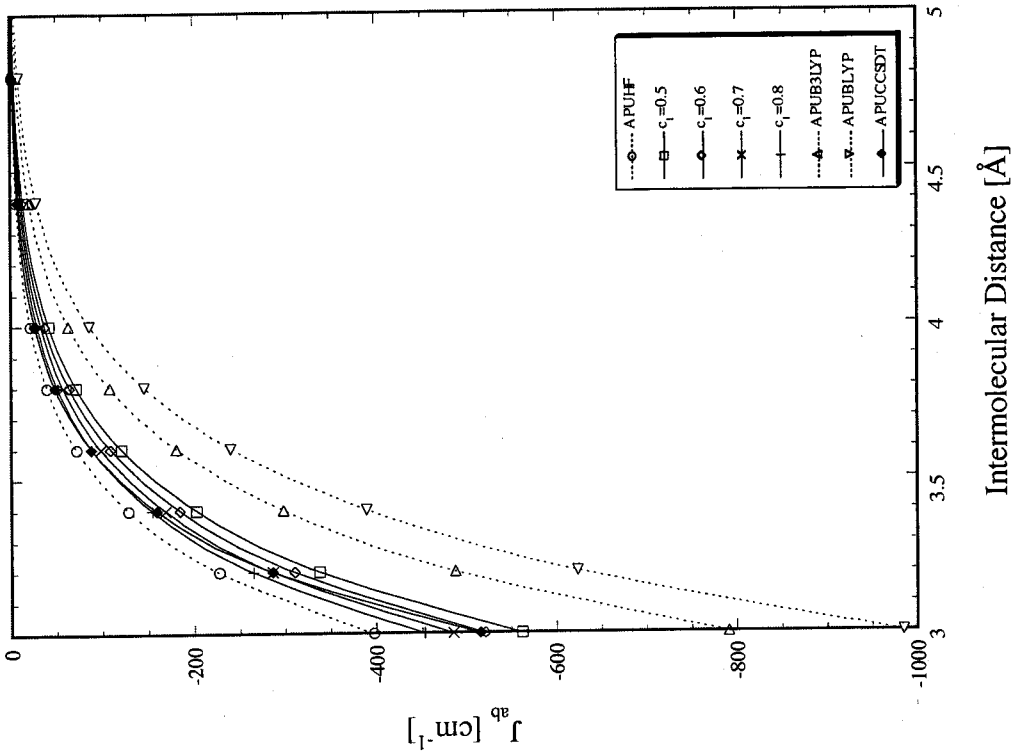

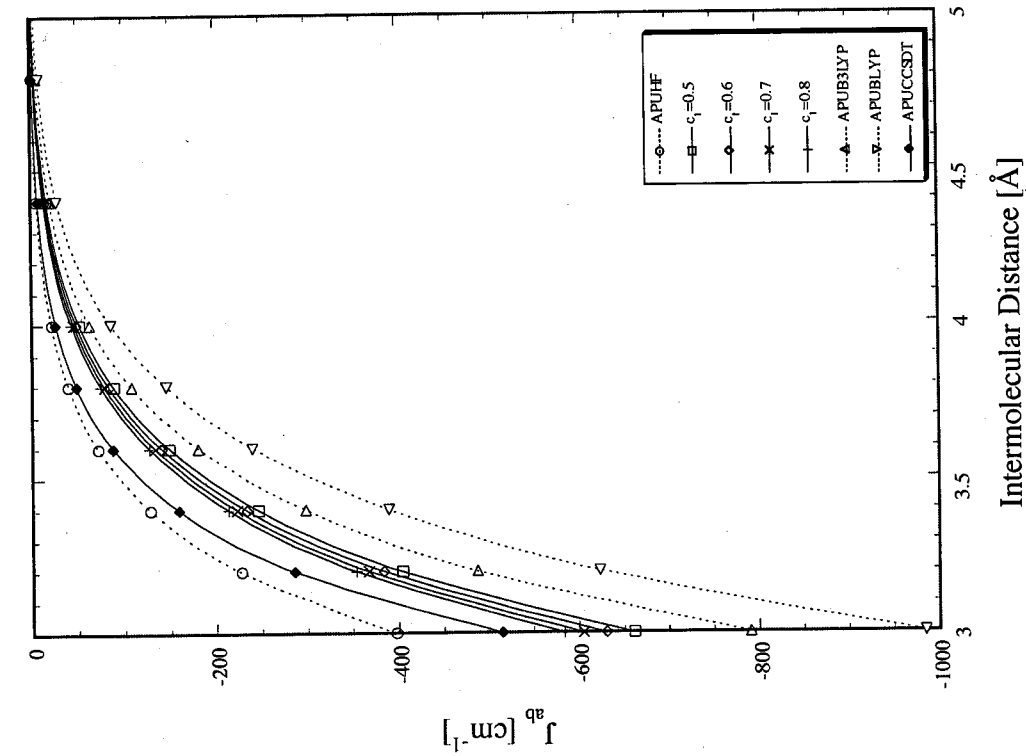

Figure 2.9 The effective exchange integrals J_{ab} between triplet methylene dimer (**3**) calculate by (a) scheme 1 and (b) scheme 2.

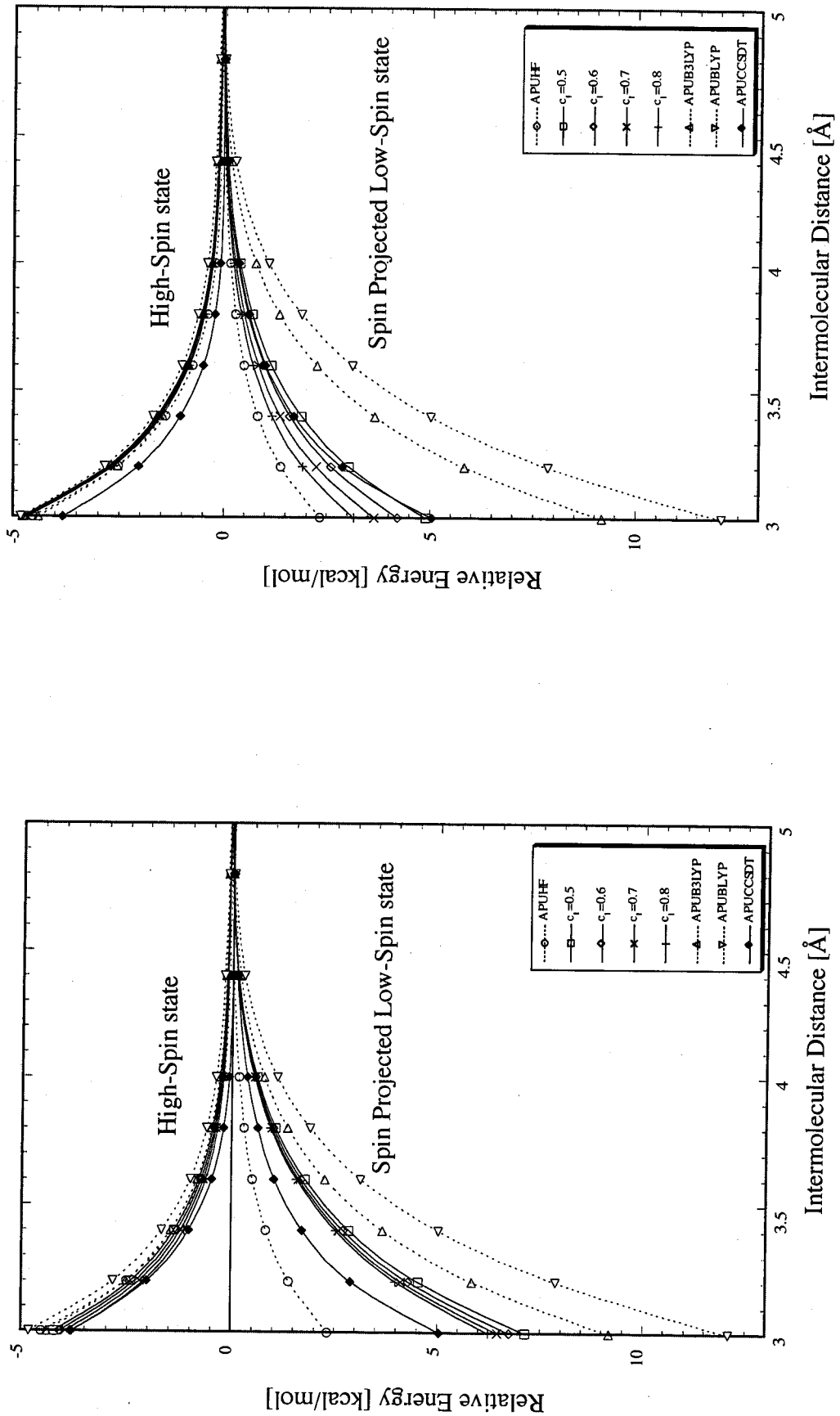

Figure 2.10 The relative energies of HS and AP-LS states of **3** calculated by (a) scheme 1 and (b) scheme 2.

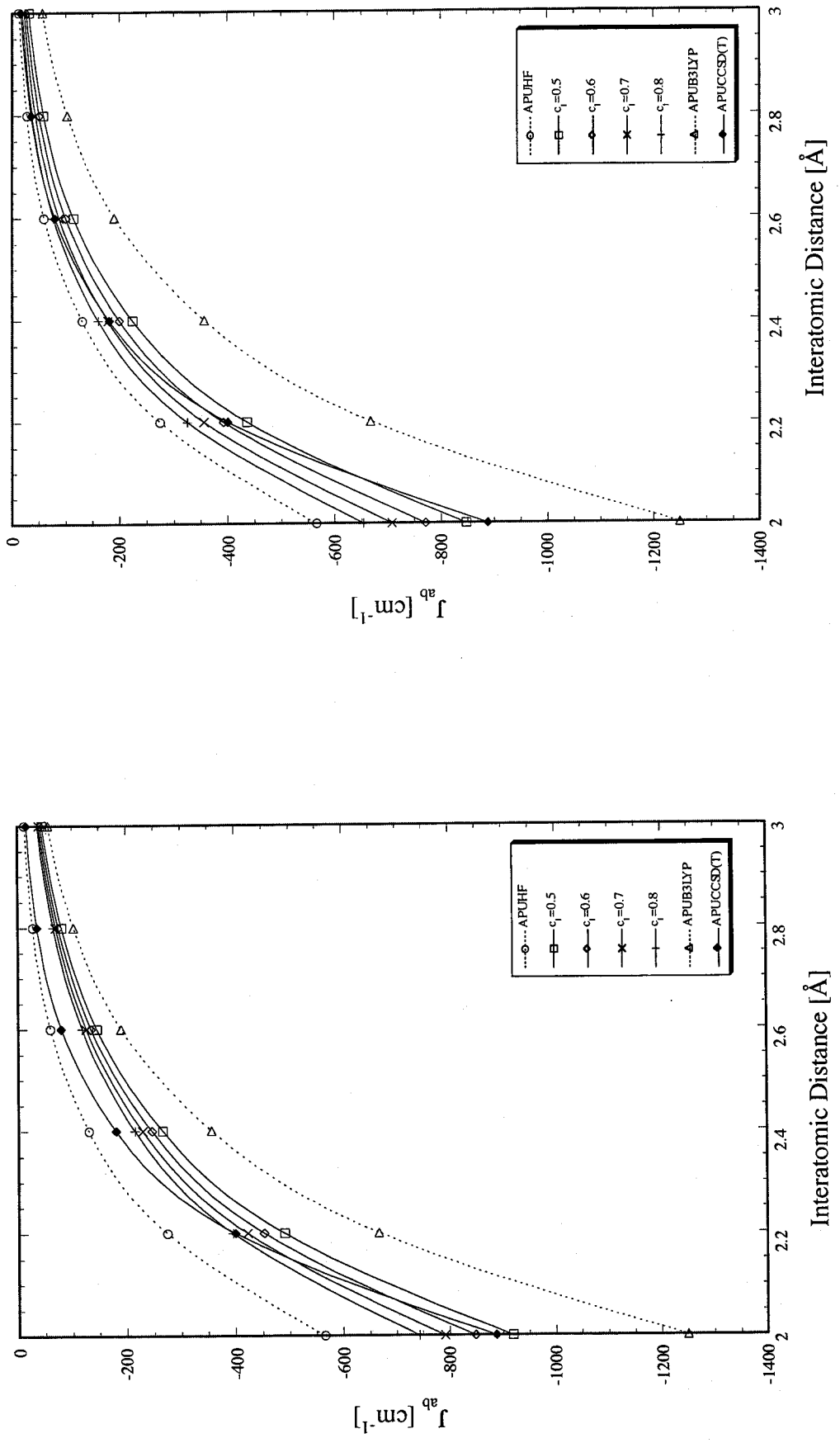

Figure 2.11 The effective exchange integrals J_{ab} between Cr(II) dimer (**4**) calculated by (a) scheme 1 (b) scheme 2.

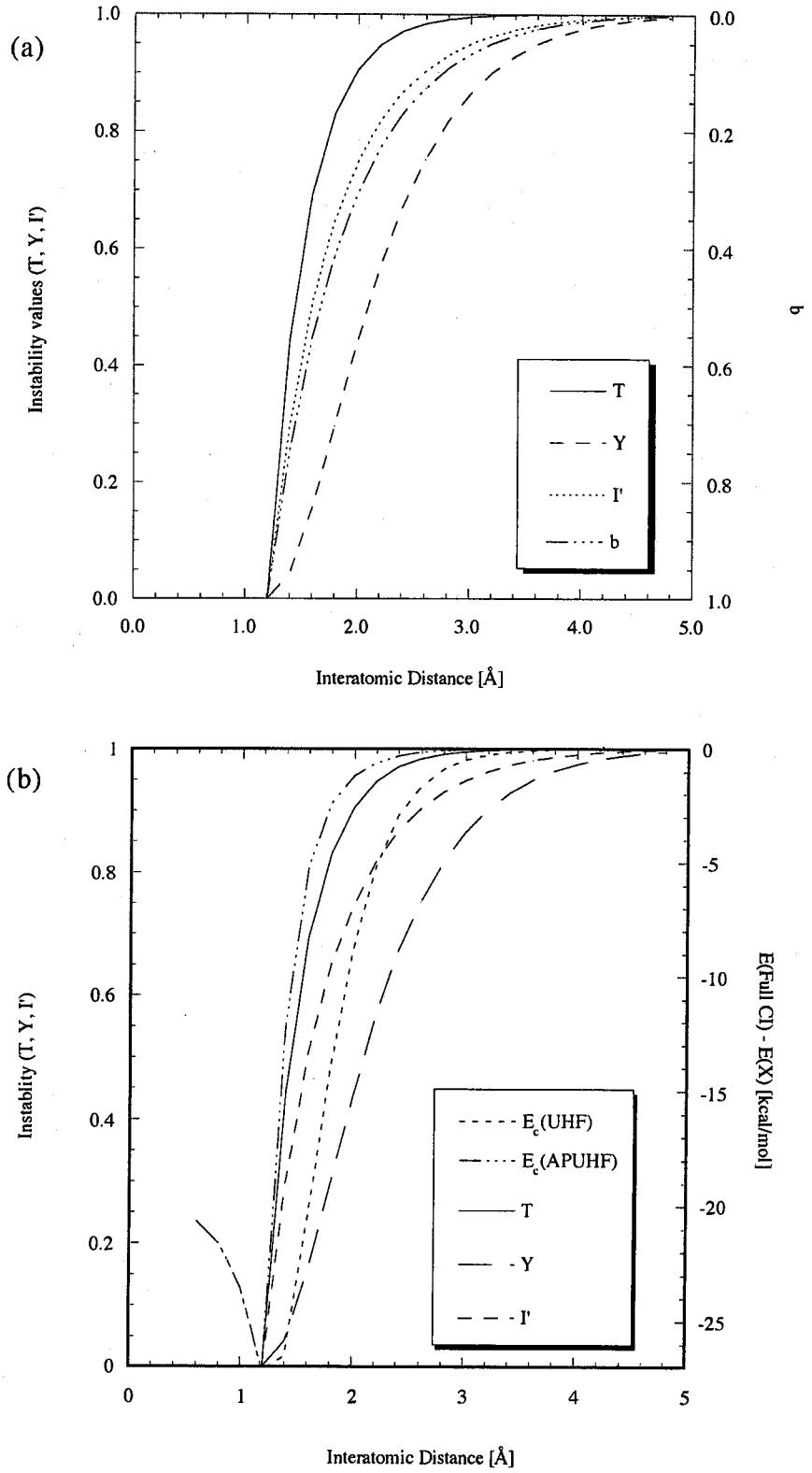

Figure 2.12 (a), (b)

(a) The relation between instability values and effective bond order and (b) the relation between instability values and E_c. Both of them are in case of hydrogen molecule.

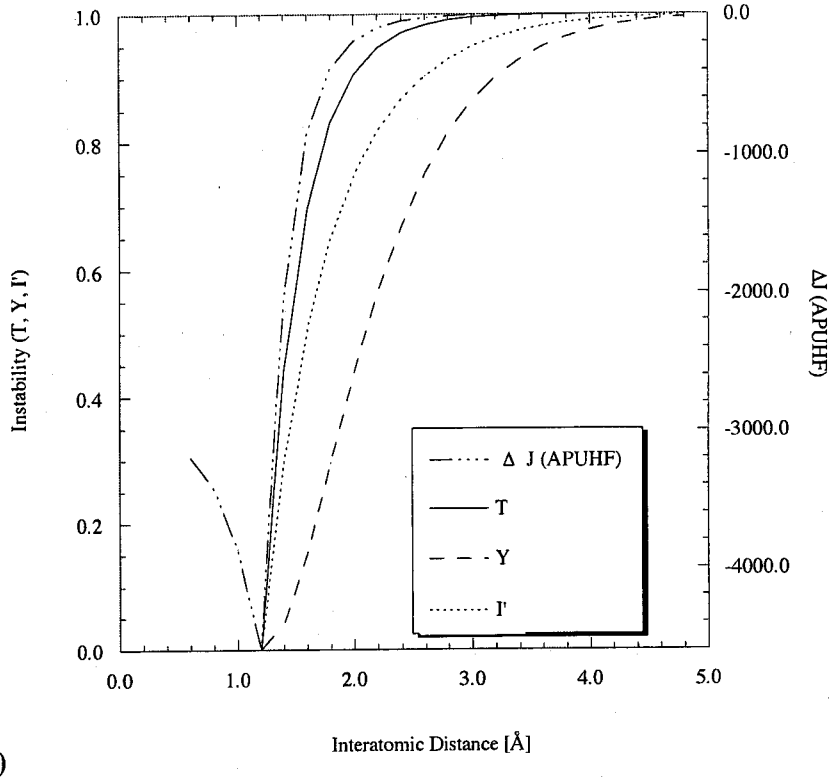

Figure 2.12 (c)

(c) The relation between instability values and ΔJ_{ab}(APUHF) i.e. J_{ab}(Full CI) - J_{ab}(APUHF) in case of hydrogen molecule.

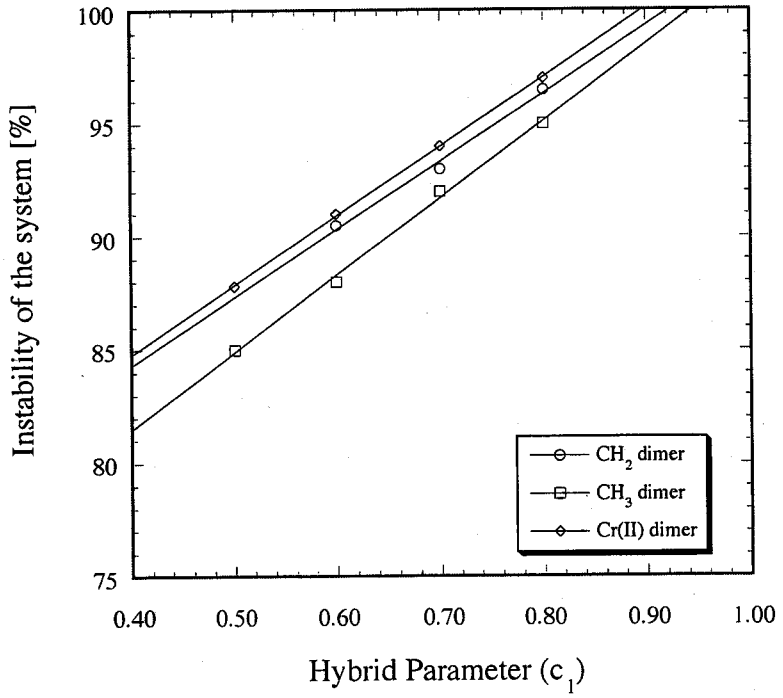

Figure 2.13

The instability of the system estimated by information entropy I'' at the intersection point of J_{ab} by post HF methods and J_{ab} by scheme 2

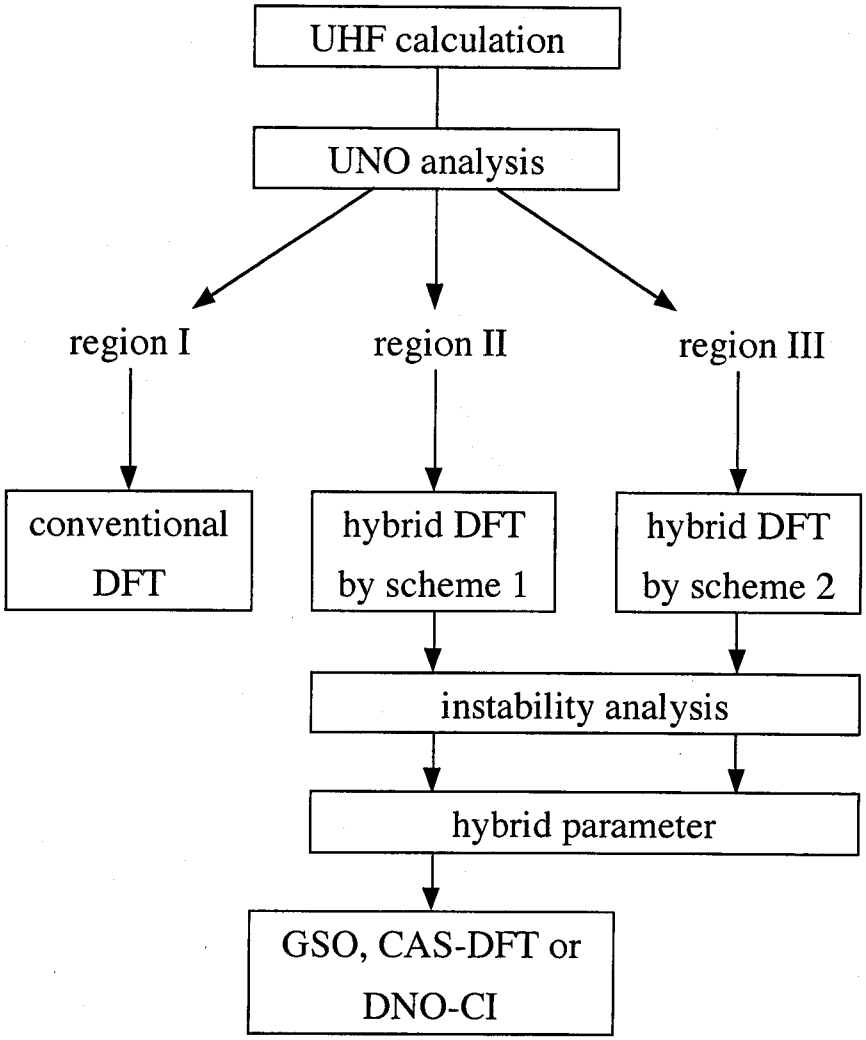

Figure 2.14

The procedure to select the appropriate scheme and parameter c_l by estimating the instabilities of the systems.

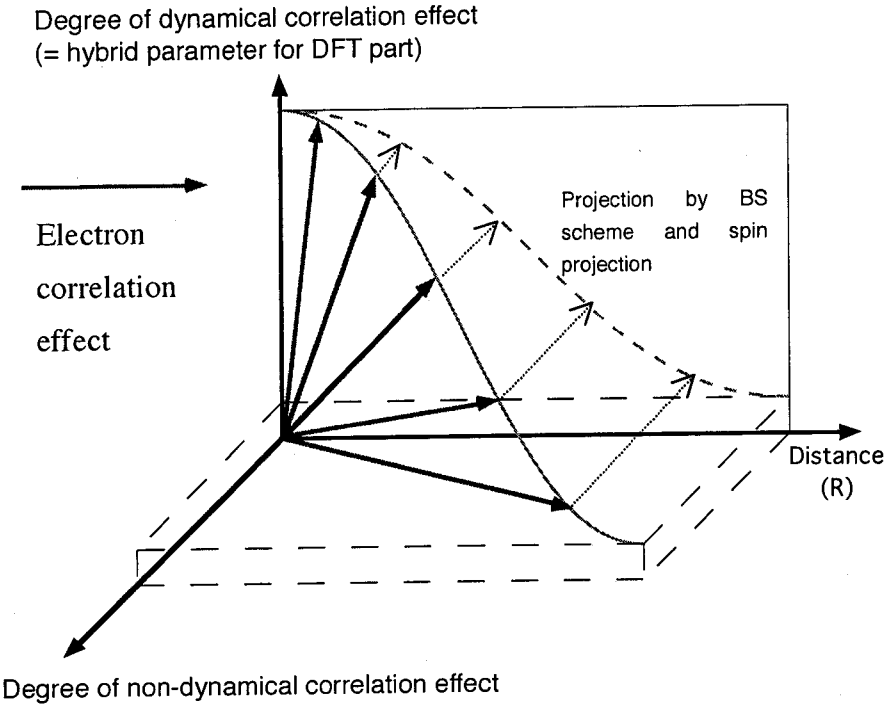

Figure 2.15(a)

Illustration of the relation between dynamical correlation effect and non-dynamical correlation effect that can not be separated.

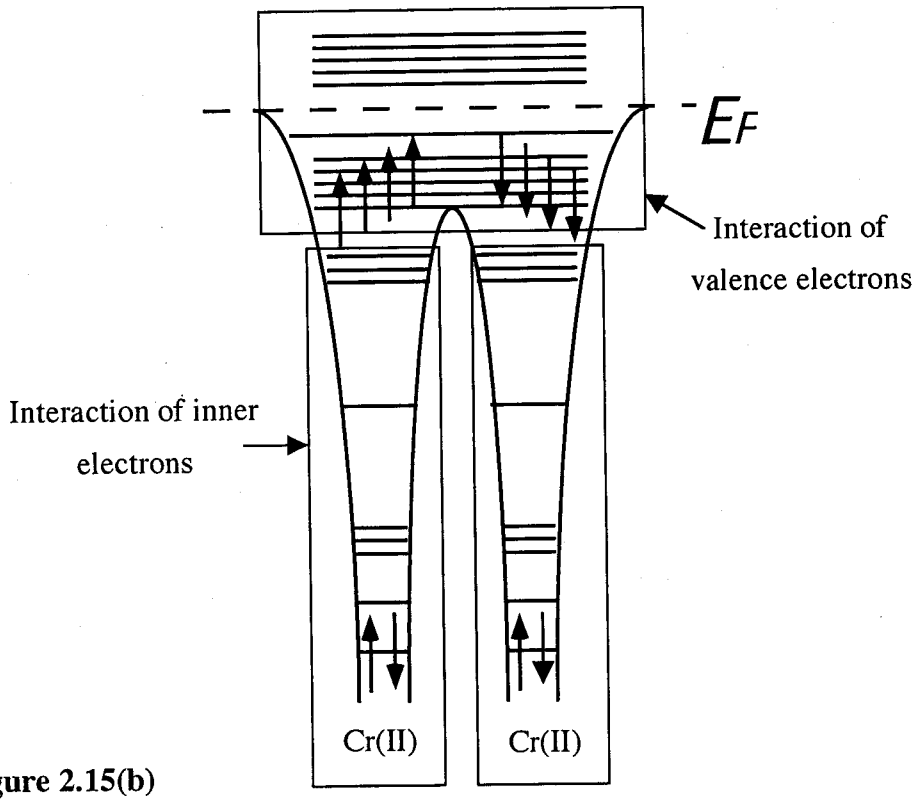

Figure 2.15(b)

Illustration of the interaction of valence electrons and inner electrons.

CHAPTER THREE

APPLICATION OF THE HYBRID DFT METHOD TO POLYNUCLEAR TRANSITION METAL COMPLEXES

Chapter Three

Application of the hybrid DFT method to Polynuclear Transition Metal Complexes

3.1 Introduction of this chapter

In recent years, many reports about metal string complexes have been presented in a field of the coordination chemistry[1][2][3][4]. Those aligned metal systems usually have unique bonding nature such as d orbital - d orbital direct bonds between metal ions (metal-metal bond), d orbital - p orbital interactions between metal and ligands (metal-ligand bond) and so on[5]. Some interesting phenomena related to them such as magnetic properties[5], non-linear optics[6] and liquid-crystals also have been investigated[7]. So, they are interesting in terms of fundamental studies of their peculiar bonding characters and applications to functional materials.

Dinuclear complexes bearing the multiple metal-metal bond are the smallest unit of metal string complexes[5]. Many experimental studies on the magnetism of these di-nuclear tetraacetate complexes such as $Cr_2(O_2CCH_3)_4(H_2O)_2$[5] have been performed. It have been, however, a difficult task to investigate electronic states using *ab initio* methods because those systems are too large to

compute with an appropriate electron correlation collection. On metal ions in those complexes, localized spins exist because of strong correlation. As mentioned in previous section, these localized spins were explained by non-dynamical correlation in the quantum chemistry. And the author has improved the spin-polarized hybrid DFT scheme for the open shell systems in terms of the magnetic interactions between the radical species, namely a magnetic effective density functional (MEDF) method.

The author applied the MEDF method to polynucler systems, which involved linearly aligned metal ions, and the magnetic interactions between metal ions were analyzed quantitatively. First, the author verified whether the MEDF method could reproduce both experimental J_{ab} values of $Cr_2(O_2CCH_3)_4(H_2O)_2$ and calculated J_{ab} value by coupled-cluster (CC) method for its naked dimer model. Total J_{ab} value was separated into direct metal-metal interaction and through-ligand interaction by complete active space (CAS) configuration interaction (CI) method using DFT natural orbitals (DNOs) together with the MEDF. Some methodological inspections such as spin-projection and so on were also examined for those analyses. In these complex, axial ligands were supposed to be influential in magnetic properties. So, the effect of the axial ligand was qualitatively investigated by using several model structures.

Next, J_{ab} values of other dinuclear tetraacetate complexes; $M_2(O_2CCH_3)_4X_2$ (M= Cu, Mo, X=none, H_2O) were calculated by using MEDF to investigate the interactions between divalent metal ions. They have characteristic metal-metal bonds, for example; Mo(II) dimer has the stable quadruple bond, while Cu(II) has the unstable single bond. Jab values, the natural orbital (NO) and the instability analysis of metal-metal bond were examined to clarify the characters of their metal-metal bonds.

Finally, the author investigated polynuclear systems that were so-called linearly aligned metal systems. As a first step for the polynuclear systems, the author focused on a tetra-chromium(II) system; $[Cr_4(DpyF)_4Cl_2]Cl_2$ where DpyF was bis(2-pyridyl)formamidine synthesized by Cotton et al[1]. As model systems, the author examined $[Cr_4(DpyF)_4Cl_2]^{2+}$ complex and its naked Cr(II) tetramer model *i.e.* no ligand model. The author applied the MEDF method to this system for an investigation of magnetic interactions between Cr(II) ions. In this system, the author estimated J_{ab} values between Cr(II) ions and elucidated the origins of those magnetic interactions. DNO and instability analyses were carried out to discuss the effects of axial and equatorial spiral ligands to the magnetic interactions. The effect of equatorial ligands and contribution of direct interaction and

through-ligand interaction for magnetic interaction between Cr(II) ions at each Cr(II)-Cr(II) distance were estimated using fitting curve of calculated results.

As a next step, the author focused on one of the aligned metal systems; $Cr_2(pyphos)_4$, where (pyphos=6-(diphenylphosphino)-2-pyridonate) and $Pt_2Cr_2(pyphos)_4(CH_3)_4$ synthesized by Mashima et al.[2]. $Pt_2Cr_2(pyphos)_4(CH_3)_4$ is interesting because different metal ions *i.e.* paltinum ions coordinate to Cr-Cr core on its axis, where electron donors such as water are usually located[5]. It has been supposed that the chromium ions in these complexes are Cr(II) and they have quadruple Cr-Cr bonds[2]. The details about electronic states of these complexes have not been elucidated well. The experimental measurement revealed their small J_{ab} values in comparison with usual $Cr_2(O_2CR)_4L_2$ complexes[2]. The author discussed the possibility of the electronic states of these complexes in terms of J_{ab} values between Cr ions.

3.2 Dichromium(II) tetraacetate complex

3.2.1 Introduction

Dichromium(II) tetraacetate dihydrate $Cr_2(O_2CCH_3)_4(H_2O)_2$ (**1a**) as shown in Figure 2.1 is one of the fundamental substances to study the nature of multiple bonds[5]. Magnetic properties were one of the important clues to study an electronic state and a bonding nature. Cotton *et al.* made the magnetic measurements of the complex **1a**, which exhibits weak temperature-dependent paramagnetism[5][8]. They found that the exchange integrals (J_{ab}) between Cr(II) ions in the Heisenberg model were -490cm^{-1}. Andersson et al. examined the structure of dichormium(II) tetraformate theoretically by using DFT and CASPT2[9]. They also reproduced experimental S-T gap value by the calculation[9]. However CASPT2 could not apply to large metal complexes. So, our MEDF is one of the most possible candidates of methods for these metal chains. The author explained the origin of experimental J_{ab} value using CASCI calculation together with MEDF. To elucidate the effects of axial ligands, several models were examined because axial ligands were supposed to be influential in magnetic properties in these complexes. The model structures that examined here are illustrated in figure 3.1. In the model **1c**, axial H_2O are removed from **1a**. The model **2a** and **2b** are taken from crystal of periodically aligned $\{Cr_2(O_2CCH_3)_4\}_n$ as illustrated figure 3.1. **2a** included axial acetates and **2b** is without axial acetates. Table 3.1 summarizing the Cr(II)-Cr(II) distances of those complexes. In comparison with them, the effect of axial ligands was investigated.

3.2.2 Computational Details

An atomic coordination of complexes **1a**, **1c**, **2a**, **2b** were taken from date of X-ray crystal structure analysis[5]. Naked model **1b** also calculated using experimental metal-metal distance of **1a**. Those calculations were performed by the use of Tatewaki-Huzinaga MIDI (533(21)/53(21)/(41))[10] puls Hay's diffuse d-basis sets[11] for Cr atoms and 6-31++G** basis sets for other atoms. DNO CAS CI calculations were carried out by using HONDO95[12] and all other calculations were carried out by using Gaussian98[13]. The hybrid parameter of MEDF was c_1=0.5 on scheme 1 (eq 2.18b)[14].

3.2.3 *Effective Exchange Integrals (J_{ab}) of $Cr_2(O_2CCH_3)_4(H_2O)_2$*

A effectiveness of the MEDF for J_{ab} values of **1a** and **1b** were examined here. Calculated electronic states are described using MO picture as follows; $(\sigma)^2(\pi)^4(\delta)^2$ for low spin state (S=0) and $(\sigma)^1(\pi)^2(\delta)^1(\delta^*)^1(\pi^*)^2(\sigma^*)^1$ for high spin state (S=4)[13]. Calculated results were compared with experimental J_{ab} values[5] for **1a** and calculated J_{ab} valued by UCCSD(T) that took single, double and triple excitations into account for **1b**. Table 3.2 summarized them. MEDF method could reproduce not only J_{ab} value of UCCSD(T) method for neked dimer model **1b** but also the experimental J_{ab} value for **1a**. UHF underestimated J_{ab} value because electron correlation effects were not considered enough especially for a singlet state[14]. On the other hand, conventional UBLYP and UB3LYP overestimated J_{ab} value because they were optimized for stable closed shell systems[14]. From these results, the author could verify that J_{ab} values calculated by MEDF reproduced J_{ab} values between Cr(II) ions in a di-Cr(II) tetraacetate complex (**1a**) and it's naked metal dimer model (**1b**).

The methodological inspection about the difference between $J_{ab}(1)$, $J_{ab}(2)$ and $J_{ab}(3)$ which are eq.2.29, eq.2.30 and eq.2.31 in previous chapter, respectively, is briefly described here[15]. The J_{ab} values obtained by them were summarized in Table 3.3. $J_{ab}(3)$, which connected small overlap region and large overlap region, was close to $J_{ab}(1)$. This fact shows that magnetic interactions between Cr(II) ions in complex **1a** could be expressed by using relatively small overlap model. The procedure of $J_{ab}(3)$ could not apply to tetra-Cr(II) models (see section 3.4) because there were several types of J_{ab}, leading the necessity of another method. This results supports that small overlap model could be applicable to estimate J_{ab} in tetra-Cr(II) models.

3.2.4. *Analysis of the contribution of each orbital using DNO*

To obtain a molecular orbital (MO)-like explanation of the effective exchange interaction, the NOs of the MEDF methods were determined by diagonalizing their first order density matrices as

$$\rho(r,r') = \sum n_i \{\phi_i(r)\}^* \phi_i(r') \qquad (3.2.1)$$

where n_i denoted the occupation number of NO ϕ_i[22]. Usually, occupation numbers of bonding and anti-bonding NOs are 2.0 and 0.0, respectively. In unrestricted calculations, however, α and β electrons split spatially to express so-called singlet diradical species. In such cases, occupation numbers are close to 1.0. An instability of a chemical bond could be discussed using this occupation number n_i. For example, n_i equals 2.0 if a chemical bond is stable, while n_i closes to 1.0 if a chemical

bond is unstable and the bond has localized spin structure. To assess this instability (diradical character), effective bond order for orbital i (b_i) were used here as follows[23],

$$b_i = \frac{n_i - n_i^*}{2} \tag{3.2.2}$$

where n_i and n_i^* were occupation number of bonding and anti-bonding orbital, respectively. b_i indicates 1.0 where a bond is stable, while b_i indicates zero where a bond is broken down and spins are localized at metal sites. This b is closely related to information entropy as mentioned in chapter 2.3. Table 3.4 summarizes the occupation numbers and effective bond orders of **1a** and **1b**. In the table, effective bond orders indicated that all those orbitals were not so stable. Especially, δ orbital shows almost localized spin structure. Compared with naked naked model **1b**, δ, π and especially σ orbitals of **1a** were stabilized by ligand effects. In Figure 3.2, σ, π and δ orbitals of low spin state of **1a** were depicted. The σ orbitals were delocalized to axial H_2O. This delocalization that could not be found in other orbitals seemed to contribute the stabilization of σ orbital. A localized spin structure could be recognized in δ orbital from the figure because of the narrow part of the NO. δ orbital almost dissociated compared with other orbitals from the table and the figure. δ orbital in Cr(II)-Cr(II) quadraple bond has originally small overlap and it is considered that δ orbital in those aligned Cr(II) chain are broken down. On the other hand, σ orbital has relatively large overlap and axial ligand also assists in stabilization of σ orbital, so it is considered that σ orbital easily conjugates in Cr(II) linear chain. The detail about the effect of axial ligands is discussed later in chapter 3.5.

3.2.5. Separation of the interaction path using CAS CI calculation

The author performed CAS CI 8-orbital and 8-electron ({8,8}) calculation by using DNO obtained by the MEDF[23]. The DNOs that selected here were '*valence*' orbitals as the view point of magnetic interest. They were related to Cr(II)-Cr(II) direct interaction, *i.e.* σ, π, δ, σ* π* and δ* orbitals that mainly constructed by metal d characters as shown in Figure 3. 2[9]. In other words, this CAS CI {8,8} calculation revealed J_{ab} value by a direct interaction between Cr(II) ions, leading to separation of metal-metal direct interaction and through-ligand interaction as follwes;

$$J_{ab}(through-ligand) = J_{ab}(total) - J_{ab}(direct). \tag{3.2.3}$$

This separation of interaction paths has never been carried out qualitatively in these complexes nevertheless it is very interesting in terms of ligand effects in magnetic interactions. While, Nishino

et al. investigated the reliability of the spin, multiplet splittings by the Heisenberg model using naked Cr(II) dimer model[13]. So, the author also examined it using complex **1a**. The J_{ab} values for the metal-metal direct exchange couplings between the Cr(II) ions were calculated from total energies *E(spin state)* by DNO CASCI [8,8] as follows;

$$J_{ab}(S-T) = \frac{E(singlet) - E(triplet)}{2} \tag{3.2.4}$$

$$J_{ab}(T-Q) = \frac{E(triplet) - E(quintet)}{4} \tag{3.2.5}$$

$$J_{ab}(S-T) = \frac{E(singlet) - E(quintet)}{6}. \tag{3.2.6}$$

Therefore, if these J_{ab} values are nearly equal, $J_{ab} \approx J_{ab}(S\text{-}T) \approx J_{ab}(T\text{-}Q) \approx J_{ab}(S\text{-}Q)$, the energy splits are reduced to those of the Heisenberg model[13]. Table 3.5 was summarizing them. From these results, the author found three points as follows. (i) The J_{ab}(S-T), J_{ab}(T-Q) and J_{ab}(S-Q) values were almost equal to one another. This was in good agreement with the energy splittings expected from Heisenberg model. (ii) J_{ab} value caused by Cr(II)-Cr(II) direct interaction was about 330cm^{-1}. This value was close to J_{ab} value of naked Cr(II) dimer model (**1b**). So, effect by ligands on direct interaction was relatively small. This meaned that σ, π and δ orbitals were localized on metal ions except for axial ligands, which was supported by Figure 3.2. (iii) The difference between J_{ab} by MEDF and J_{ab} by CAS CI [8,8] showed the effect of the through-ligand interactions. For example, about 190 cm^{-1} was the through-ligand effect caused by four acetate ligands. It was brought to light that the ratio of Cr(II)-Cr(II) direct and through-ligand interactions in terms of the magnetic interactions between Cr(II) ions was about 3 to 2. This was showing that a through-ligand effect were important in the Cr(II) di-nuclear complexs.

3.2.6 The effect of axial ligand

To clarify the effect of the axial ligands, the electronic states of several model structures; **1a**, **1c**, **2a** and **2b** as illustrated in Figure 3.1, were investigated in terms of the magnetic interaction. In the model **1c**, axial H_2O are removed from **1a**. The model **2a** and **2b** are taken from crystal of periodically aligned $\{Cr_2(O_2CCH_3)_4\}_n$ as illustrated figure 3.2. **2a** included axial acetates and **2b** is without axial acetates. Cr(II)-Cr(II) distances of those complexes were summarized in Table 3.1. Calculated J_{ab} values by eq 2.31 ware summarized in Table 3.6. The calculated J_{ab}s were influenced by the axial ligands. To explain this effect, the author examined the relation between J_{ab}

values and metal-metal bond. Figure 3.4 depicts the orbital energies of valence orbitals of each model. The energy difference of sigma orbital is larger than other orbitals. Figure 3.5 is summarizing the instabilities of each valence bond using effective bond order (b_i) in eq 3.2.2. The change of b_i of sigma orbital is also larger than other orbitals. Figure 3.6 is indicating the relation between J_{ab} values and average values of effective bond order b_i. This figure is showing that J_{ab} is the closely related to the instability of valence orbitals of metal-metal bond. Adding that, sigma orbital, which is easily affected by axial ligands in comparison with other pi, delta orbitals, dominates the instability of valence orbital of metal-metal bonds. From those results, the author summarized as follows; (i) the absolute value of J_{ab} ($|J_{ab}|$) decreases when the absolute value of orbital energy increases. (So, $|J_{ab}|$ is in inverse proportion to |orbital energy|) (ii) $|J_{ab}|$ value increases when instability of valence bond decreases. (So, $|J_{ab}|$ is in inverse proportion to instability of valence bond) (iii) sigma orbital dominates the instability of valence metal-metal bonds.

The reason of these results is considered as illustrated in Figure 3.7. The sigma orbital of metal-metal bond is delocalized to axial ligands because sigma orbital and lonepair of axial ligands, which coordinate to metal ions, make sigma type conjugation[28]. The conjugated sigma bonds split to ligand part and meta-metal part if difference of orbital energies between metal-metal bond and lonepair of ligands is large. The valence sigma orbital of metal-metal bond that is depicted in Figure 3.2 comes from 'anti bonding orbital' between metal-metal bond and lonepair of ligands. So, if the conjugation between metal-metal bond and axial ligands, 'anti-bonding' metal-metal valence sigma bond becomes unstable. But the conjugation makes metal-metal distance short, therefore the instability of metal-metal bond becomes stable because of large overlap integrals. As a consequence, J_{ab} value is enlarged.

3.2.7 Concluding remarks of chapter 3.2

The magnetic interactions between Cr(II) ions in $Cr_2(O_2CCH_3)_4(H_2O)_2$ (**1a**) and related complexes (**2a**) were investigated qualitatively using MEDF method. The J_{ab} by direct and through-ligand interactions were estimated separately, together with CAS CI{8,8} calculation. Those analyses revealed the importance of axial and equatorial ligands of magnetic interactions. The axial ligands directly influenced the stability of σ orbitals, so J_{ab} values changed with the existence of axial ligands. Furthermore, it is also possible to vary J_{ab} with axial ligands. J_{ab} value of through-ligand

interaction was smaller than J_{ab} values of direct interaction, leading the decrease of the ratio of through-ligand interaction at short distance. While, J_{ab} values of through-ligand interaction competed with J_{ab} values of direct interaction. The δ orbitals were easily affected and unstabilized by spiral structure of equatorial ligands. δ orbitals originally tended to localize on Cr(II) ions, so d-electrons in δ orbitals might be able to act as localized spin completely if spiral structure was designed well. It is very interesting to realize the coexistance of anti-ferromagnetic coupling by σ and π orbitals and ferromagnetic coupling by δ orbital. Through these studies, our MEDF approach seemed to be available for the di- and more aligned metal complexes and other related substances at this stage.

3.3 Comparison with dichromium tetraacetate complex and other dinuclear acetate complexes

3.3.1 *Introduction*

Here, the author examined fundamental nature of those Cotton-type complexes and found our hybrid method are appropriate method for those systems. The author focused on di-Cu(II) tetra-acetate and di-Mo(II) tetra-acetate that had characteristic metal-metal bonds. For example, Mo(II) dimer has the stable quadruple bond, while Cu(II) has the unstable single bond. The J_{ab} values of those metal-acetate complexes are calculated by using hybrid DFT methods to investigate the interactions between divalent metal ions. Furthermore natural orbital (NO) and molecular orbital (MO) analysis also examined to clarify the species of the interactions. Metal-Metal distances were summarized in Table 3.7.

3.3.2. *Computational Details*

Those calculations were performed by the use of Tatewaki-Huzinaga MIDI (533(21)/53(21)/(41))[10] puls Hay's diffuse[11] d-basis sets for Cr, Cu atoms and 6-31++G** basis sets for other atoms. In the calculations of Mo(II)-acetate complex, Tatewaki-Huzinaga MIDI (4333(21)/433(21)/4(21))[10] for Mo atoms and 6-31G** basis sets for other atoms were used. The coordinations for $Cu_2(OCCH_3)_4(H_2O)_2$ (**3a**) and $Mo_2(O_2CCH_3)_4$ (**4a**) are according to X-ray measurement study. J_{ab} values were estimated by eq. 2.31.

3.3.3. *Naked metal ion dimers*

Before the calculations about the metal-acetate complexes, the author examined the properties of the naked metal dimers to elucidate the tendency of the methods and the original nature of metal dimers, which are involved in metal-acetate complexes. To consider the effectiveness of the methods, UHF, MEDF and UB3LYP methods were compared with the UCCSD(T) method. Each calculated electron configuration was similar to the full model complex; $\sigma^2\pi^4\delta^2$ (low spin state, S=0) and $(\sigma)^1(\pi)^2(\delta)^1(\sigma*)^1(\pi*)^2(\delta*)^1$ (high spin state, S=4) and for Mo(II), Cr(II) dimer, and $(\sigma)^2(\pi)^4(\delta)^4(\pi^*)^4(\sigma^*)^2(\delta^*)^2$ (low spin stete, S=0) and $(\sigma)^2(\pi)^4(\delta)^3(\pi^*)^4(\sigma^*)^2(\delta^*)^3$ (high spin state, S=1) for Cu(II) dimer, respectively. The J_{ab} values of Cu(II) and Mo(II) naked dimers calculated by

several methods are shown in Table3.8. The author could not obtain appropriate electronic state for naked Mo(II) dimer. However, strong anti-ferromagnetic coupling is expected from the results of full model complex. The J_{ab} value of Cr(II) was negative so that the interactions between metal atoms are anti-ferromagnetic. From the magnitudes of the J_{ab} values, it was found that Cu(II) dimer had the very week interaction. The J_{ab} values and the instability values at the bonding distance in each metal-acetate complex are shown in Table.3.7 in comparison with Cr(II) naked dimer (**1b**). By using the idea of the regions as mentioned before, it could be predicted that Mo(II) dimer that had small instability value could be considered in region I and J_{ab} value of Mo(II) dimer will be reproduced by APUB3LYP. While Cu(II) dimer that had large instability value could be considered in region III and J_{ab} value of Cu(II) dimer could be reproduced by APUHF. In fact, the author found that the J_{ab} value of Mo(II) dimer by using APUB3LYP was corresponding with the J_{ab} value by using APUCCSD(T) method at the bonding distance in Mo(II)-acetate complex. The J_{ab} value of Cu(II) dimer by using APUHF was corresponding with the J_{ab} value by using APUCCSD(T).

3.3.4. Dinuclear tetraacetate complexes

Next, The author examined the metal-acetate models. In those systems, the calculations that include the electron correlation effects such as the post Hartree-Fock (HF) methods are impossible because of their size. So, hybrid DFT method is applied to these systems to investigate the magnetic interactions. The J_{ab} value of the each metal-acetate complex is summarized in Table 3.9. The experimental J_{ab} value of Cu(II)-acetate is -142cm^{-1} [29] nevertheless the J_{ab} value of naked Cu(II) dimer was smaller than -10cm^{-1} from Table.3.7. CASCI{2,2} result in Table 3.7 also supports it. This interaction between Cu(II) ions is considered mainly through-bond effect because the author estimated that the through-ligand effect by acetate ligands was about -135 to -193cm^{-1} in previous section. Natural Orbitals (NOs) of the magnetic orbitals of Cr(II), Mo(II) and Cr(II)-acetate complexes calculated by using MEDF (DFT-NOs: DNOs) are shown in Figure 3.8 (a) - (b) and Figure 3.2, respectively. The DNOs of Cu(II)-acetate that spread to the ligands evidently explain that the interaction through acetete ligands is stronger than other metal-acetate complexes. Molecular orbitals (MOs) of Cu(II)-acetate by MEDF shown in Figure 3.9 that have little overlap with another Cu(II) ion also elucidate that direct interaction is very week. Furthermore, The author found that the instability value of Cu(II)-acetate complex was more than 100 [%]. This means that Highest Occpied

Molecular Orbital (HOMO) is anti-bonding orbital and Lowest Unoccupied Molecular Orbital (LUMO) is bonding orbital in terms of metal-metal bond as depicted in Figure 3.8(a). This phenomenon that is not obtained in naked Cu(II) dimer, also suggests the existence of the stronger through-bond interaction than direct interaction. On the other hand, it is considered that the metal-metal interaction in Mo(II)-acetate complex mainly comes from metal-metal direct interaction because the J_{ab} value of Mo(II) dimer is almost -3000cm^{-1} from Table 3.7. Because DNOs of Mo(II)-acetate are similar to closed shell type NO, the strong metal-metal direct interaction is expected in comparison with the other metal-acetate complexes. The results that J_{ab} value calculated by CASCI{8,8}, which could estimate the Mo(II)-Mo(II) valence interaction, was almost same to J_{ab} value calculated by APUB3LYP also supported it. There is no experimental J_{ab} values of **4a**, such a large anti-ferromagnetic interaction might be observed as diamagnetic interaction.

di-Cr(II) tetra-acetate complex; **3a** has both direct and through-bond interactions and takes a middle position between di-Cu(II) tetra-acetate; **1a** complexes and di-Mo(II) tetra-acetate complexes; **4a**.

3.3.5. Concluding remarks of chapter 3.3

The J_{ab} values of the typical metal-acetate complexes (metal=Cr(II), Cu(II) and Mo(II)) were calculated by using HF and hybrid DFT methods to investigate the interactions between metal atoms. The hybrid DFT methods such as APUB3LYP and MEDF ware examined on the metal dimers and they could reproduce J_{ab} value calculated by APUCCSD(T) method. By using MEDF methods, which has variable hybrid parameter, J_{ab} values the large sized characteristic di-nuclear tetra-acetate systems were investigated with the appropriate electron correlation effects. By comparing naked dimer to complex, The author found the characters of interaction as follows, the interactions between metal atoms for di-Cu(II) tetra-acetate complex are mainly through-ligand effect. On the other hand, they are mainly direct interaction for di-Mo(II) tetra-acetate complex. NO analysis and MO analysis also examined to clarify the type of interactions. They expressed the effects of through-ligand interaction and direct interaction. Those Cotton-type complexes of early transition metals such as Cr-acetate complex that was investigated here are good candidates for the atom three-terminal devices[28]. The hybrid DFT methods are effective methods to investigate those electronic states as theoretical approaches.

3.4 Linearly aligned tetra-Cr(II) complex

3.4.1. Introduction

The author focused on aligned tetra chromium(II) systems; $[Cr(II)_4(DpyF)_4Cl_2]Cl_2$ where DpyF was bis(2-pyridyl)formamidine synthesized by Cotton et al, which was reliable approach to a metal chain[1]. As model systems, the author examined $[Cr(II)_4(DpyF)_4Cl_2]^{2+}$ complex model (**5a**) and its naked model *i.e.* without ligand model (**5b**) as illustrated in Figure 3.10. The author applied the MEDF method to this system for an investigation of magnetic interactions between Cr(II) ions. In this system, the author estimated J_{ab} values between Cr(II) ions and elucidated the origins of those magnetic interactions. DNO and instability analyses were carried out to discuss the effects of axial and equatorial spiral ligands to the magnetic interactions. The contribution of Cr(II)-Cr(II) direct interaction and through-ligand interaction to total J_{ab} value at each Cr(II)-Cr(II) distance was also examined here.

3.4.2. Computational details

Atomic coordination of complex **5a** was taken from date of X-ray crystal structure analysis[1]. Naked model **5b** also calculated using experimental metal-metal distance of **5a**. Each calculation was performed by the use of Tatewaki-Huzinaga MIDI[10] plus p type wavefunctions for Cr atoms and 4-31G basis set for other atoms for complex **5a** and naked model **5b**. All calculations were carried out by using Gaussian98[13].

3.4.3. Effective Exchange Integrals (J_{ab}) of $[Cr(II)_4(DpyF)_4Cl_2]^{2+}$

Next, The author attempted to calculate J_{ab} values of larger and reliable metal chain system; $[Cr(II)_4(DpyF)_4Cl_2]^{2+}$ model[1]. This complex contains two Cr(II)-Cr(II) quadruple bonds and it is considered that there are little or no bonding between the two inner chromium atoms[1]. Approximated spin projection by eq 2.31 could not use in this system because three types of magnetic interactions between Cr(II) ions *i.e.* J_1, J_2 and J_3 as illustrated in Figure 3.11(a) were assumed to clarify magnetic interactions qualitatively. So, J_{ab} values were directly obtained from Heisenberg model under the approximation of small overlap model by calculating four electronic states as illustrated in Figure 3.11(b). Calculated results of J_{ab} values were summarized in Table 3.11. The author could

not compare with experimental results because the experimental magnetic measurement has never been performed. The J_1 of full model **5a** showed the relatively strong anti-ferromagnetic interactions and consistent with the naked model **5b**. Therefore J_1 mainly originated from metal-metal direct interactions. On the other hand, J_2 and J_3 in model **5a** were larger than ones in naked model **5b**. Especially, J_3 in model **5a** showed small anti-ferromagnetic interaction although the J_3 interaction in model **5b** almost disappeared. From those results, J_2 in model **5a** mainly originated from a through-ligand interaction. Similarly, it was considered that the J_3 in model **5a** was also caused by a through-ligand interaction. In this way, magnetic interactions between Cr(II) ions at a long distance were dominated by through-ligand effects, while they at a short distance could be described by metal-metal direct interactions.

3.4.4. DNO and instability analyses of $[Cr(II)_4(DpyF)_4Cl_2]^{2+}$

The DNOs of this complex **5a** were examined to elucidate contributions of each orbital to magnetic properties. In Figure 3.12(a)-(c), σ, π and δ orbitals of most stable LS(III) state in Figure 3.11(b) were depicted. The σ orbitals were delocalized to axial terminal Cl ligands same as **1a**. π orbitals were constructed by pairs of orthogonal doubly degenerated orbitals. δ orbitals had spiral structures that were reflecting a spiral structure of ligands. The author found that the δ orbitals easily affected by the structure of ligands. Occupation numbers and effective bond orders were summarized in Table 3.12. σ orbitals were much stabilized than π orbitals. This was also the effect of axial ligands same as **1a**. In comparison with the data of complex **1b** summarized in Table 3.4, all orbitals of complex **5b** were stabilized. These were understandable by taking account of a conjugation stabilization of d-electrons. The effects of ligands that stabilized σ and π orbitals were also same to the case of **1a** and **1b**. However, δ orbitals were not so stabilized by the ligands in comparison with **1a** and **1b**. It is considered that this was originated in spiral structure affected by the ligands.

3.4.5 The effects of ligands on magneic interactions

Here, The author discuss about ligand effects that were important to consider magnetic interactions between Cr(II) ions in Cr(II) aligned complexes. The author focused on two different types of ligands *i.e.* axial and equatorial ligand that were defined as a ligand on metal aligned axis and a ligand connecting Cr(II) ions, respectively. The first point was the effects of axial ligands to

magnetic interactions. The detail about it was discussed in chapter 3.2.6. The second point was the equatorial ligands which connects two Cr(II) ions. In above chapter, The author pointed out that magnetic interactions between Cr(II) ions at a long distance were dominated by through-ligand effects, while they at a short distance could fully be described by metal-metal direct interactions. To clarify the contributions by through-ligand and direct interaction at each distance, The author fitted calculated J_{ab} values with a gauss-type function

$$J_{ab} = p \exp(-qR^2) \qquad (3.4.5)$$

where p and q were fitting parameters. The J_{ab} curve of total magnetic interactions (direct plus through-ligand interaction) was fitted with J_{ab} of **1a** and J_1, J_2, J_3 of **5a** in Table 3.1 and Table 3.11 using their experimental Cr(II)-Cr(II) distance, respectively. The J_{ab} curve of direct interaction was approximately estimated by fitting with J_{ab} of naked Cr(II) dimer model. The through-ligand J_{ab} values were obtained by subtraction in eq. 3.2.3. Fitting curves were depicted in Figure 3.13. The change of the strength of direct interaction with distance was larger than one of through-ligand interaction. Consequently, the direct interaction is far stronger than the through-ligand interaction at short distance, while the through-ligand interaction competes with direct interaction at long distance.

3.4.6. Concluding remarks of chapter 3.4

The magnetic interactions between Cr(II) ions in $[Cr_4(DpyF)_4Cl_2]^{2+}$ (**5a**) was investigated qualitatively using MEDF method. These analyses revealed the importance of equatorial ligands of magnetic interactions. J_{ab} value of through-ligand interaction was smaller than J_{ab} values of direct interaction at the bonding distances of usual di-Cr(II) complexes, leading the decrease of the ratio of through-ligand interaction at short distance. On the other hand, J_{ab} values of through-ligand interaction competed with J_{ab} values of direct interaction at relatively long distance. And it finally become dominantly at considerably longer Cr(II)-Cr(II) distance.

The δ orbitals were easily affected and unstabilized by spiral structure of equatorial ligands. δ orbitals originally tended to localize on Cr(II) ions, so d-electrons in δ orbitals might be able to act as localized spin completely if spiral structure was designed well. It is very interesting to realize the coexistance of anti-ferromagnetic coupling by σ and π orbitals and ferromagnetic coupling by δ orbital. Through these studies, our MEDF approach seemed to be available for the di- and more aligned metal complexes and other related substances at this stage.

3.5 Other linearly aligned tetra-metal complex

3.5.1. *Introduction*

The author focused on one of the aligned metal systems; $Cr_2(pyphos)_4$ where (pyphos=6-(diphenylphosphino)-2-pyridonate) and $Pt_2Cr_2(pyphos)_4(CH_3)_4$ synthesized by Mashima et al.[2]. $Pt_2Cr_2(pyphos)_4(CH_3)_4$ is interesting because different metal ions *i.e* paltinum ions coordinate to Cr-Cr core on its axis, where electron donors such as water are usually located[5]. Spin sources in those complexes were Cr ions and Cr-Cr distances of **6a** and **7a** were 2.015Å and 2.389Å, respectively. It has been supposed that the chromium ions in these complexes are Cr(II) and they have quadruple Cr-Cr bonds[2]. The details about electronic states of these complexes have not been elucidated well. The experimental measurement revealed their small J_{ab} values in comparison with usual $Cr_2(O_2CR)_4L_2$ complexes[2]. J_{ab} values of **6a** observed by SQUID and NMR were -340cm^{-1} and -520cm^{-1}, respectively[2]. While observed J_{ab} value of **7a** was -29cm^{-1}[2]. The author discussed the electronic states of these complexes in terms of J_{ab} values between Cr ions.

3.5.2. *Computational details*

In those calculations, the author used Heisenberg model (in eq.2.26) and size-consistent spin projection (in eq.2.31) to estimate J_{ab}. Those spin projected J_{ab} values calculated by the method X called AP - X such as APUHF. All atomic coordinations except for hydrogen atoms were taken from date of X-ray crystal structure analyses. Hydrogen atoms were added based on the general chemical bonds. Those calculations were performed by the use of Tatewaki-Huzinaga MIDI (533(21)/53(21)/(41))[10] for Cr, Pt and 4-31G basis sets for other atoms. All calculations were carried out by using Gaussian98[13].

3.5.3. *J_{ab} calculations presuming Cr(II)*

First, The author calculated J_{ab} values of $Cr_2(pyphos)_4$ (**6a**) presuming Cr(II) and Cr(II)-Cr(II) $\sigma^2\pi^4\delta^2$ quadruple bond. SQUID and NMR measurements indicated different J_{ab} values that were -340 cm^{-1} and -520 cm^{-1}, respectively[2]. The both values were smaller than usual J_{ab} value between Cr(II) ion at a distance of 2.015Å[5]. Here, The author calculated J_{ab} values of the full model (**6a**) and naked dimer core model (**6b**) as illustrated in Figure 3.14. The calculated results

were summarized in Table 3.13. The calculated J_{ab} values of naked dimer model **6b** were larger than experimental values. The J_{ab} value calculated by the MEDF method of c_i=0.5 in eq 2.18(b) that was optimized for the Cr(II) dimer[25] close to J_{ab} by the UCCSD(T). The J_{ab} value of full model (**6a**) was calculated by using UHF and MEDF. The author found that calculated J_{ab} values were about twice as large as experimental J_{ab} values. The J_{ab} between Cr(II) ions estimated by the S-T gap plot by Cotton et al. was about 1000cm^{-1} at a distance of 2.0Å[5][26]. The J_{ab} value by MEDF (-1202cm^{-1}) was consistent with it. So, it was conceived that MEDF reproduced J_{ab} between Cr(II) ions in full model, well. From these results, The author could not reproduce experimental J_{ab} values of **6a** presuming that Cr ions in **6a** were +2 cation. This was suggested that Cr ions were not Cr(II). On the other hand, the difference between J_{ab} of full model (**6a**) and naked core model (**6b**) estimated by UHF and MEDF was about -200cm^{-1} and -330cm^{-1},respectively. This was leading that the magnetic interaction through ligand, namely through-ligand J_{ab}, was expected to be about 70 percent of the J_{ab} of the full model. Therefore it would be expected that Cr-Cr direct interaction in **6a** was so small in comparison with experimental J_{ab} value, -520cm^{-1}.

Next, The author examine J_{ab} of $Pt_2Cr_2(pyphos)_4(CH_3)_4$ (**7a**). It was reported that this complex showed extremely small J_{ab} (-29 cm^{-1})[2] as compared with usual J_{ab} value between Cr(II) ion at a distance of 2.389Å[5][14]. Here, The author also presumed that Cr and Pt ions were +2. The calculated results were summarized in Table 3.14. In every model of Cr-Cr naked core (**7c**), Pt-Cr-Cr-Pt naked core (**7b**) and complex (**7a**), the calculated J_{ab} values were larger than the experimental value. The J_{ab} between Cr(II) ions estimated by the S-T gap plot by Cotton et al. was about -450 cm^{-1} at a distance of 2.4Å[26]. Calculated J_{ab} by MEDF (-407cm^{-1}) was consistent with it. In these models, The author could not reproduce experimental J_{ab} values of **7a** presuming that Cr and Pt were +2 cation again. The through-ligand effect in this complex could also be estimate from the difference between J_{ab} of full model (**7a**) and Pt-Cr-Cr-Pt naked core model (**7b**). They were about -50cm^{-1} by UHF and -230cm^{-1} by MEDF, respectively and it accounted for about 50 percent of the J_{ab} value of the full model. Of course these were values presuming Cr(II) and they could not be applied to other cases as they were. These results, however, suggested that Cr-Cr direct exchange interactions must be smaller than the experimental J_{ab} value. On the other hand, The author found the effect of Pt(II) ions that decreased J_{ab} value between Cr(II) ions in comparison with J_{ab} of **7b** and **7c**. This meant that Pt(II) ions made Cr(II)-Cr(II) bond unstable and the interaction between spins on Cr(II) ions decreased.

From these results, The author could not reproduced the experimental J_{ab} values by theoretical calculations presuming Cr(II).

3.5.4. J_{ab} calculation preasuming of Cr(III)

Here, The author examined the possibility of Cr(III) in $Cr_2(pyphos)_4$ (**1a**) and $Pt_2Cr_2(pyphos)_4(CH_3)_4$ (**7a**) using their naked models (**6b**), (**7b**) and (**7c**) as illustrated in Figure 3.14. There were three candidates of the electron configuration for Cr(III)-Cr(III) triple bonds; $\sigma^2\pi^2\delta^2$, $\sigma^2\pi^4$, and $\pi^4\delta^2$. The author calculated J_{ab} values for each electronic configuration.

At first, The author calculated J_{ab} values of $Cr_2(pyphos)_4$ (**6a**) presuming Cr(III). The calculated J_{ab} values of $\sigma^2\pi^2\delta^2$, $\sigma^2\pi^4$, and $\pi^4\delta^2$ configurations were summarized in Table 3.15. J_{ab} values were smaller than one's of naked Cr(II) dimer model in Table 3.13, except for $\sigma^2\pi^4$ state. Their order was $| J_{ab}(\sigma^2\pi^4) | > | J_{ab}(\sigma^2\pi^2\delta^2) | > | J_{ab}(\pi^4\delta^2) |$. This tendency reflected the stability of chemical bonds; $\sigma > \pi > \delta$ because the stable chemical bonds contributed to large negative J_{ab} values[14]. For example, the calculated $J_{ab}(\pi^4\delta^2)$ was small because the $\pi^4\delta^2$ state did not have σ bonding which gave large negative J_{ab} value. These naked models did not take through-ligand effects into account. The author found through-ligand effects in (**6b**) was relatively large presuming Cr(II). So, possible candidate of electronic stete of $Cr_2(pyphos)_4$ seemed to be $\pi^4\delta^2$ state of Cr(III) dimer core that had smallest J_{ab} value. However a possibility of $\sigma^2\pi^2\delta^2$ could not deny because it has smaller J_{ab} value than the experimental value. There was little possibility of the $\sigma^2\pi^4$ state of Cr(III) dimer core that had larger J_{ab} value than the experimental value.

Next, the electronic state of $Pt_2Cr_2(pyphos)_4(CH_3)_4$ was also examined by using Cr-Cr naked core model (**7c**) and Pt-Cr-Cr-Pt naked core model (**7b**) assuming Pt(II) and Cr(III), respectively. These calculations, however, were very difficult to converge. So, The author substituted point charges for ligand atoms. Only the atoms that had connections to metal ions (P, N ,O atoms of pyphos ligands and C atoms of CH_3 ligands) were used as point charges and they were based on the calculated results of pyphos$^-$ and CH_3^- by RHF. They were located on same arrangement with real complex (**7a**). Here, The author calculated J_{ab} values of $\sigma^2\pi^2\delta^2$ and $\pi^4\delta^2$ configurations of Cr(III)-Cr(III) core because they were candidates for the electronic state for $Cr_2(pyphos)_4$. The results were summarized in Table 3.16. In comparison with the data of $Cr_2(pyphos)_4$ in Table 3.14, calculated J_{ab} values were decreased drastically. Especially, J_{ab} value by APUHF was slightly positive in case of

$\pi^4\delta^2$ state of **7b**. Because of the suggestion that Cr-Cr direct exchange interactions must be very small from the estimation of through-ligand J_{ab} presuming Cr(II), The author concluded that the $\pi^4\delta^2$ configurations of Cr(III)-Cr(III) core was the possible candidate for $Pt_2Cr_2(pyphos)_4(CH_3)_4$.

To clarify such a peculiar J_{ab} of the $\pi^4\delta^2$ state, The author analyzed its natural orbitals (NOs) and instabilities of orbitals as illustrated in Figure 3.15. Instabilities of each orbitals were estimated by using the information entropy as mentioned in chapter 2.3. There are some attempts to apply the information theory to the studies of atomic and molecular systems. Ramírez et al [26] indicated that the entropy of the system is calculated as follows;

$$I = -\sum_i n_i \ln n_i . \qquad (3.5.1)$$

Here n_i is occupation number of occupied natural orbital. The author improved it as follows[14];

$$I_i' = 1 - \frac{n_i \ln n_i}{2 \ln 2} . \qquad (3.5.2)$$

This normalized information entropy; I_i' for orbital i indicates zero in the region strong bonding region while it indicates 1.0 in fully dissociated region. Here, The author used this I_i' to estimate the instabilities of metal-metal bonds. Calculated I_i' of **7b** by UHF was summarized in Table 3.17. From the pictures of NOs as illustrated in Figure 3.15, The author found that HOMO was Cr-Cr δ bond. While HOMO-1 to HOMO-4 were conjugated orbitals of Cr-Cr π bonds and Pt(II)'s orbital. It was considered that interaction between Pt and Cr-Cr center was week because there were dδ-like component of Pt(II)'s orbital and overlap between Pt and Cr-Cr center was small. This dδ component of Pt(II) reflected the effects of point charges. Instability values of these HOMO to HOMO-5 orbitals in Table 3.17 were more than 95%. Especially, HOMO-1 and HOMO-2 that were originated in π orbitals of Cr-Cr bonding became more unstable than **7c** (see values in parentheses). This unstabilization contributed to the decrease of J_{ab} of **7b**. HOMO-5 to HOMO-8 and HOMO-12, HOMO-13 orbitals were mainly derived from Pt(II)'s orbitals. HOMO-5 and HOMO-6 orbitals were σ-type orbitals that derived from Pt(II)'s orbitals and they were slightly unstable. The vacant σ orbital of Cr-Cr core contributed to this instability of Pt(II)'s σ-type orbital.

3.5.5. Concluding remarks of chapter 3.5

The author studied the electronic states of $Cr_2(pyphos)_4$ (**6a**) and $Pt_2Cr_2(pyphos)_4(CH_3)_4$ (**7a**) by using J_{ab} values. The calculated values of **6a** and **7a** did not reproduce experimental J_{ab} presuming

Cr(II). Therefore there was a possibility of another oxidation states of Cr in those complexes. The author, next, carried out the J_{ab} calculations by using naked models, presuming Cr(III). $\pi^4\delta^2$ triple bonded state gave smallest J_{ab} than $\sigma^2\pi^2\delta^2$ and $\sigma^2\pi^4$ in the **6b** model. This $\pi^4\delta^2$ triple bonded state seemed to be possible candidate for the electronic states of **6a**. In the **7b** model, electronic state which involved $\pi^4\delta^2$ triple bonded Cr(III)-Cr(III) core gave slightly positive J_{ab} values by APUHF calculation. This was good agreement with experimental result, which showed very small J_{ab}. The electronic state which involved $\pi^4\delta^2$ triple bonded Cr(III)-Cr(III) core also seemed to be possible candidate for the electronic states of **7a**. NO analysis and the instability analysis were performed to explain its peculiar J_{ab}. The π bonding orbitals of Cr(III)-Cr(III) core and the orbital of Pt(II) were conjugated. Instability values of the π type conjugated orbitals and the δ bonding orbital of Cr(III)-Cr(III) core were more than 95% and π orbitals of Cr(III)-Cr(III) core were unstabilized by the existance of Pt(II). The instability of these π conjugations seemed to contribute to the small J_{ab} values of **7c**. From these results, The author found that Cr-Cr σ bond have great influence on J_{ab}. By withdrawing electrons from σ orbital of Cr(II)-Cr(II) quadruple bond, J_{ab} values in di-chromium complexes decreases significantly. In this study, The author demonstrated that calculated J_{ab} clued us in about the unknown electronic states of complexes.

3.6 Concluding remarks of chapter three

In this chapter, the author applied MEDF method to polynuclear systems that had linearly aligned metal chain to elucidate their electronic states. Their electronic states were investigated in terms of magnetic interactions between spins by using effective exchange integrals (J_{ab}) values. First, the author investigated Cotton type complex; $Cr_2(O_2CCH_3)_4(H_2O)_2$ as a smallest unit of polynuclear complexes. J_{ab} values calculated MEDF could reproduce not only experimental J_{ab} value for full model but also calculated J_{ab} value by APUCCSD(T) for naked Cr(II) dimer model. In this way, it was verified that MEDF was a effective method to these di-Cr(II) systems. In this complex, the path of magnetic interaction was analyzed quantitatively by separating J_{ab}(through-ligand) and J_{ab}(direct meta-metal interaction) by using DNO-CASCI{8,8} together with MEDF. It was found that through-ligand interaction was smaller than direct interaction but not negligible. Natural orbital analyses and their instability was examined to explain magnetic interaction in terms of 'orbital'. The tendency of stability was $\sigma > \pi > \delta$. δ orbital was almost dissociated and it seemed that electrons in δ orbital had localized spin structures. The σ orbitals were delocalized to axial ligands and were easily affected by them. And J_{ab} values were also closely related to the axial ligands because σ orbitals were strongly contributed to the magnetic interactions. Therefore the author proposed the possibility of chemical control of Jab by axial ligands.

Next, the author examined tetra-Cr(II) system; $[Cr(II)_4(DpyF)_4Cl_2]^{2+}$ as a reliable model to polynuclear complexes. Several Jab interactions were presumed and estimated by MEDF method. The calculated J_{ab} values were analyzed in terms of interaction path. Natural orbital and its instability analyses were carried out and it was found that δ orbitals was unexpectedly unstable in comparison with $Cr_2(O_2CCH_3)_4(H_2O)_2$. The author found that δ orbitals were strongly affected by spiral structure of equatorial ligands. Therefore unexpected instability of δ orbital occurred.

Finally, the electronic states of linearly aligned di- and tetra-metal complex synthesized by Mashima et al; $Cr_2(pyphos)_4$ where (pyphos=6-(diphenylphosphino)-2-pyridonate), $Pt_2Cr_2(pyphos)_4(CH_3)_4$, respectively was examined. The experimental J_{ab} values of them was small in comparison with usual di-Cr(II) complexes and calculated J_{ab} results presuming Cr(II) also could not reproduced experimental results. The author examined possibility of Cr(III). The magnetic interaction between Cr(III) was drastically decreased when $\pi 4\delta 2$ configuration was presumed. This $\pi^4\delta^2$ configuration of Cr(III)-Cr(III) seemed that one of the possibility of $Cr_2(pyphos)_4$ and

$Pt_2Cr_2(pyphos)_4(CH_3)_4$. In this way, the procedure that investigate the unknown electronic state of polynuclear complexes using experimental J_{ab} value as a clue, was unique and promising to the analyses of these complexes of strongly correlated electron systems.

References of chapter three

[1] Cotton, F. A.; Daniels, L. M.; Murillo C. A.; Wang, X. *Chem. Commun.* **1998**, 39.

[2] (a) Mashima, K.; Tanaka, M.; Tani, K.; Nakamura, A.; Takeda, S.; Mori, W.; Yamaguchi, K. *J. Am. Chem. Soc.* **1997**, *119*, 4307. (b) Tanaka, M.; Mashima, K.; Nishino, M.; Takeda, S.; Mori, W.; Tani, K.; Yamaguchi, K.; Nakamura, A.; *Bull. Chem. Soc. Jpn.* **2001**, *74*, 67.

[3] Prater, M.E.; Pence, L.E.; Clérac, R.; Finniss, G.M.; Campana, C.; Auban-Senzier, P.; Jérome, D.; Canadell E.; Dunber, K.R. *J. Am. Chem. Soc.* **1999**, *121*, 8005.

[4] Lai, S-Y.; Lin, T-W.; Chen, Y-H.; Wang, C-C.; Lee, G-H.; Yang, M-h.; Leung M-k.; Peng, S-M. *J. Am. Chem. Soc.* **1999**, *121*, 250. (b) Wang, C-C.; Lo, W-C.; Chou, C-C.; Lee, G-H.; Chen, J-M.; Peng, S-M. *Inorg. Chem.* **1998**, *37*, 4059.

[5] Cotton, F. A.; Walton, R. A. Multiple Bonds between Metal Atoms; Clarrendon Press: Oxford, 1993, and references therein.

[6] Kishida, H.; Matshhzaki, H.; Okamoto, H.; Manabe, T.; Yamashita, M.; Taguchi, Y,; Tokura, Y. *Nature* **2000**, *405*, 929

[7] Chisholm, M. H., *Acc. Chem. Res.* **2000**, *33*, 53.

[8] Cotton, F. A.; Chen,H.; Daniels, L. M.; Feng, X. *J. Am. Chem. Soc.* **1992**, *114*, 8980.

[9] Andersson, K.; Bauschlicher Jr, C. W.; Persson, B. J.; Roos, B. O. *Chem. Phys. Lett.* **1996**, *257*, 238.

[10] Tatewaki, H.; Huzinaga, S. *J. Chem. Phys.* **1979**, *71*, 4339.

[11] Hay, P.J. *J. Chem. Phys.* **1977**, *66*, 4377.

[12] Dupuis, M.; Marguez, A.; Davidson, E. R. "HONDO95.3 from CHEMSTATION", (1995) IBM Corporation, Neighborhood Road, Kingston, NY.12401.

[13] Gaussian 98, Frisch,M,J., Trucks,G.W., Schlegel,H.B., Scuseria,G.E., Robb,M.A., Cheeseman,J.R., Zakrzewski,V.G., Montgomery,J.A.,Jr., Stratmann,R.E., Burant,J.C., Dapprich,S., Millam,J.M., Daniels,A.D., Kudin,K.N., Strain,M.C., Farkas,O., Tomasi,J., Barone,V., Cossi,M., Cammi,R., Mennucci,B., Pomelli,C., Adamo,C., Clifford,S., Ochterski,J., Petersson,G.A., Ayala,P.Y., Cui,Q., Morokuma,K., Malick,D.K., Rabuck,A.D., Raghavachari,K., Foresman,J.B., Cioslowski,J., Ortiz,J.V., Stefanov,B.B., Liu,G., Liashenko,A., Piskorz,P., Komaromi,I., Gomperts,R., Martin,R.L., Fox,D.J., Keith,T., Al-Laham,M.A., Peng,C.Y., Nanayakkara,A., Gonzalez,C., Challacombe,M., Gill,P.M.W., Johnson,B., Chen,W., Wong,M.W., Andres,J.L., Gonzalez,C., Head-Gordon,M., Replogle,E.S. and J. A. Pople, Gaussian, Inc., Pittsburgh PA, 1998.

[14] (a) Nishino, M.; Yamanaka, S.; Yoshioka, Y.; Yamaguchi, K. *J. Phys. Chem. A.* **1997**, *101*, 705. (b) Kitagawa, Y.; Soda, T.; Onishi, T.; Takano, Y.; Nishino, M.; Yoshioka Y.; Yamaguchi, K. *Mol. Cryst. Liq. Cryst.* **2000**, *343*, 145.

[15] (a) Kitagawa, Y.; Soda, T.; Shigeta, Y.; Yamanaka, S.; Yoshioka Y.; Yamaguchi, K. *Int. J. Quant. Chem.* **2001**, *84*, 592. (b) Kitagawa, Y.; Kawakami K.; Yamaguchi, K. *Mol. Phys.* **2002**,

100, 1829.

[16] Yamaguchi,K.; Kawakami, T.; Takano, Y.; Kitagawa, Y.; Yamashita, Y.; Fujita, H. *Int.J.Quant.Chem.* **2002**, *90*, 370.

[17] (a) Nagao, H.; Nishino, M.; Shigeta, Y.; Soda, T.; Kitagawa, Y.; Onishi, T.; Yoshioka, Y.; Yamaguchi, K. *Coord. Chem. Rev.* **2000**, *198*, 265. (b) Soda, T.; Kitagawa, Y.; Onishi, T.; Takano, Y.; Shigeta, Y.; Nagao, H.; Yoshioka, Y.; Yamaguchi, K. *Chem. Phys. Lett.* **2000**, *319*, 223.

[18] (a) Kawakami, T.; Yamanaka, S.; Yamada, S.; Mori, W.; Yamaguchi, K. In *Molecular-Based Magnetic Materials, Theory, Technique and Applications;* Turnbull, M. M.; Sugimoto, T.; Thompson, L. K. Eds.; ACS Symposium Series 644; American Chemical Society: Washington, DC, 1996; p30. (b) Yamaguchi, K. In *Self-Consistent Field, Theory and Applications*; Carbeó, R.; Klobukowski, M. Eds.; Studies in physical and theoretical chemistry 70; Elsevier: Amsterdam-Oxford-New Tork-Tokyo, 1990; p727.

[19] (a) Nagao, H.; Nishino, M.; Shigeta, Y.; Soda, T.; Kitagawa, Y.; Onishi, T.; Yoshioka, Y.; Yamaguchi, K. *Coord. Chem. Rev.* **2000**, *198*, 265. (b) Soda, T.; Kitagawa, Y.; Onishi, T.; Takano, Y.; Shigeta, Y.; Nagao, H.; Yoshioka, Y.; Yamaguchi, K. *Chem. Phys. Lett.* **2000**, *319*, 223.

[20] (a) Ginsberg, A. P. *J. Am. Chem. Soc.* **1980**, *102*, 111, (b) Noodleman, L. *J. Chem. Phys.* **1981**, *74*, 5737, (c) Noodleman, L.; Davidson, E. R. *Chem. Phys.* **1985**, *109*, 131

[21] (a) Bencini, A.; Totti, F.; Daul, C. A.; Doclo, K.; Fantucci, P.; Barone, V. *Inorg. Chem.* **1997**, *36* 5022, (b) Ruiz, E.; Cano, J.; Alvarez, S.; Alemany, P. *J. Comp. Chem.* **1999**, *20*, 1391

[22] Takatsuka, K.; Fueno, T.; Yamaguchi, K. *Theoret.Chem.Acta.* **1978**, *48*, 175

[23] Takano, Y.; Kitagawa, Y.; Onishi, T.; Yoshioka, Y.; Yamaguchi, K.; Koga N.; Iwamura, H. *J. Am. Chem. Soc.* **2002**, *124*, 450.

[24] (a) Mitani, M.; Takano, Y.; Yoshioka, Y.; Yamaguchi, K. *J. Chem. Phys.* **1999**, *111*, 1309. (b) Mitani, M.; Yamaki, D.; Takano, Y.; Kitagawa, Y.; Yoshioka, Y.; Yamaguchi, K. *J. Chem. Phys.* **2000**, *113*, 10486.

[25] Kitagawa, K.; Soda, T.; Onishi, T.; Takano, Y.; Nishino, M.; Yoshioka, Y.; Yamaguchi, K. *Mol. Cryst. Liq. Cryst.* 2000, 343, 463.

[26] Cotton, F. A.; Chen, H. ; Daniels, L. M.; Feng, X. *J. Am. Chem. Soc.* **1992**, *114*, 8980

[27] Ramílez, J. C.; Rodolfo, C. S.; Esquivel, O.; Sagar, P. R.; *Phys. Rev. B.* **1997**, *56*, 4477.

[28] Yamaguchi, K. in Organometalic Conjugation, (Eds, Nakamura, A.; Ueyama, N.; Yamaguchi, K. Kodansha Scientific, 2000)

[29] Weder, J. E.; Hambley, T. W.; Kennedy, B.J.; Lay, P.A.; MacLachelan, D.; Bramley,, C.D.Delfs, R.; Murray, K.S.; Moubaraki, B.; Warwick, B.; Biffin, J.R.; Regtop, H.L. *Inorg. Chem.* **1999**, *38*, 1736

Table 3.1

Cotton type complex models; $Cr(II)_2L_4X_2$ that were used here and their Cr(II)-Cr(II) distances where L is bridging equatorial ligand and X is axial ligand.

Moldel	Cr(II)-Cr(II) distance	L	X
1a	2.362Å	CH_3COO^-	H_2O
1b	2.362Å	none	none
1c	2.362Å	CH_3COO^-	none
2a	2.287Å	CH_3COO^-	CH_3COOH
2b	2.287Å	CH_3COO^-	none

Table 3.2

Effective exchange integrals (J_{ab}) values[a] of $Cr_2(O_2CCH_3)_4(H_2O)_2$ (**1a**) and its naked dimer model (**1b**)

Method	**1a**	**1b**
UHF	-281	-151
MEDF	-520	-299
UB3LYP	-733	-402
UBLYP	-1042	——[b]
UCCSD(T)		-210
Expt.	-490	

a) in cm^{-1}, b) Appropriate electronic state could not obtained by UBLYP

Table 3.3

The effective exchange integrals (J_{ab}) values[a] of $Cr_2(O_2CCH_3)_4(H_2O)_2$ (**1a**) calculated by several methods[b]

$J_{ab}(1)$	$J_{ab}(2)$	$J_{ab}(3)$
-529	-423	-520

a) in cm^{-1}, b) see text

Table 3.4

Occupation numbers, effective bond orders of low spin state for $Cr_2(O_2CCH_3)_4(H_2O)_2$ (**1a**) and its naked model (**1b**) calculated by using MEDF method

Orbital	Occupation number		Effective bond order	
	1a	**1b**	**1a**	**1b**
δ	1.075	1.022	0.075	0.022
π(2)	1.161	1.149	0.161	0.149
π(1)	1.162	1.149	0.162	0.149
σ	1.455	1.282	0.455	0.282

Table 3.5

Effective exchange integrals (J_{ab}) values[a] of $Cr_2(O_2CCH_3)_4(H_2O)_2$ (**1a**) calculated by CASCI {8,8} method using DFT natural orbitals (DNOs)

DNO CASCI	J_{ab}
J_{ab}(S-T)	-327
J_{ab}(T-Q)	-334
J_{ab}(S-Q)	-332

a) in cm^{-1}

Table 3.6

Effective exchange integrals (J_{ab}) values[a] of $Cr_2(O_2CCH_3)_4(H_2O)_2$ (**1a**), its without axilai ligand model (**1c**), The model taken from crystal of periodically aligned $\{Cr_2(O_2CCH_3)_4\}_n$ (**2a**) and its without ligand model (**2b**) calculated by MEDF.

Model	J_{ab}
1a	-520 (-490[b])
1c	-467
2a	-620
2b	-574

a) in cm-1, b) experimental value

Table 3.7

Cotton type complex models; $M(II)_2L_4X_2$ that were used here and their M(II)-M(II) distances, where M is metal ion, L is bridging equatorial ligand and X is axial ligand, respectively.

model	M	L	X	distance[a)]
1a	Cr	CH_3COO^-	H_2O	2.362
3a	Cu	CH_3COO^-	H_2O	2.618
4a	Mo	CH_3COO^-	none	2.089

a) in Å

Table 3.8

Effective exchange integrals (J_{ab}) values[a] of naked Cr(II) dimer (**1a**), Cu(II) dimer (**3b**) calculated by MEDF[b)]

Method	Models	
	1b	**3b**
APUHF	-151	-2.7
MEDF	-299	-4.2
APUB3LYP	-402	-6.3
APUCCSD(T)	-210	-3.7

a) in cm^{-1}, b) scheme1 c_1=0.5 were used

Table 3.9

The Effective exchange integrals[a)] of neked dimer models; **1a**, **3a** and **4a** calculated by using several methods.

Method	Model		
	1a	**3a**	**4a**
APUHF	-281	-21	-2702
MEDF[b)]	-520	-80	-3736
APUB3LYP	-733	-266	-4378
CAS CI [m,m]	-327[c)]	-11[d)]	-4864[e)]
Expt.	-490.[f)]	-142.[g)]	

a) cm^{-1}, b) scheme 1 c_1=0.5, c) m=8 using MEDF-NO of scheme1 c_1=0.5, d) m=2 using UHF-NO, e) m=8 using UB3LYP-NO, f) in ref. 5, g) in ref. 29

Table 3.10

The instability value[a)b)] of several metal-acetate complexes

metal	distance[Å]	instability	
		naked dimer	complex
Mo(II)	2.089		22.3
Cr(II)	2.362	81.2	75.2
Cu(II)	2.618	99.7	102.3

a) estimated by using Yamaguchi's method i.e. Y value, b) in %

Table 3.11

Effective exchange integrals (J_{ab}) values[a] between Cr(II) ions in $[Cr_4(DpyF)_4Cl_2]^{2+}$ (**5a**) and its naked Cr(II) tetramer model (**5b**) calculated by MEDF method

	R[b]	**5a**	**5b**
J_1	2.013 (2.002)	-1260	-1125
J_2	2.726	-180.2	-39.2
J_3	4.739	-30.4	+4.7

a) in cm^{-1}, b) Cr(II)-Cr(II) distance[Å]

Table 3.12

Occupation numbers, effective bond orders and of $[Cr_4(DpyF)_4Cl_2]^{2+}$ (**5a**) and its Cr(II) naked tetramer model (**5b**) calculated by using MEDF method

Orbital[a]	Occupation number		Effective bond order	
	5a	**5b**	**5a**	**5b**
δ_2	1.057	1.054	0.057	0.054
δ_1	1.134	1.061	0.134	0.061
π_4	1.357	1.300	0.357	0.300
π_3	1.357	1.300	0.357	0.300
π_2	1.403	1.349	0.403	0.349
π_1	1.403	1.349	0.403	0.349
σ_2	1.486	1.459	0.486	0.459
σ_1	1.659	1.563	0.659	0.563

a) see Figure12(a)-(c)

Table 3.13

Effective exchange integrals (J_{ab})[a] between Cr(II) ions in $Cr_2(pyphos)_4$ (**6a**) and its naked core model (**6b**)

Method	**6a**	**6b**
APUHF	-739	-532
MEDF[b]	-1202	-870
APUMP2		-607
APUMP4(SDTQ)*		-644
APUCCSD(T)		-831
UNO-CASCI[8,8]		-656
Expt.	-340[c], -520[d]	

a) in cm^{-1}, b) c_i=0.5 in eq (2.17b), c) SQUID value in ref [2], d) NMR value in ref [2]

Table 3.14

Effective exchange integrals (J_{ab})[a] between Cr(II) ions in $Pt_2Cr_2(pyphos)_4(CH_3)_2$ (**7a**), its naked Pt-Cr-Cr-Pt core model(**7b**) and its naked Cr-Cr core model (**7c**)

Method	**2a**	**2b**	**2c**
APUHF	-185	-103	-136
MEDF[b]	-407	-178	-275
APUMP2		-126	-155
APUMP4(SDTQ)		-135	-164
APUCCSD(T)			-189
Expt.	-29[c], -10[d]		

a) in cm^{-1}, b) c_i=0.5 in eq (2.17b), c) SQUID in ref [2], d) NMR in ref [2]

Table 3.15

Effective exchange integrals (J_{ab})[a] between Cr(II) ions of several electronic states in naked core model (**6b**)

Method	$\sigma^2\pi^4$	$\sigma^2\pi^2\delta^2$	$\pi^4\delta^2$
APUHF	-629	-423	-263
MEDF[b]	-1018	-679	-423
APUCCSD(T)	-527		-278
APUMP2	-678	-449	-347
APUMP4(STDQ)	-705	-465	-285
Expt. (**6a**)		-340[c], - 520[d]	

a) in cm^{-1}, b) c_i=0.5 in eq (2.17b), c) SQUID in ref [2], d)NMR in ref [2]

Table 3.16

Effective exchange integrals (J_{ab})[a)] between Cr(III) ions of several electronic states in naked Pt-Cr-Cr-Pt core model (**7b**) and naked Cr-Cr core model (**7c**) of $\sigma^2\pi^2\delta^2$ and $\pi^4\delta^2$ states

Method	$\sigma^2\pi^2\delta^2$		$\pi^4\delta^2$	
	(**7b**)	(**7c**)	(**7b**)	(**7c**)
APUHF	-74	-77	10	-33
APUMP2	-83	-82	-17	-35
APUMP4(SDTQ)	-84	-84	-31	-36
Expt.		-29		

a) in cm^{-1}, 2) SQUID value of complex (**7a**) in ref[2]

Table 3.17

Occupation numbers and instability values[a)b)] I_i' of magnetic orbitals of **7b**, where Cr(III)-Cr(III) core was $\pi^4\delta^2$ configuration calculated by UHF.

Orbital	Occupation Number	Instability value
HOMO	1.00544	99.6 (99.5)[c)]
HOMO-1	1.02070	98.5 (96.5)[c)]
MOHO-2	1.03189	97.7 (96.5)[c)]
MOHO-3	1.04975	96.3
HOMO-4	1.06322	95.3
MOHO-5	1.98730	1.55
HOMO-6	1.99096	1.10
MOHO-7	1.99920	0.0977
MOHO-8	1.99964	0.0440
HOMO-12	1.99998	0.00244
HOMO-13	1.99999	0.00122

a) in [%], b) Information entropy was used c) instability values of **7c** were written in parentheses.

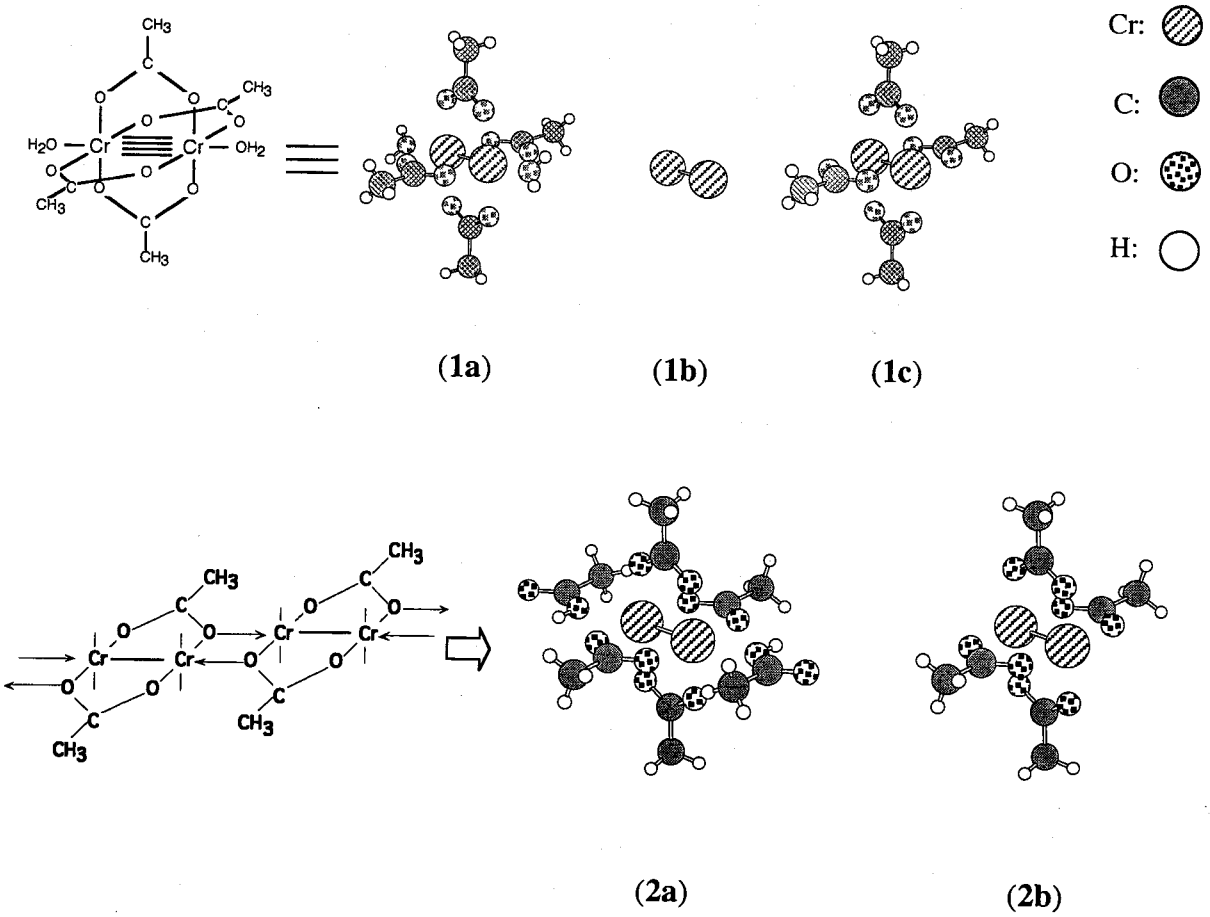

Figure 3.1

Calculated models. Dichromium(II) tetraacetate dihydrate $Cr_2(O_2CCH_3)_4(H_2O)_2$ (**1a**), its naked Cr(II) dimer model (**1b**) and model without axial H_2O ligand from **1a** (**1c**). The model **2a** and **2b** are taken from crystal of periodically aligned $\{Cr_2(O_2CCH_3)_4\}_n$. **2a** included axial acetates and **2b** is without axial acetates.

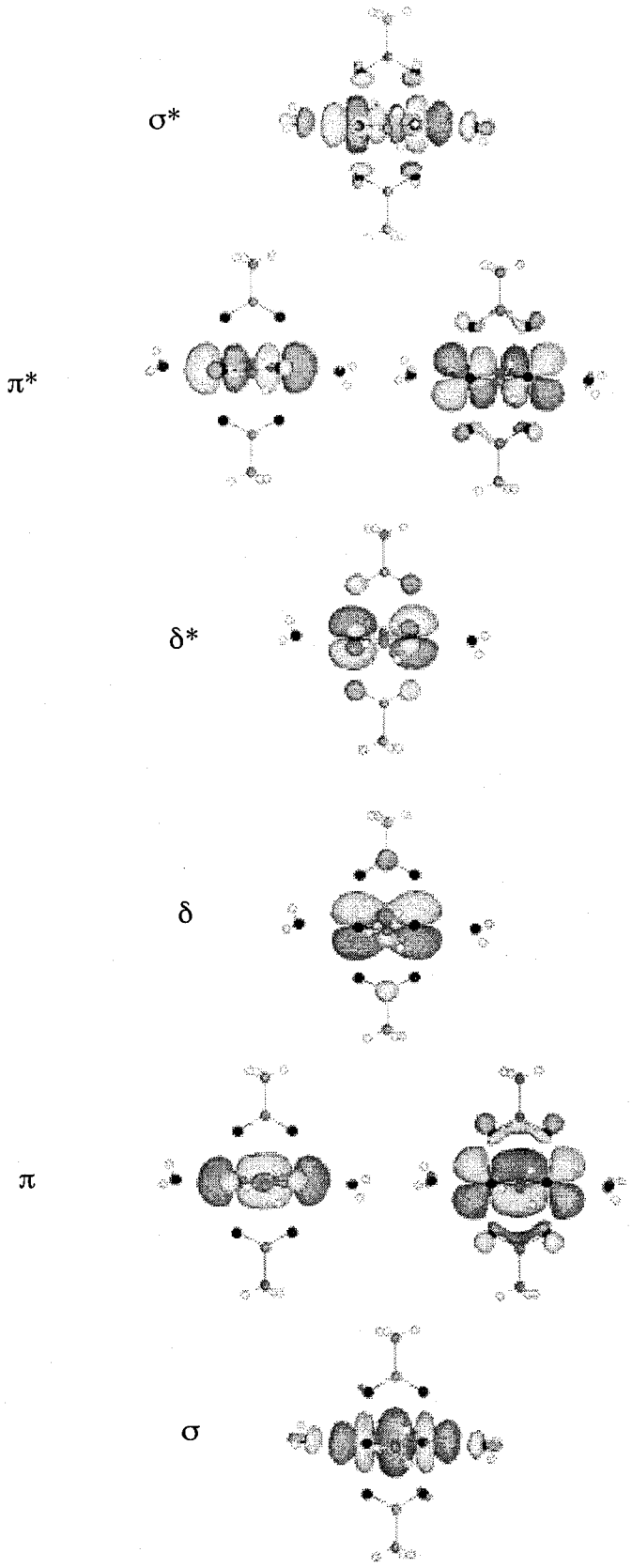

Figure 3.2
Natural orbitals (NOs) of magnetic orbitals of $Cr_2(O_2CCH_3)_4(H_2O)_2$ (**1a**) by using

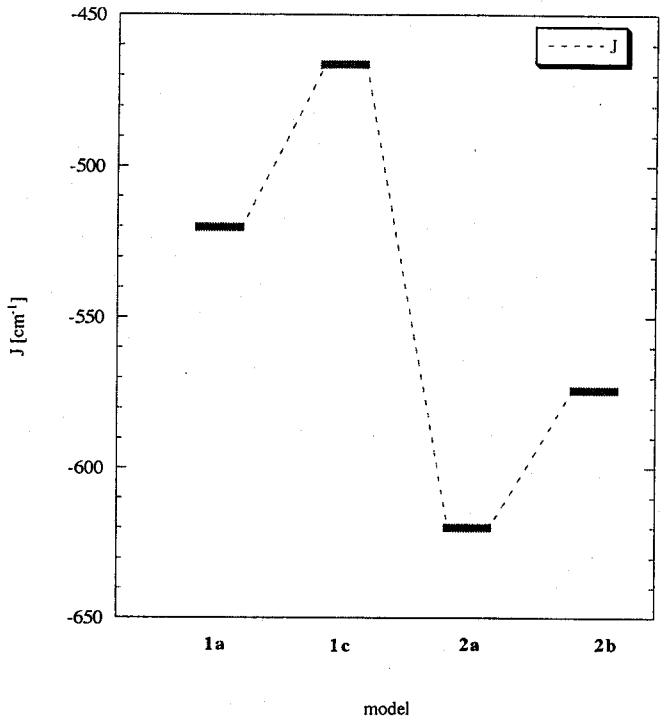

Figure 3.3
Effective exchange integrals (J_{ab}) values of each model calculated by MEDF

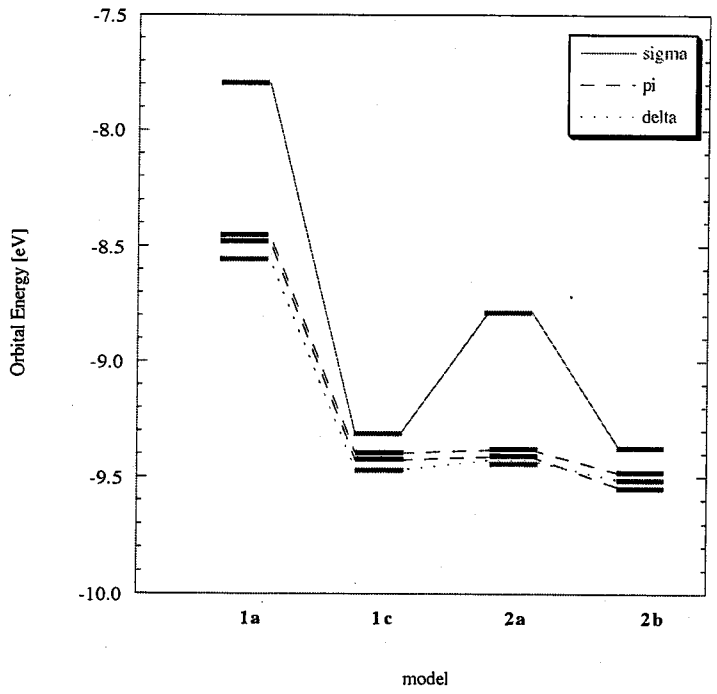

Figure 3.4
Orbital energies of valence orbitals of each model calculated by MEDF

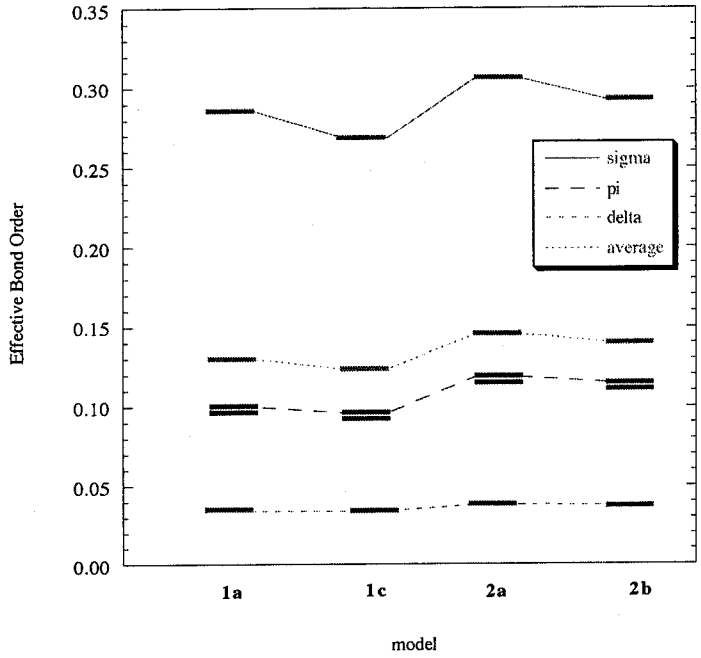

Figure 3.5
Effective bond orders (b_i) of valence orbitals and their average value of each model calculated by MEDF

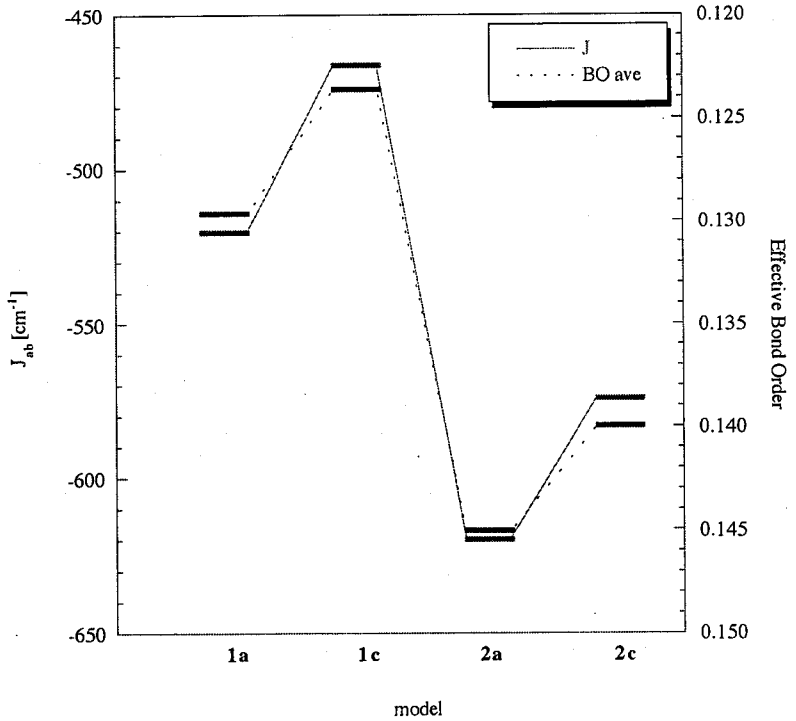

Figure 3.6
Figure of the relation between J_{ab} value and averaged effective bond order for each model calculated by MEDF

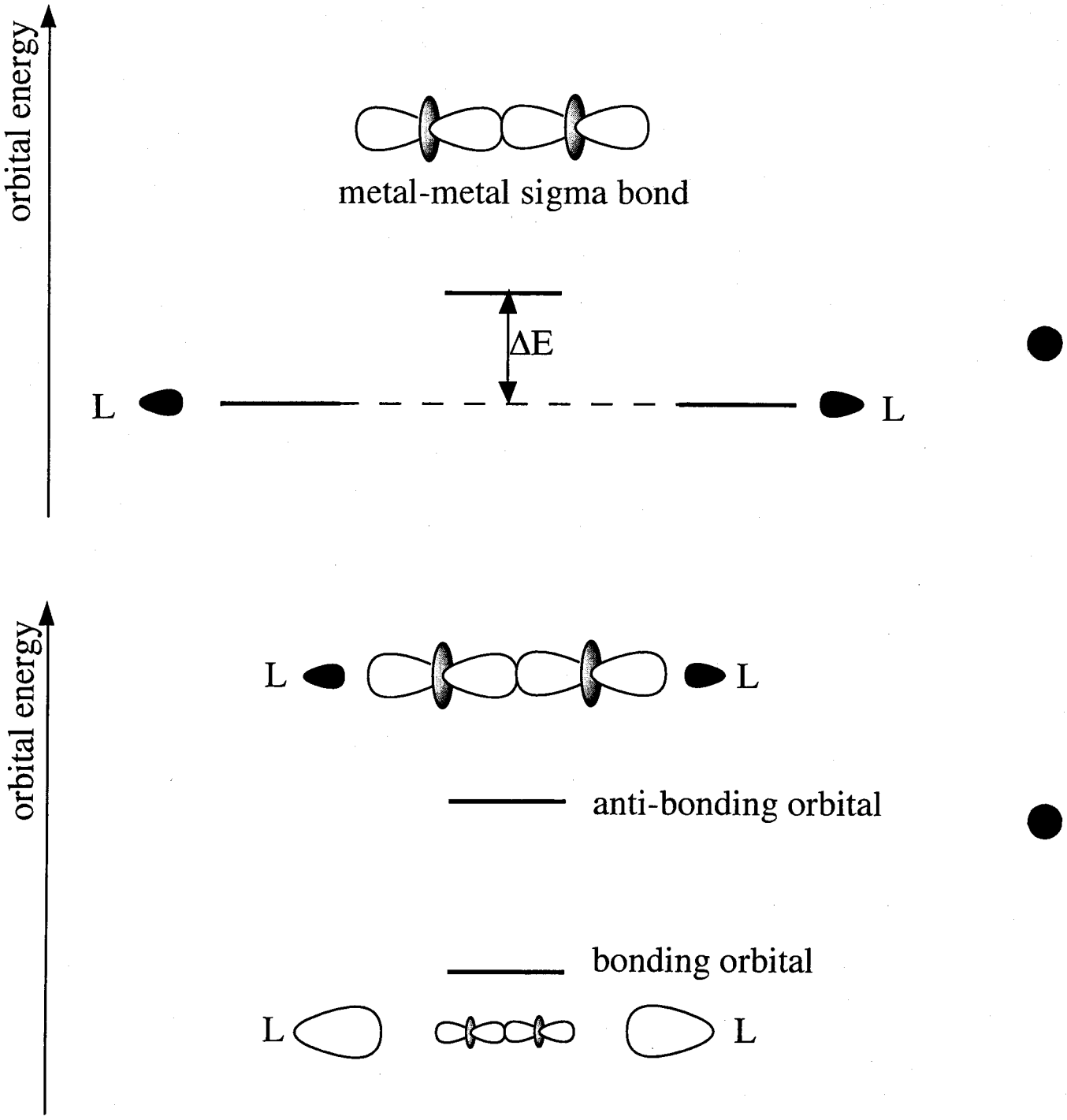

Figure 3.7
The illustration of the relation between metal-metal direct sigma bond and lonepair of axial ligands

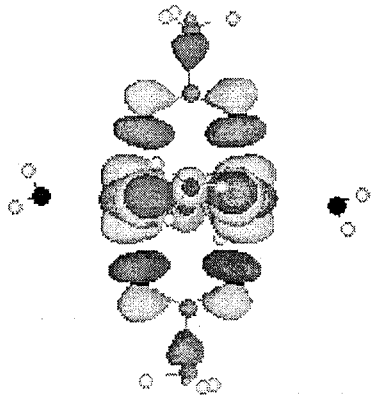

Lowest unoccupied natural orbital

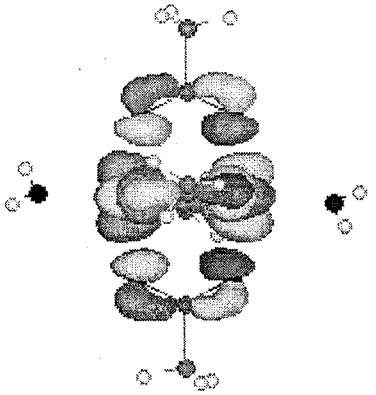

Highest occupied natural orbital

Figure 3.8 (a)
Natural orbitals (NOs) of magnetic orbitals of $Cu_2(O_2CCH_3)_4(H_2O)_2$ (**3a**) calculated by using MEDF

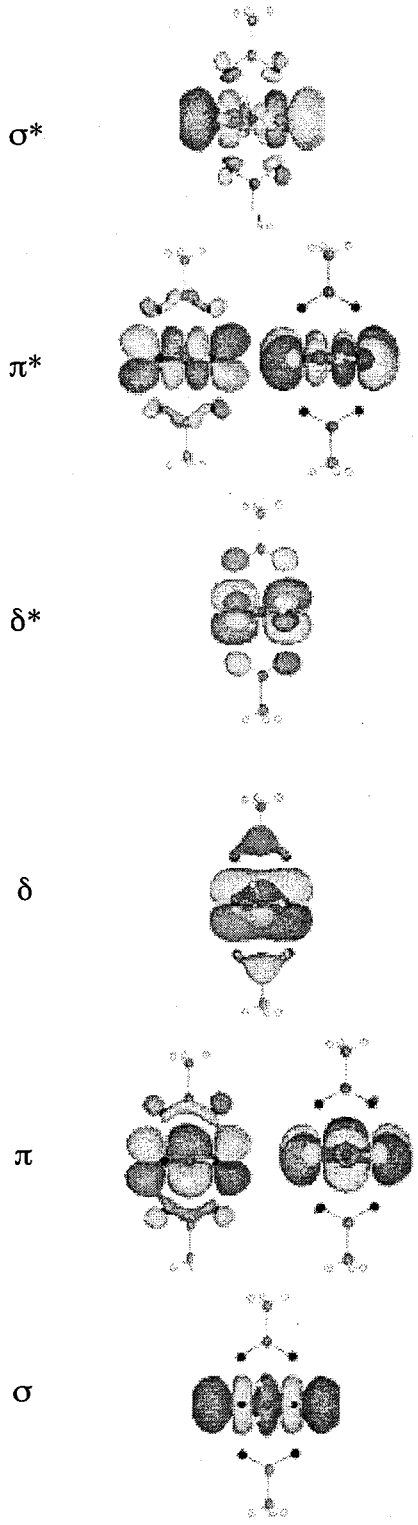

Figure 3.8 (b)
Natural orbitals (NOs) of magnetic orbitals of $Mo_2(O_2CCH_3)_4$ (**4a**) calculated by using MEDF

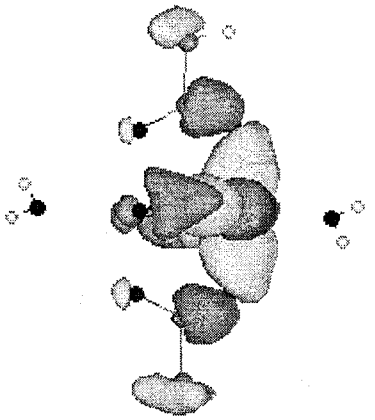

LUMO

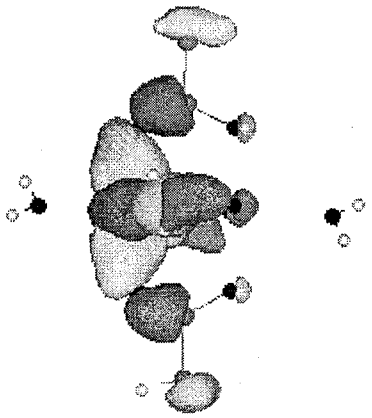

HOMO

Figure 3.9
Molecular orbitals of $Cu_2(O_2CCH_3)_4(H_2O)_2$ calculated by UHF.

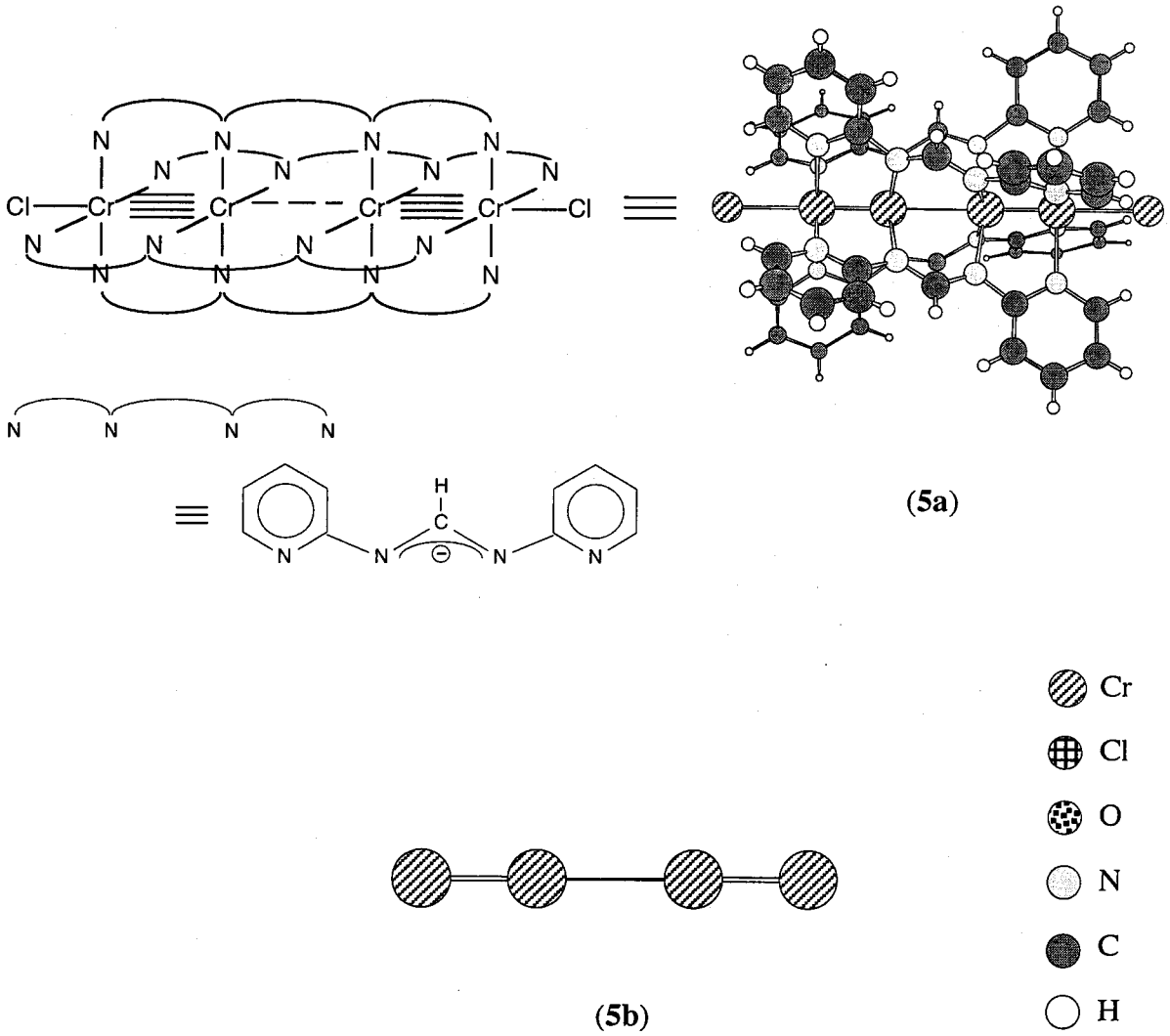

Figure 3.10
$[Cr(II)_4(DpyF)_4Cl_2]^{2+}$ complex model (**5a**) , its naked Cr(II) tetramer model (**5b**).

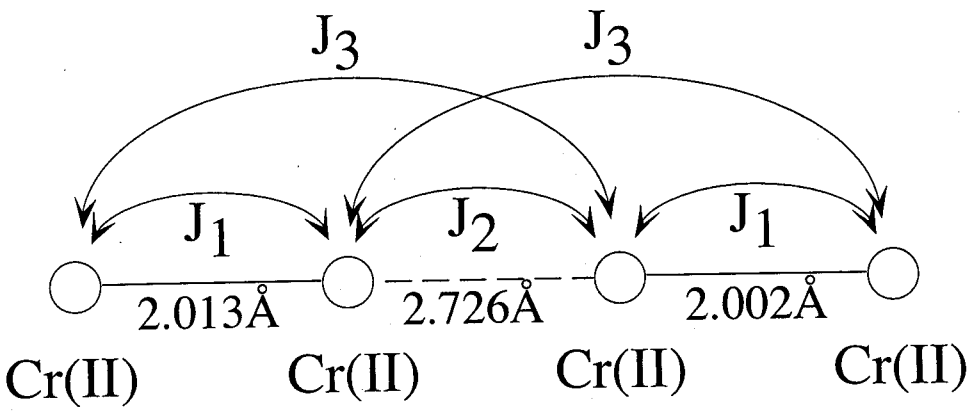

(a)

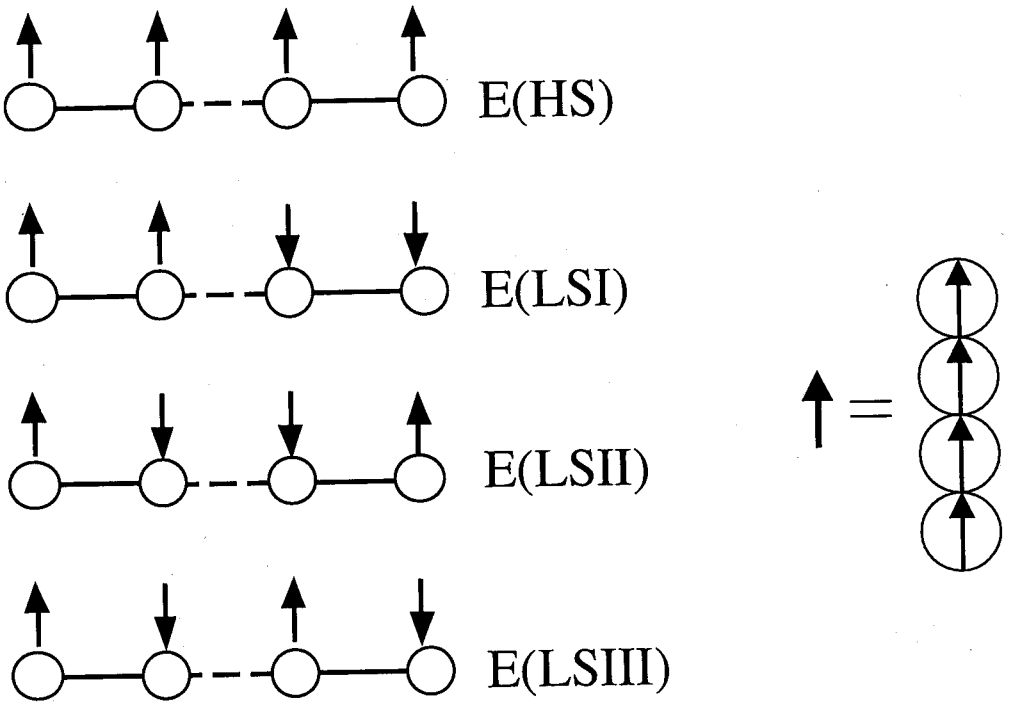

(b)

Figure 3.11
(a) The notation for J_1, J_2 and J_3 in model **5a** and **5b**, (b) The calculated four states to obtain J_{ab} value by eq. 2.26, where one bold arrow means four electron spins on one Cr(II) ion.

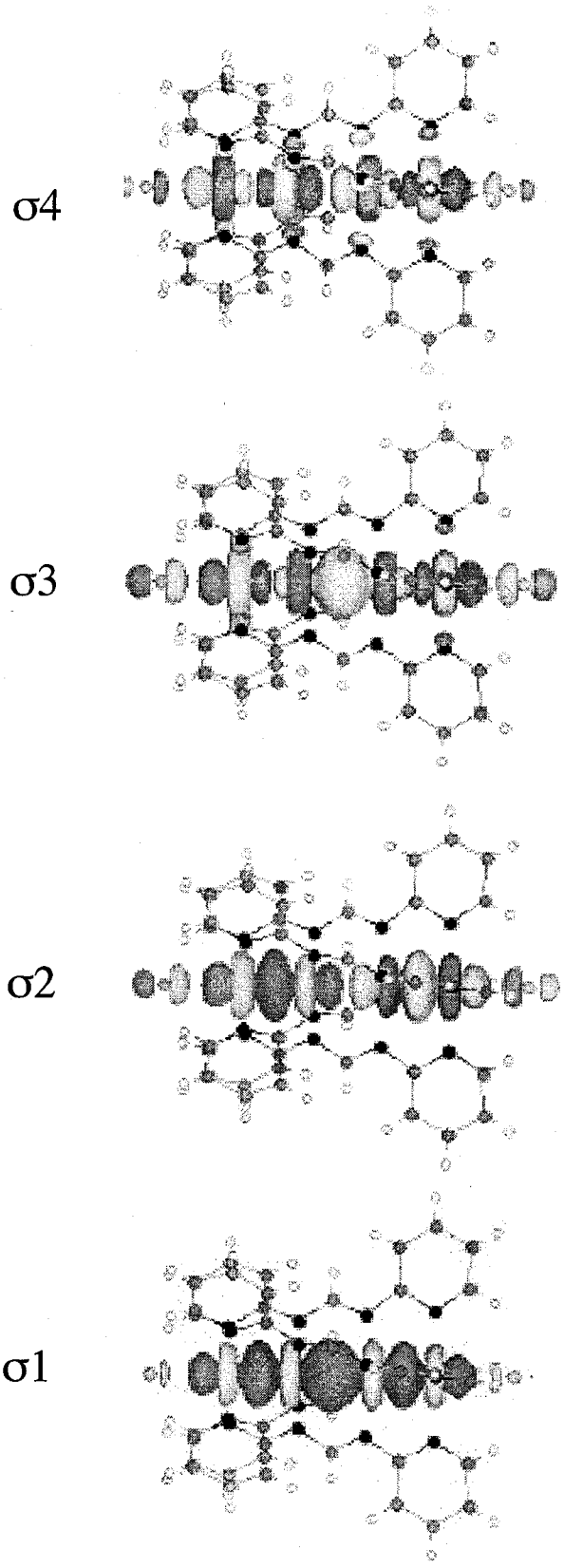

Figure 3.12 (a)
The natural orbitals of sigma orbital of model **5a** calculated by using MEDF.

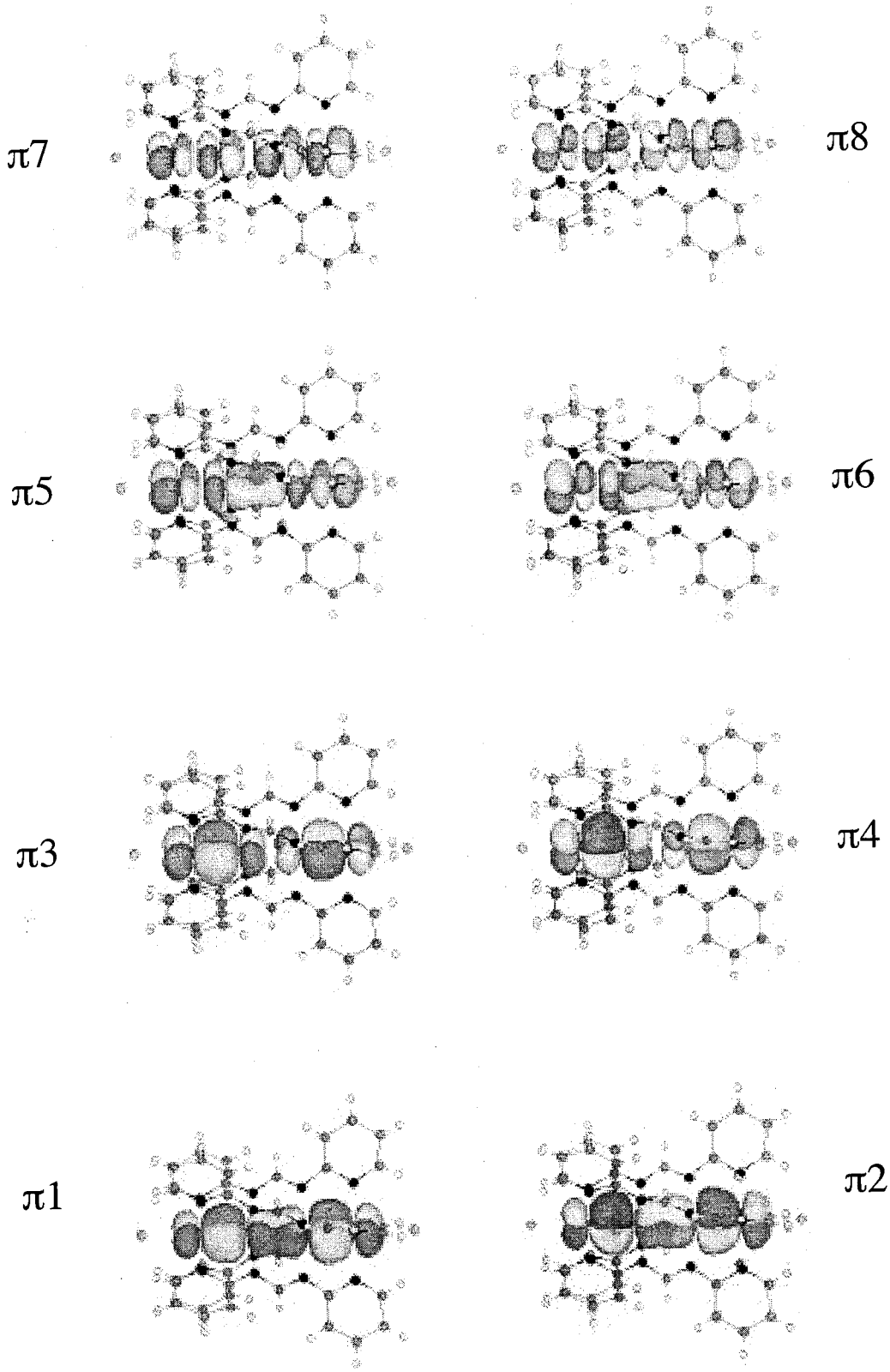

Figure 3.12 (b)
The natural orbitals of pi orbitals of model **5a** calculated by using MEDF.

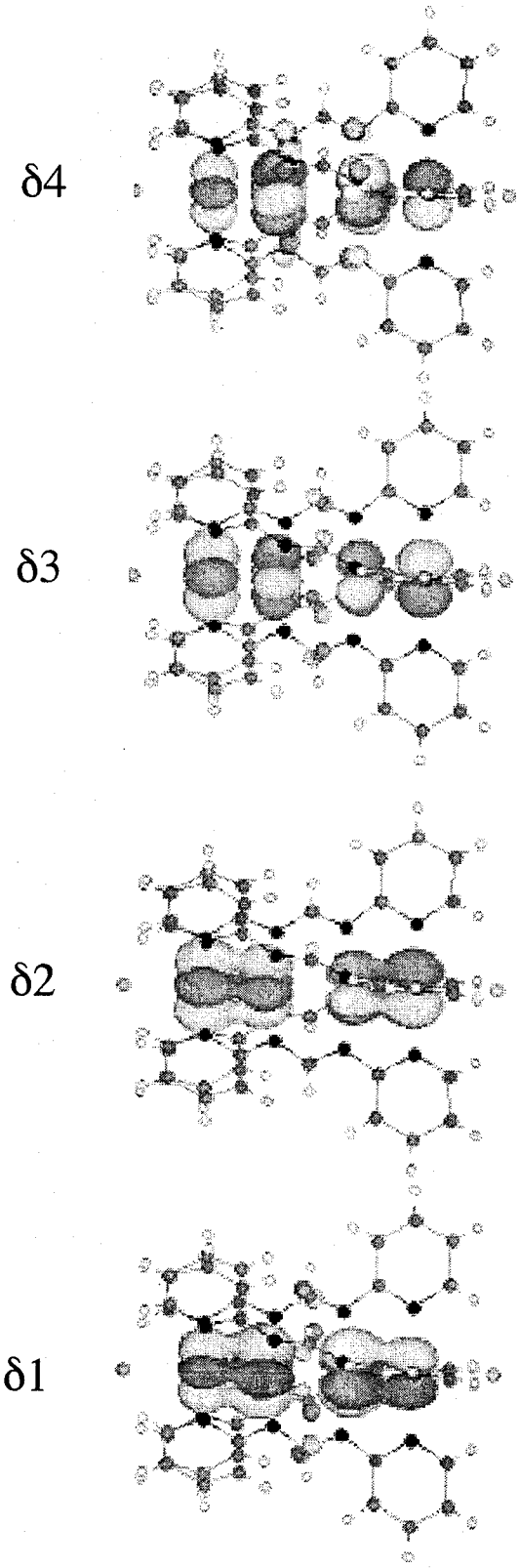

Figure 3.12 (c)
The natural orbitals of delta orbital of model **5a** calculated by using MEDF.

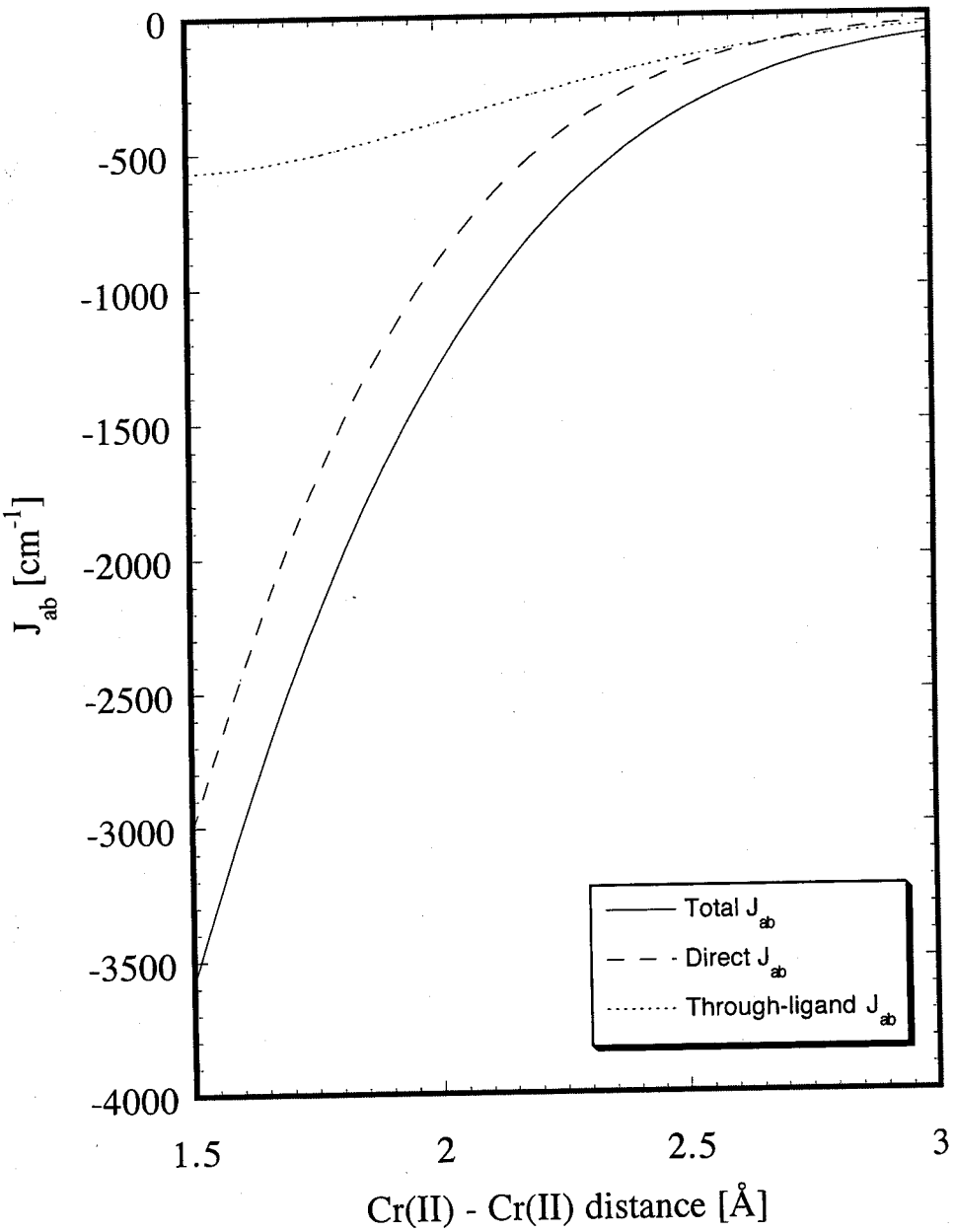

Figure 3.13

J_{ab} curves by fitteng function (eq 3.4.5 in the text). Fiiting parameters for total Jab were p = -14144 and q = 0.68632, while for direct J_{ab} were p = -13229 and q = 0.58023. J_{ab} values of through-ligand were estimated by eq.3.2.3 in the text.

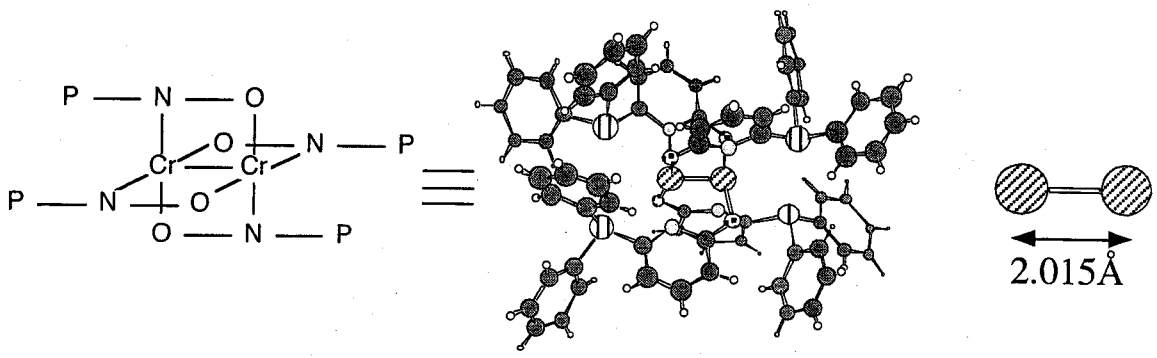

(6a) **(6b)**

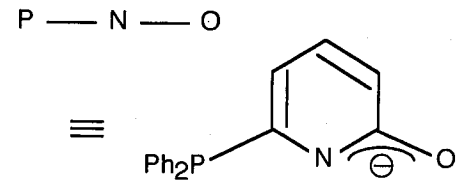

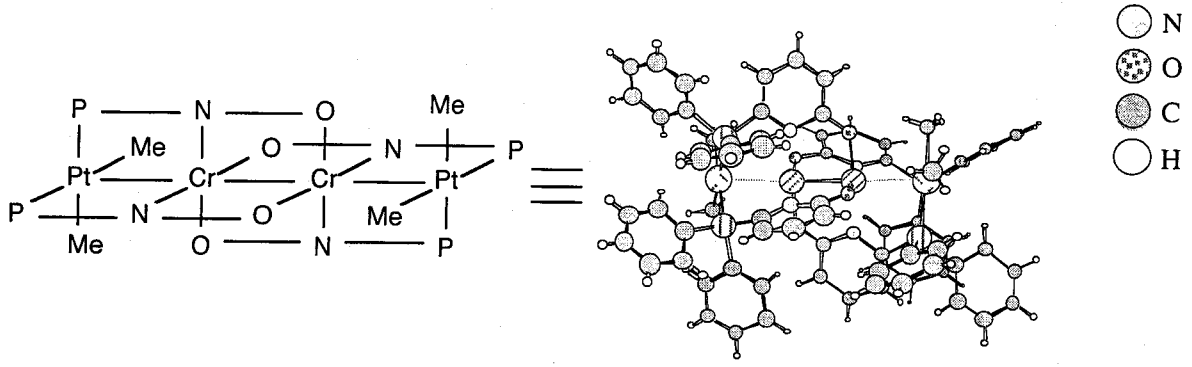

(7a)

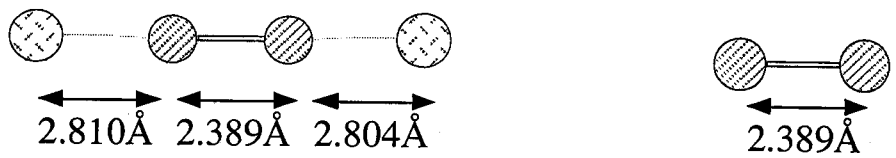

(7b) **(7c)**

Figure3.14

Model figures of full model of $Cr_2(pyphos)_4$ (**6a**), its Cr-Cr naked core model (**6b**). And model figures of full model of $Cr_2(pyphos)_4(CH_3)_4$ (**7a**), its naked Pt-Cr-Cr-Pt core model (**7b**) and its naked Cr-Cr model (**7c**)

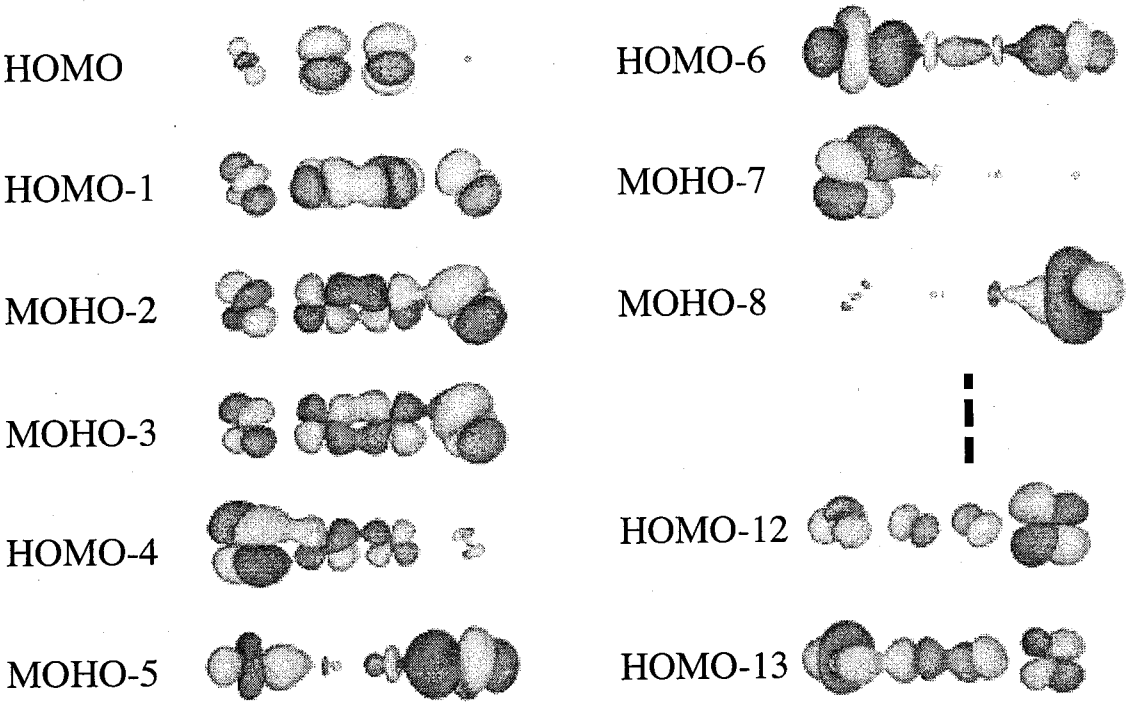

Fig.3.15
Natural Orbitals (NOs) of naked Pt-Cr-Cr-Pt core model (**7b**) of $\pi^4\delta^2$ state.

CHAPTER FOUR

GENERAL CONCLUSION OF THIS THESIS AND FUTURE PROSPECT

Chapter Four

General Conclusion of This Thesis and Future Prospect

4.1 General conclusion

In this thesis, the author developed the hybrid UDFT method to investigate magnetic interaction between radical species for strongly correlated systems, namely MEDF method. And the author applied the MEDF method to polynuclear complexes that involved linearly aligned metal ions to examine their electronic states using the effective exchange integrals (J_{ab}) values. The MEDF aimed to correct dynamical correlation effect, which Hartree-Fock method did not include, by DFT term under the approximation that non-dynamical correlation effect was taken into account by unrestricted calculation and spin-projection. The MEDF could reproduce J_{ab} values of Full CI or APUCCSD(T) method by adjusting its hybrid parameter. This hybrid parameter was closely related to instability of magnetic orbitals. The author found that the instability of magnetic orbitals could be used as indices to decide the hybrid parameter.

The electronic states of Polynuclear complexes were investigated by using MEDF.

Especially, details about magnetic interactions between metal ions in them were examined by effective exchange integrals (J_{ab}). The fundamental character of metal-metal bond and magnetic interactions between metal ions in linearly aligned metal complexes were investigated using $Cr_2(O_2CCH_3)_4(H_2O)_2$ and other Cotton type complexes in detail. From these results, the effect of metal ions, equatorial ligands and axial ligands to the magnetic interaction were elucidated. Furthermore, tetra-metal systems that were reliable models to metal chain, were also investigated using MEDF. The calculations of these strongly correlated electron systems need high calculating techniques. The author succeeded the calculation of J_{ab} of tetra-Cr(II) system using full complex model for the first time in the world. From the results, the author found that δ orbitals were easily affected by spiral equatorial ligands. Finally, the author examined the electronic state of polynuclear complexes that detail about its electronic states had not been elucidated except for J_{ab} values. The author could present the new strategy for those polynucler complexes that electronic state was determined with experimental J_{ab} value. This strategy was realized by quantitative analyses of J_{ab} calculated by MEDF.

This MEDF method is now applied to the several regions. Only a part of them are introduced here. Kawakami et al. applied the MEDF method to the calculation of J_{ab} in organic ferromagnets[1]. Usually, magnetic interactions in the crystal of organic ferromagnets are small. So, experimental J_{ab} values are small and conventional DFT methods such as UBLYP are overestimated them. The MEDF works well in those calculations. Onishi et al. and Nakano et al. investigated the electronic states of strong correlated copper-oxide clusters[2][3]. In these systems, conventional UDFT also overestimated twice as much as experimental J_{ab} values. MEDF could reproduce experimental J_{ab} values and they succeeded quantitative analyses on magnetic interaction. Nakano et al. also applied MEDF to the tight-binding band calculations for the copper-oxide lattice model[4] and two-dimensional C_{60}[5]. This was the first trial that connected band calculation and MEDF. The calculated results of copper-oxide explained the interaction of d- and π-hole that depended on the structure, well. On the other hand, Isobe et al. applied MEDF to the chemical reactions[6]. MEDF could compensate for the week point of conventional calculation methods, *i.e.* the UHF tends to estimate radical reaction path to be stable, while UDFT tends to estimate concerted reaction path to be stable. On the same strategy, Takano et al. investigated the magnetic coupling of non-Heme oxygen transport protein[7].

4.2 Future prospect

In this way, there are a lot of strongly correlated electron systems that are too large to calculate with post HF methods. The conventional DFT methods, however, do not reproduce appropriate electronic states, especially magnetic interactions. So, MEDF is powerful for the large strong correlated electron systems that have several localized spins. One of the most suitable systems is the metaloprotein that involves several metal ions. There are still a lot of such systems that electronic states and reaction mechanisms have not been elucidated well. In those systems, one can examine those electronic states or reaction path on the same strategy explained in chapter 3.5, if one can obtain the information about their X-ray structures and J_{ab} values.

The extension of MEDF to band calculation brought us so many possibilities. Very recently, interesting reports about so-called MX and MMX chain, which is one of the linearly aligned metal complex system have been presented because periodic conditions are necessary for calculations of electronic states of these complexes. Very strong anti-ferromagnetic interaction and non-linear optical effect on MX chain were reported by Yamashita et al.. Band calculation with MEDF seems to be the most possible candidate to analyze their electronic states and electronic properties.

As mentioned in chapter 2.7, the serious week points of MEDF still exist. One is the procedure for decision of hybrid parameter. Although this is performed by the semi-empirical way now, the more sophisticated theoretical framework, which determines hybrid parameter uniquely, is necessary. Another is the analysis of electronic states around bifurcation point, leading a necessity of CASDFT. Takeda et al. is developing the CASDFT procedure, which treats strong interaction between HOMO and LUMO exactly by CI and dynamical correlation effect of inner electrons by DFT[8]. By treating non-dynamical correlation effect by CASCI together with DFT, the electronic states are elucidated well.

Polynuclear systems are considered as good candidates for quantum wires, which can be used for quantum dots and atom relay transistor[11]. The resonant electron transfer occur via σ- or σ*-orbital energy levels of the chains in the complexes as illustrated in Figure 4.1. The so-called Kondo effect forming the singlet pair between transferred electrons must be taken into consideration often since the electron-electron repulsion (U) is significant in the case of transition metal clusters. Present calculations clearly demonstrated that σ-type d-d conjugations were feasible in such linearly

aligned transition metal complexes. And the energy level of σ-type conjugating orbitals was easily affected axial ligands. The hole (or electron) doping into these conjugated systems has received much interested with regard to conductivity and other properties such as nonlinear optical response. The author demonstrated the possibility of +3 oxidation state of chromium in $Cr_2(pyphos)_4$ and $Pt_2Cr_2(pyphos)_4(CH_3)_4$. Some hints might be hidden for such doping in those complexes. Such axial ligands and metal oxidation state are good candidates for chemical control of such molecular devices. In this sense, Cotton-type complexes constructed of early transition metals are promising for this purpose if they are linearly assembled as illustrated in Figure 4.2.

Although further improvements are needed on MEDF, it will contribute to the investigation of electronic states of strong correlated electron systems such as polynuclear systems as theoretical approach.

References of chapter four

[1] Kawakami, T.; Taniguchi, T.; Kitagawa, Y.; Takano Y.; Nagao, H.; Yamaguchi, K.; *Mol. Phys.* **2002**, *100*, 2641.

[2] Onishi, T.; Takano, Y.; Kitagawa, Y.; Kawakami, T.; Yoshioka, Y.; Yamaguchi, K. *Polyhedron*, **2001**, *20*, 1177.

[3] Nakano, S.; Kitagawa, Y.; Kawakami, T.; Nagano, H.; Yamaguchi, K. *Mol. Cryst. Liq. Cryst.* **2002**, *379*, 513.

[4] Nakano, S et al. on the domestic presentation.

[5] Nakano, S.; Kitagawa, Y.; Kawakami, T.; Yamaguchi, K. *Synthetic Metals* to be published.

[6] Isobe H.; Takano, Y.; Kitagawa, Y.; Kawakami, T.; Yamanaka, S.; Yamaguchi, K.; Houk, K. *Mol. Phys.* **2002**, *100*, 717.

[7] Takano Y; Kitagawa Y; Onishi T; Yoshioka Y; Yamaguchi K; Koga N; Iwamura H, *J. Am. Chem. Soc.* **2002**, *124*, 450.

[8] Takeda, R.; Yamanaka S.; Yamaguchi K. Chem. Phys. Lett. 2002. 366. 321

[9] Yamanaka, S.; Yamaki, D.; Kiribayashi, S.; Yamaguchi, K. *Int. J. Quant. Chem.* **2001**, *85*, 421.

[10] Yamanaka, S.; Yamaki, D.; Shigeta, Y.; Nagao, H.; Yoshioka, Y.; Suzuki, N.; Yamaguchi, K. *Int. J. Quant. Chem.* **2000**, *80*, 664.

[11] In Organometalic Conjugation, Eds, Nakamura, A.; Ueyama, N.; Yamaguchi, K. Kodansha Scientific, 2000.

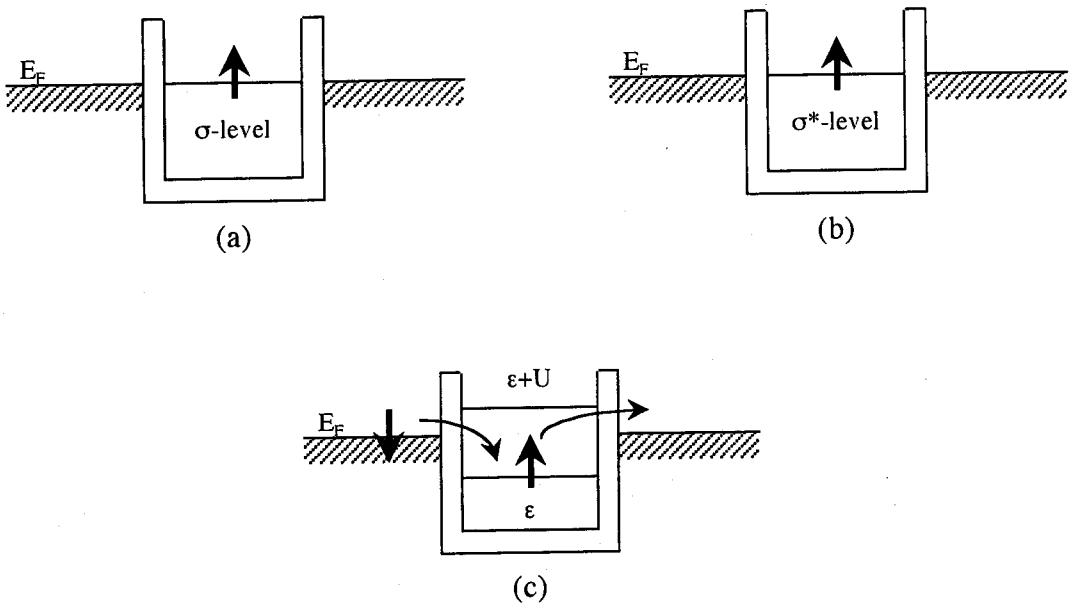

Figure 4.1
σ- and σ*-energy level diagrams for quantum dots (a and b) and Kondo effect in the dot (c).

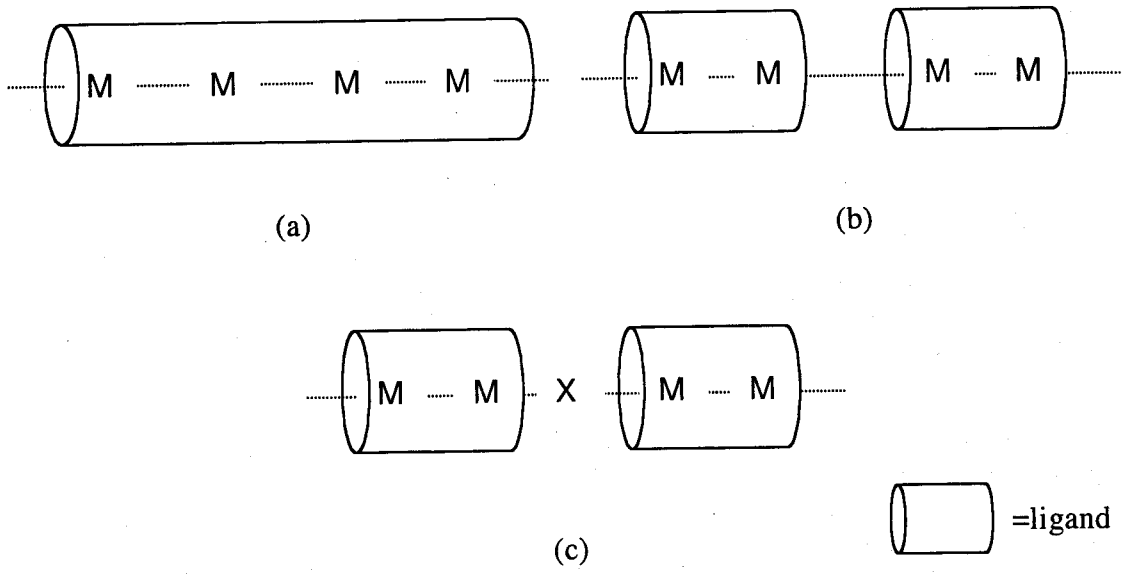

Figure 4.2
Quantum wires constructed of transition metal complexes.

List of publications

Main Publications

1) Kitagawa Y; Kawakami T; Yamaguchi K, Instability of a system and its estimation in terms of the hybrid density functional theory method, A magnetic effective density functional (MEDF) approach, *Mol. Phys.*, **2002**, *100*, 1829-1838.

2) Kitagawa Y; Soda T; Shigeta Y; Yamanaka S; Yoshioka Y; Yamaguchi K, Improvement of the hybrid density functional method from the viewpoint of effective exchange integrals, *Int. J. Quant. Chem.*, **2001**, *84*, 592-600

3) Kitagawa Y; Soda T; Onishi T; Takano Y; Nishino M; Yoshioka Y; Yamaguchi K, Theoretical studies on magnetic interactions of dichromium tetraacetate by using hybrid density functional method, *Mol. Cryst. Liq. Cryst.*, **2000**, *343*, 463-468

4) Kitagawa Y; Kawakami T; Yoshioka Y; Yamaguchi K, Theoretical studies on magnetic interactions of the metal dimers and their acetate complexes, *Polyhedron*, **2001**, *20*, 1189-1196

5) Kitagawa Y; Nakano S; Kawakami T; Mashima K; Tani K; Yamaguchi K, Theoretical Studies on Magnetic Interactions of Aligned Tetrametal Systems by Using Magnetic Effective Density Functional (MEDF) Method, *Mol. Cryst. Liq. Cryst.*, **2002**, *379*, 525-530.

6) Kitagawa Y; Nishino M; Kawakami T; Yoshioka Y; Yamaguchi K, Theoretical Studies on Magnetic Interactions of Aligned Tetrametal System by Using Hybrid Density Functional Method, *Mol. Cryst. Liq. Cryst.*, **2002**, *376*, 347-352.

7) Kitagawa Y; Nakano S; Kawakami T; Mashima K; Yamaguchi K, Magnetic Effective Density Functional Studies on Electronic States of $Cr_2(pyphos)_4$ and $Pt_2Cr_2(pyphos)_4(CH_3)_4$, *Polyhedron*, *submitted.*

8) Yamaguchi K; Kitagawa Y; Onishi T; Isobe H; Kawakami T; Nagao H; Takamizawa S, Spin-mediated superconductivity in cuprates, organic conductors and pi-d conjugated systems, *Coord. Chem. Rev.*, **2002**, *226*, 235-259

9) Isobe H; Takano Y; Kitagawa Y; Kawakami T; Yamanaka S; Yamaguchi K; Houk KN, Extended Hartree-Fock (EHF) theory of chemical reactions VI: hybrid DFT and post-Hartree-Fock approaches for concerted and non-concerted transition structures of the Diels-Alder reaction, *Mol. Phys*, **2002**, *100*, 717-727

10) Takano Y; Kitagawa Y; Onishi T; Yoshioka Y; Yamaguchi K; Koga N; Iwamura H, Theoretical studies of magnetic interactions in Mn(II)(hfac)(2){di(4-pyridyl)phenylcarbene} and Cu(II)(hfac)(2){di(4-pyridyl)phenylcarbene}, *J. Am. Chem. Soc.*, **2002**, *124*, 450-461

11) Okumura M; Kitagawa Y; Haruta M; Yamaguchi K, DFT studies of interaction between O-2 and Au clusters. The role of anionic surface Au atoms on Au clusters for catalyzed oxygenation, *Chem. Phys. Lett.*, **2001**, *346*, 163-168

12) Isobe H; Soda T; Kitagawa Y; Takano Y; Kawakami T; Yoshioka Y; Yamaguchi K, EHF theory of chemical reactions V. Nature of manganese-oxygen bonds by hybrid density functional theory (DFT) and coupled-cluster (CC) methods, *Int. J. Quant. Chem.*, **2001**, *85*, 34-43

13) Takano Y; Onishi T; Kitagawa Y; Soda T; Yoshioka Y; Yamaguchi K, Density functional and post-Hartree-Fock studies on effective exchange interaction of d-pi-d conjugated systems involving m-phenylene-type bridge, *Int. J. Quant. Chem.*, **2000**, *80*, 681-691

14) Takano Y; Soda T; Kitagawa Y; Onishi T; Yoshioka Y; Yamaguchi K, Theoretical study on magnetic interactions of Mn-pi conjugated system, *Mol. Cryst. Liq. Cryst.*, **2000**, *342*, 291-296

15) Soda T; Kitagawa Y; Onishi T; Takano Y; Yoshioka Y; Yamaguchi K, Theoretical studies on magnetic interaction of di-mu-oxo bridged manganese dimers, *Mol. Cryst. Liq. Cryst.*, **2000**, *343*, 475-480

16) Soda T; Kitagawa Y; Onishi T; Takano Y; Shigeta Y; Nagao H; Yoshioka Y; Yamaguchi K, Ab initio computations of effective exchange integrals for H-H, H-He-H and Mn2O2 complex: comparison of broken-symmetry approaches, *Chem. Phys. Lett.*, **2000**, *319*, 223-230

17) Yoshioka Y; Kitagawa Y; Takano Y; Yamaguchi K; Nakamura T; Saito I, Experimental and theoretical studies on the selectivity of GGG triplets toward one-electron oxidation in B-form DNA, *J. Am. Chem. Soc.*, **1999**, *121*, 8712-8719

18) Yamaguchi K; Yamanaka S; Nishino M; Takano Y; Kitagawa Y; Nagao H; Yoshioka Y, Symmetry and broken symmetries in molecular orbital descriptions of unstable molecules II. Alignment, flustration and tunneling of spins in mesoscopic molecular magnets, *Theoret. Chem. Acc.*, **1999**, *102*, 328-345

19) Takano Y; Soda T; Kitagawa Y; Yoshioka Y; Yamaguchi K, Theoretical studies of the effective exchange interactions and photoinduced magnetism in manganese and copper di(4-pyridyl)carbene complexes, *Chem. Phys. Lett.*, **1999**, *301*, 309-316

Others

20) Yamaguchi K; Kawakami T; Takano Y; Kitagawa Y; Yamashita Y; Fujita H, Analytical and ab initio studies of effective exchange interactions, polyradical character, unpaired electron density, and information entropy in radical clusters (R)(N): Allyl radical cluster (N=2-10) and hydrogen radical cluster (N=50), *Int. J. Quant. Chem.*, **2002**, *90*, 370-385.

21) Kawakami T; Kitagawa Y; Taniguchi T; Nakano S; Yamaguchi K, Theoretical studies on pi-d magnetic interactions between BETS donor and transition metal halides in kappa-BETS2MX4 crystals, *Mol. Cryst. Liq. Cryst.*, **2002**, *379*, 489-494.

22) Nagao H; Saito H; Suzuki R; Kitagawa Y; Kawakami T; Yamaguchi K, Field-induced superconductivity, *Mol. Cryst. Liq. Cryst.*, **2002**, *379*, 495-500.

23) Nakano S; Kitagawa Y; Kawakami T; Nagao H; Yamaguchi K, Theoretical studies on SDW and CDW states of Cu and Ag oxides under the periodic boundary condition, *Mol. Cryst. Liq. Cryst.*, **2002**, *379*, 513-518.

24) Kawakami T; Taniguchi T; Kitagawa Y; Takano Y; Nagao H; Yamaguchi K, Theoretical investigation of magnetic parameters in two-dimensional sheets of pure organic BEDT-TTF and BETS molecules by using ab initio MO and DFT methods, *Mol. Phys.*, **2002**, *100*, 2641-2652.

25) Onishi T; Takano Y; Kitagawa Y; Yoshioka Y; Yamaguchi K, Theoretical study on the magnetic interaction for manganese oxides, *Mol. Cryst. Liq. Cryst.*, **2002**, *376*, 335-340.

26) Kawakami T; Matsuoka F; Yamashita Y; Kitagawa Y; Yamaguchi K, Theoretical studies on magnetic properties of TCNQ organic crystals with ab initio and DFT methods, *Mol. Cryst. Liq. Cryst.*, **2002**, *376*, 441-416.

27) Nagao H; Kitagawa Y; Kawakami T; Yoshimoto T; Saito H; Yamaguchi K, Theoretical studies on field-induced superconductivity in molecular crystals, *Int. J. Quant. Chem.*, **2001**, *85*, 608-618

28) Kawakami T; Kitagawa Y; Matsuoka F; Yamashita Y; Isobe H; Nagao H; Yamaguchi K, Possibilities of molecular magnetic metals and high T-c superconductors in field effect transistor configurations, *Int. J. Quant. Chem.*, **2001**, *85*, 619-635

29) Matsuoka F; Yamashita Y; Kawakami T; Kitagawa Y; Yoshioka Y; Yamaguchi K, Theoretical investigation on the magnetic interaction of the tetrathiafulvalene-nitronyl nitroxide stacking model: possibility of organic magnetic metals and magnetic superconductors, *Polyhedron*, **2001**, *20*, 1169-1176

30) Onishi T; Takano Y; Kitagawa Y; Kawakami T; Yoshioka Y; Yamaguchi K, Theoretical study of the magnetic interaction for M-O-M type metal oxides. Comparison of broken-symmetry approaches, *Polyhedron*, **2001**, *20*, 1177-1184

31) Kawakami T; Takamizawa S; Kitagawa Y; Maruta T; Mori W; Yamaguchi K, Theoretical studies of spin arrangement of adsorbed organic radicals in metal-organic nanoporous cavity, *Polyhedron*, **2001**, *20*, 1197-1206

32) Kawakami T; Kitagawa Y; Matsuoka F; Yamashita Y; Yamaguchi K, Theoretical studies of

strong direct magnetic interactions of 5-methyl-1,2,4-triazole nitronylnitroxide, *Polyhedron*, **2001**, *20*, 1235-1242

33) Kawakami T; Matsuoka F; Yamashita Y; Kitagawa Y; Nakano M; Yamaguchi K, Theoretical design of organo-magnetic conducting crystal, *Synthetic Metals*, **2001**, *121*, 1826-1827

34) Shigeta Y; Kitagawa Y; Nagao H; Yoshioka Y; Toyoda J; Nakasuji K; Yamaguchi K, Theoretical studies on the proton and electron transfer (PET) in a pseudo one-dimensional hydrogen bonded network system, *J. Mol. Liq.*, **2001**, *90*, 69-74

35) Mitani M; Yamaki D; Takano Y; Kitagawa Y; Yoshioka Y; Yamaguchi K, Density-functional study of intramolecular ferromagnetic interaction through m-phenylene coupling unit (II): Examination of functional dependence, *J. Chem. Phys.*, **2000**, *113*, 10486-10504

36) Oda A; Nagao H; Kitagawa Y; Shigeta Y; Yamaguchi K, Theoretical studies on magnetic behavior in clusters by the genetic algorithms, *Int. J. Quant. Chem.*, **2000**, *80*, 646-656

37) Takamizawa S; Mori W; Yokomichi Y; Kitagawa Y; Maruta T; Kawakami T; Yoshioka Y; Yamaguchi K, Molecular simulations of argon, nitrogen, and hydrogen adsorption in microporous complexes, *Mol. Cryst. Liq. Cryst.*, **2000**, *342*, 285-290

38) Onishi T; Soda T; Kitagawa Y; Takano Y; Yamaki D; Takamizawa S; Yoshioka Y; Yamaguchi K, Theoretical study of the antiferromagnetic model clusters for K2MX4 type solids, *Mol. Cryst. Liq. Cryst.*, **2000**, *343*, 451-456

39) Nishino M; Kitagawa Y; Onishi T; Soda T; Takano Y; Nagao H; Yoshioka Y; Yamaguchi K, Theoretical study on necessary conditions for reversible photoinduced magnetization: Cobalt-iron cyanide system, *Mol. Cryst. Liq. Cryst.*, **2000**, *343*, 469-474

40) Kawakami T; Takamizawa S; Kitagawa Y; Matsuoka F; Maruta T; Mori W; Yamaguchi K, Theoretical studies on radical spin arrangements in the cavity of nanoporous complexes, *Mol. Cryst. Liq. Cryst.*, **2000**, *343*, 533-538

41) Nagao H; Nishino M; Shigeta Y; Soda T; Kitagawa Y; Onishi T; Yoshioka Y; Yamaguchi K, Theoretical studies on effective spin interactions, spin alignments and macroscopic spin tunneling in polynuclear manganese and related complexes and their mesoscopic clusters, *Coord. Chem. Rev.*, **2000**, *198*, 265-295

42) Yamaki D; Kitagawa Y; Nagao H; Nakano M; Yoshioka Y; Yamaguchi K, Visualization of two-body electron densities and wave functions of magnetic molecules, *Int. J. Quant. Chem.*, **1999**, *75*, 645-654